DIMENSIONAL STABILITY OF ENGINEERED CEMENTITIOUS COMPOSITES

A THESIS SUBMITTED TO
THE GRADUATE SCHOOL OF NATURAL AND APPLIED SCIENCES
OF
MIDDLE EAST TECHNICAL UNIVERSITY

BY

SÜLEYMAN BAHADIR KESKİN

IN PARTIAL FULFILLMENT OF THE REQUIREMENTS
FOR
THE DEGREE OF DOCTOR OF PHILOSOPHY
IN
CIVIL ENGINEERING

SEPTEMBER 2012

Approval of thesis:

DIMENSIONAL STABILITY OF ENGINEERED CEMENTITIOUS COMPOSITES

submitted by **SÜLEYMAN BAHADIR KESKİN** in partial fulfillment of the requirements for the degree of **Doctor of Philosophy in Civil Engineering Department, Middle East Technical University** by,

Prof. Dr. Canan Özgen _____
Dean, Graduate School of **Natural and Applied Sciences**

Prof. Dr. Güney Özcebe _____
Head of Department, **Civil Engineering**

Prof. Dr. İsmail Özgür Yaman
Supervisor, **Civil Engineering Dept., METU** _____

Assoc. Prof. Dr. Mustafa Şahmaran
Co- Supervisor, **Civil Eng. Dept., Gaziantep University** _____

Examining Committee Members:

Prof. Dr. Mustafa Tokyay
Civil Engineering Dept., METU _____

Prof. Dr. İsmail Özgür Yaman
Civil Engineering Dept., METU _____

Assoc. Prof. Dr. Recep Birgül
Civil Engineering Dept., Muğla Sıtkı Koçman University _____

Asst. Prof. Dr. Sinan T. Erdoğan
Civil Engineering Dept., METU _____

Asst. Prof. Dr. Tahir Kemal Erdem
Civil Engineering Dept., İzmir Institute of Technology _____

Date: September 14, 2012

I hereby declare that all information in this document has been obtained and presented in accordance with academic rules and ethical conduct. I also declare that, as required by these rules and conduct, I have fully cited and referenced all material and results that are not original to this work.

Name, Last Name : Süleyman Bahadır Keskin

Signature :

ABSTRACT

DIMENSIONAL STABILITY OF ENGINEERED CEMENTITIOUS COMPOSITES

Keskin, Süleyman Bahadır

Ph.D., Department of Civil Engineering

Supervisor : Prof. Dr. İ. Özgür Yaman

Co-Supervisor: Assoc. Prof. Dr. Mustafa Şahmaran

September 2012, 165 pages

Cementitious materials with strain-hardening property and high tensile ductility are promising materials on account of their mechanical and durability performances. These materials require special ingredients which make it costly to be used in conventional constructions. Hence, potential applications of Engineered Cementitious Composites (ECC) generally focus on layered systems or repairs which require the use of ECC together with another material. For it to be used especially as a repair material, it should have sufficient dimensional compatibility for preventing restrained shrinkage cracking. In this thesis, a strain-hardening fiber-reinforced cementitious composite, named Engineered Cementitious Composites, was produced with local ingredients and their mechanical performance, dimensional stability properties were investigated.

For investigating the effect of materials and mix proportions on mechanical properties, compressive strength, flexural strength with mid-span beam deflections and matrix fracture toughness tests were conducted. For determining the

dimensional compatibility properties, autogenous, drying and restrained shrinkage tests were conducted along with tensile creep tests. As a result it was shown that, mechanical and dimensional stability properties are affected by the ingredients and mix proportions. It was shown that especially autogenous shrinkage of mixtures was relatively high which can cause early age cracking. In order to mitigate the adverse effect of autogenous shrinkage, the effect of pre-soaked expanded perlite aggregate replacement on mechanical, shrinkage and dimensional compatibility properties was investigated. As a result it was found out that autogenous shrinkage can be mitigated by the use of pre-soaked expanded perlite aggregate replacement.

Keywords: Engineered Cementitious Composites, Mechanical Properties, Dimensional Stability, Tensile Creep

ÖZ

TASARLANMIŞ ÇİMENTOLU KOMPOZİTLERİN BOYUTSAL KARARLILIĞI

Keskin, Süleyman Bahadır
Doktora, İnşaat Mühendisliği Bölümü
Tez Yöneticisi : Prof. Dr. İ. Özgür Yaman
Ortak Tez Yöneticisi: Doç. Dr. Mustafa Şahmaran

Eylül 2012, 165 sayfa

Mekanik ve dayanıklılık performansları açısından şekil değiştirme sertleşmesi ve çekme altında yüksek süneklik gösteren çimentolu malzemeler gelecek vaat eden malzemelerdir. Bu malzemeler içerisinde bulundurdukları özel bileşenlerden dolayı normal beton gibi geleneksel yapılarda kullanılamayacak kadar maliyetlidir. Bu yüzden, Tasarlanmış Çimentolu Kompozitlerin (TÇK) potansiyel uygulamaları TÇK'nın başka bir malzemeyle birlikte kullanılmasını gerektiren, genel olarak tabakalı sistemlere veya tamir işlerine odaklanmaktadır. Bu sebeple, özellikle tamir malzemesi olarak kullanılabilmeleri için, kısıtlanmış rötre çatlaklarının engellenebilmesi açısından yeterli boyutsal uyumluluğa sahip olmalıdır. Bu tezde Tasarlanmış Çimentolu Kompozitler olarak adlandırılan, şekil değiştirme sertleşmesi gösteren, lif donatılı kompozitler, yerel bileşenler ile üretilmiş ve mekanik performansı, boyutsal karalılığı incelenmiştir.

Malzemelerin ve karışım oranlarının mekanik özellikler üzerine etkisini incelemek için, basınç dayanımı, orta açıklık kiriş eğilmesiyle birlikte eğilme dayanımı ve

matris kırılma tokluğu testleri gerçekleştirilmiştir. Boyutsal uyumluluk özelliklerinin belirlenmesi için, otojen, kuruma ve tutulmuş rötre testlerinin yanı sıra çekme altında sünme testleri yapılmıştır. Sonuç olarak, mekanik ve boyutsal stabilite özelliklerinin malzeme ve karışım oranlarından etkilendiği gösterilmiştir Ayrıca, karışımların özellikle otojen rötrelerinin, bu karışımlarda erken yaşta çatlama oluşabilecek şekilde nispeten yüksek olduğu gösterilmiştir. Otojen rötrenin olumsuz etkilerinin azaltılması için önceden ıslatılmış genleştirilmiş perlit agregası ikamesinin mekanik, rötre ve boyutsal uyumluluk özellikleri üzerine etkisi de incelenmiştir. Sonuç olarak, otojen rötrenin, önceden ıslatılmış genleştirilmiş perlit ikamesi ile azaltılabileceği bulunmuştur.

Anahtar kelimeler: Tasarlanmış Çimentolu Kompozitler, Mekanik Özellikler, Boyutsal Kararlılık, Çekme Altında Sünme

To Selin

ACKNOWLEDGEMENTS

I would like to express great appreciation to my supervisor Prof. Dr. İ. Özgür Yaman not only for his suggestions, support and supervision throughout my PhD life but also for his sincerity. Thanks are extended to my co-supervisor Assoc. Prof. Dr. Mustafa Şahmaran for his assistance, guidance and for always being available whenever I need help.

I would also express my gratitude to thesis progressive committee members Prof. Dr. Mustafa Tokyay and Assoc. Prof. Dr. Recep Birgül for their support, comments and directions. Also, I would like to thank Asst. Prof. Dr. Sinan T. Erdoğan and Asst. Prof. Dr. Tahir Kemal Erdem for their comment and advice on the thesis.

I wish to thank Burhan Aleessa Alam not only for his friendship but also for his help during the experimental work. I would also like to thank my friends and colleagues Şevki Öztürk, Volkan Kalpakçı, Murat Şahin, Melek Yılmaztürk and Dr. Onur Pekcan for their moral support.

I acknowledge the personnel of Materials of Construction Laboratory, Cuma Yıldırım, Ali Sünbüle, and Şahismail Tekin for their full support and contribution to the experiments.

I would like to express my sincere gratitude to my wife Dr. Özlem Kasap Keskin, my parents and my sisters for their patience, understanding, encouragement, and full support not only during my PhD study but also throughout my life. Finally, I am grateful to my late grandmother for her love and for everything she did for me.

This thesis was partially supported by the Scientific and Technical Research Council of Turkey (TÜBİTAK) provided under Project: MAG-108M495, and METU Scientific Research Project: BAP-03-03-2010-03.

TABLE OF CONTENTS

LIST OF TABLES

TABLES

LIST OF FIGURES

FIGURES

CHAPTER 1

INTRODUCTION

1.1 General

The requirement to build safe and durable structures necessitates the development of new materials to be used in constructions. In this context, cementitious materials of different types were brought to scene, by altering conventional concrete ingredients and their amounts, to meet different constructional needs. As a result of this search, high performance concretes arose. American Concrete Institute (ACI) defines high performance concrete as "a concrete meeting special combination of performance and uniformity requirements that cannot always be achieved routinely using conventional constituents and normal mixing, placing, and curing practices" (Russell, 1999). According to Aïtcin, (1998); concrete possessing a water to binder ratio lower than 0.4 can be considered as high performance concrete. Those concretes per se, exhibit high compressive strength.

High compressive strength concretes have been used in past years for structural purposes. However, high strength concrete exhibits a brittle behavior (Tasdemir et al., 1998). In addition, as the compressive strength of concrete increases, brittleness also increases. This case brings about potential dangers in structural applications. Although, concrete is not assumed to bear tension in engineering calculations, its poor tensile strength and tensile strain capacity are reasons of its low durability. Internal and external restraints generate tensile stresses and if the tensile strength

and/or tensile strain capacity of the material is not sufficient, cracks may form and open up which further stakes the durability of the material as they serve to ingress of liquids and detrimental chemical solutions to material.

To obtain a cementitious material with enhanced durability properties, fiber-reinforced cementitious composites which can also be considered as a type of high performance concrete according to ACI definition, were developed. According to Japan Society of Civil Engineers [JSCE], (2008) a special type of fiber-reinforced concrete, high performance fiber-reinforced cementitious composites (HPFRCC), is defined as "a material that exhibits strain-hardening characteristics under uniaxial tensile stress among short fiber-reinforced cementitious composites (FRCC)'s". The strain-hardening property of HPFRCC is attributed to fine and dense multiple crack formation. One major example of HPFRCC is "Engineered Cementitious Composites".

Engineered Cementitious Composites (ECC) is a new type of a cementitious material possessing high ductility hence high durability. The ingredients of ECC are similar to fiber-reinforced concrete as it contains cement, fly ash, aggregate, fiber, water and water reducing admixture. Compressive strength of ECC is also high enough to be used in most engineering structures. However, the characteristics of the used materials may be different to ensure superior tensile properties. ECC mixture design is conducted by a micromechanical method which elaborates individual ingredient properties to achieve desired composite properties.

Contrary to ordinary and fiber-reinforced concrete (FRC), after the first crack formation, ECC strain-hardens and demonstrates a strain capacity about 300-500 times greater than conventional concrete (Li, 2002). Also, unlike ordinary concrete and most FRC, ECC exhibits self-controlled crack widths under increased loads. Under tensile stresses, independent from the ultimate tensile strain, average crack widths remain at about 60 μm or even less (Şahmaran and Li, 2009-a). This behavior is achieved by micromechanical tailoring of ECC meaning tailoring its

microstructure for achieving the desired mechanical performance from the composite. Moreover, as a result of narrow crack widths and high tensile ductility; this construction material shows also high durability.

Although ECC is a preferable material in most respects, special constituents of ECC makes it an expensive material to be used instead of concrete. For this reason, in general ECC is used in critical regions of reinforced concrete structures instead of concrete or in repair of deteriorated concrete structures like concrete pavements and bridge decks. In this context, a repair material should have sufficiently high dimensional stability, hence compatibility to substrate for a crack free repair. That is, when placed on a dimensionally stable substrate which has lower shrinkage due to long term exposure to environmental conditions and advanced hydration, the repair material should have adequate shrinkage, tensile creep and elastic properties.

1.2 Objective and Scope

The cracking potential or dimensional compatibility of cementitious materials depend on four main factors, mentioned frequently in literature, which are modulus of elasticity, tensile strength, shrinkage strain and tensile creep.

The aim of this study is twofold; i) to produce ECC with locally available materials and high volumes of fly ash and ground granulated blast furnace slag to improve its mechanical and dimensional compatibility performances, and ii) to investigate the effect of expanded perlite aggregate replacement as pre-soaked lightweight aggregate on mechanical and dimensional stability properties. While producing ECC mixes, in addition to the water binder ratio, binder to cement ratio, aggregate to cement ratio and aggregate size of mixtures were altered to obtain standard ECC properties mentioned in the literature. When the related ECC properties were achieved, the tendency of produced materials to cracking was investigated. In addition, for mitigating shrinkage strains and cracking potential, pre-soaked lightweight aggregate usage was also investigated.

Tensile creep of ECC specimens was investigated under direct tension loads by using a setup designed and manufactured for this purpose. Drying shrinkages of the specimens were determined according to ASTM C 157 (American Society for Testing and Materials [ASTM], 2006-b) after the age of 28 days. Autogenous shrinkage was determined by sealing shrinkage drains which provides direct linear strain measurements up to 28 days. Thermal shrinkage was not determined since the experiments were conducted under stable environmental conditions. These experiments provided data on the resistors and drivers of the cracking potential of the ECC mixes. The appearance and number of shrinkage cracks were examined at early ages utilizing restrained shrinkage rings to evaluate the materials dimensional compatibility.

In the scope of the thesis, in Chapter 2, brief information about the various types of fiber-reinforced cementitious materials is provided. Design principles, properties and distinctive features of ECC and its field of applications are also given. The concept of dimensional compatibility, its importance and properties of cementitious materials that affect it are discussed. In addition, methods of determining the stability properties and relation between these properties are also given. In Chapter 3, details of the experimental study are presented. Properties of the ingredient materials used in production of ECC, proportions of the designed ECC mixtures, experimental methodology followed to determine the mechanical and dimensional properties are given in the same chapter. Results of the conducted tests both for determining the effect of mixture proportions and expanded perlite replacement on mechanical and dimensional properties are given separately in Chapter 4. Results of tests are discussed and correlated. In Chapter 5, a summary of the results and final remarks on the results are presented. Finally in Chapter 6, recommendations are given for further studies on the subject.

CHAPTER 2

LITERATURE REVIEW

2.1 Fiber-Reinforced Cementitious Composites

2.1.1 General

Cementitious materials, without any reinforcement, are characterized with low tensile strength and low tensile strain capacity; hence they exhibit brittle behavior (Bentur and Mindess, 2007). Structural use of concrete with very high compressive strength has been in progress in the last decades but brittleness also increases as the compressive strength of the concrete increases which is potentially dangerous and limits the use of high strength concrete in structural applications. This is more pronounced in locations where steel and concrete are in contact or in connections of steel-concrete hybrid structures since fracture failure of concrete may be resulted due to high stress concentrations. Furthermore, behavior of a structural element (brittle or ductile) affects the seismic response of overall structure; after all, ductile behavior of concrete can improve the seismic behavior of the structure significantly (Li and Kanda, 1998).

For this reason, using cementitious materials as a construction material requires reinforcement. Generally, this reinforcement is in a form of continuous steel reinforcement bars which are placed in appropriate places of the structure to bear the imposed tensile and shear stresses. Fibers, on the contrary, are discontinuous

and usually randomly distributed through the cementitious matrix (Bentur and Mindess, 2007). Fiber-reinforcement is not a replacement for conventional steel reinforcement as they have different intended usage. Conventional reinforcement bars are used to withstand the loads or increase the load bearing capacity whereas fibers are used for crack control. Steel and fiber reinforcement can also be used together to enhance the behavior of structural elements in case of blast, impact or seismic loading (Mindess et al., 2003).

According to the volume fraction of fibers and the intended function of the fibers in the composite, fiber-reinforced cementitious composites (FRC) can be divided into three groups. FRC's containing a low volumetric fiber amount (less than 1%) are generally intended for reducing shrinkage cracks. Fibers in FRC's containing low fiber fraction generally do not perform any structural function. FRC's containing moderate fiber fractions of 1 to 2% are adaptable materials that are potentially used for various structural functions as they can be produced as pre-cast or cast-in-place with employing regular concrete mixing and casting procedures. This type of FRC's demonstrate advanced mechanical properties like improved modulus of rupture (MOR), resistance to fatigue and impact loads, fracture toughness etc. Steel fibers are generally utilized in this type of FRC's and can serve as a secondary reinforcement in partial replacement of shear reinforcement and for crack width control. Third type of FRC, called high performance FRC (HPFRC), exhibits strain-hardening behavior by employing a high volumetric fraction of fibers between 5 and 20%. HPFRC's exhibit perfect mechanical properties with improved strength properties and fracture toughness. They are regarded as important as main reinforcement for a structural member due to their enhanced mechanical performance. However HPFRC's require special processing on account of high fiber content which hinders wider usage and restricts to precast members. Steel fibers are commonly used in HPFRC which along with the high fiber content results cost and weight associated problems. Also, material processing dependent on fiber orientation brings forth anisotropic properties and existence of weak planes (Li, 1998; Li, 2002).

Another way of classifying FRC is established by Japan Society of Civil Engineers [JSCE] (2008) as shown in Figure 2.1. This classification depends on composite ductility and strength rather than fiber content. Among fiber-reinforced cementitious composites (FRCC), fiber-reinforced concrete exhibits strain-softening behavior (a decrease in tensile strength after the formation of first crack) under tensile stresses with a strength range between low and high. A ductile fiber-reinforced cementitious composite is another class which may possess deflection-hardening characteristics under bending or pseudo strain-hardening characteristics under uniaxial tensile stresses. Deflection-hardening behavior can be explained as increase in flexural strength of a material accompanying an increase in flexural deformation. Ultra high strength fiber-reinforced concrete is the major example of this class which is also characterized with high strength. Deflection-hardening materials cannot be counted as ductile as strain-hardening materials, on account of damage localizations at relatively lower loads depending on loading rate and specimen dimensions and the difficulty of crack width control. Through short fiber-reinforced cementitious composites, high performance fiber-reinforced cement composites with multiple cracks (HPFRCC) was defined as a material that exhibits pseudo strain-hardening behavior under tensile loads. Strain-hardening behavior is described as an increase in tensile strain with a simultaneous increase in tensile stress after first crack formation as shown in Figure 2.2. The term “pseudo strain-hardening” is generally used rather than the term “strain-hardening” when dealing with cementitious materials since the mechanism of strain-hardening in HPFRCC is attributed to tight and dense multiple cracks rather than the mechanism of strain-hardening behavior observed in metallic materials (JSCE, 2008).

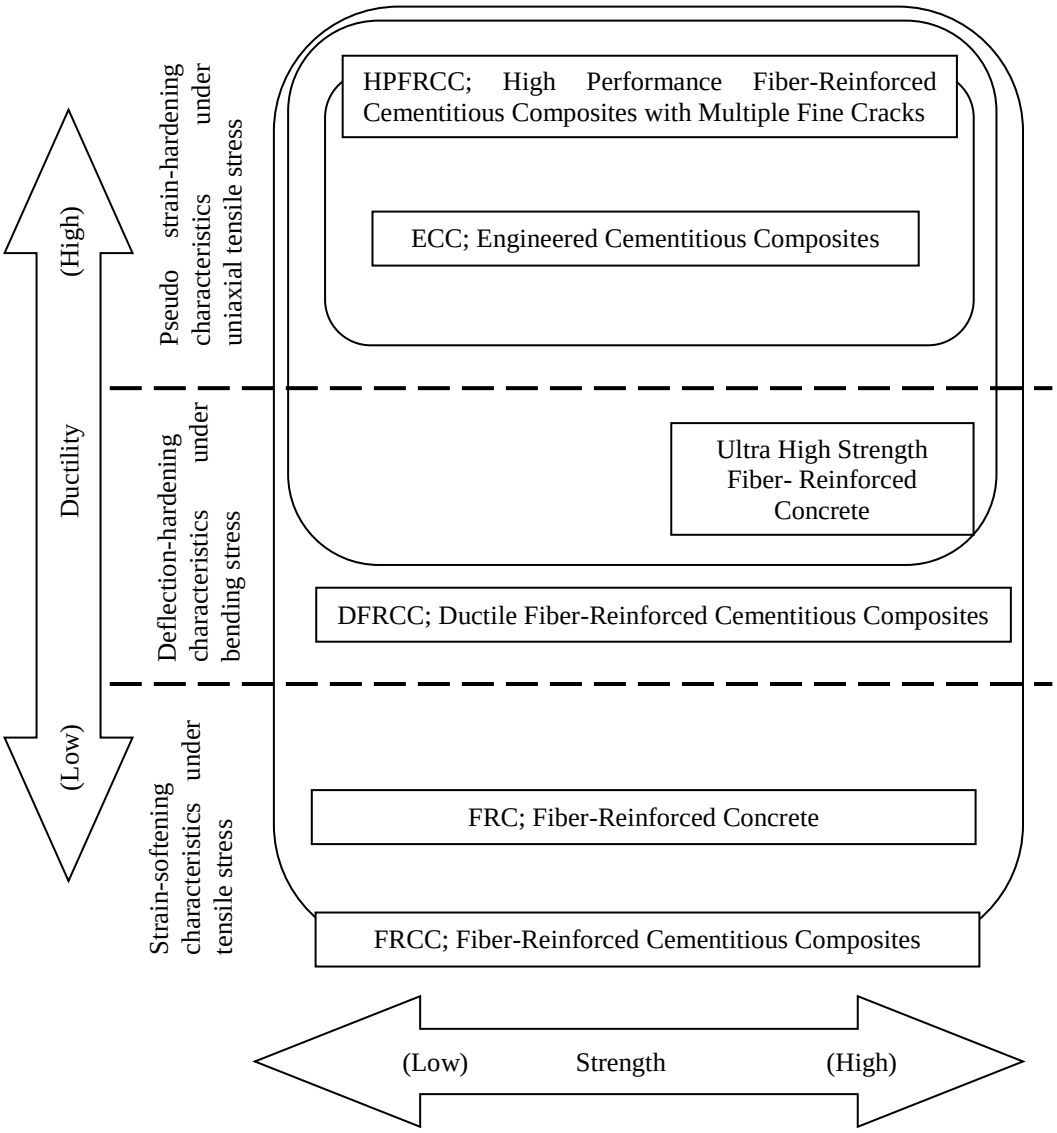

Figure 2.1 Classification of fiber-reinforced cemetitious composites according to Japan Society of Civil Engineers (JSCE, 2008)

Because of the deficiencies of low, moderate and high volume fiber containing fiber-reinforced cementitious composites mentioned above, development of cement-based composite materials with high ductility is needed for structural applications. In recent years, as a result of the studies at the University of Michigan, a high performance fiber-reinforced composite material with a patent name of "Engineered Cementitious Composites (ECC)" has been developed. ECC is the major example of HPFRCC.

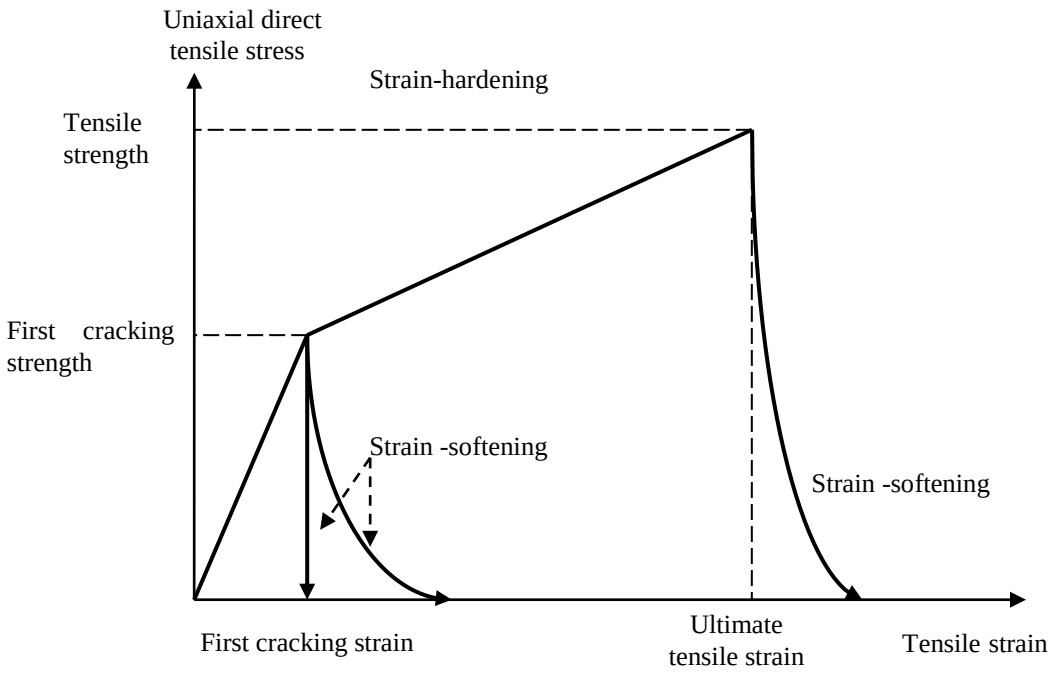

Figure 2.2 Strain-hardening and strain-softening concepts (JSCE, 2008)

2.1.2 Properties of ECC

In terms of many features ECC is similar to moderate and high strength concrete. For instance the compressive strength of ECC is within the range of 30 to 100 MPa. However, different from other normal and high performance concrete, this composite material has a very high tensile strain capacity (in the range of 3-5%) as

can be seen in Figure 2.3 (Li, 1998; Li et al., 2001). When the tensile strain capacity which is approximately 300-500 times that of normal concrete is taken into account, ECC can be considered as a ductile material. On the other hand, the ductility of ECC under bending loads is also assured (Figure 2.4) (Li and Kanda, 1998; Li et al., 1994; Li, 1998).

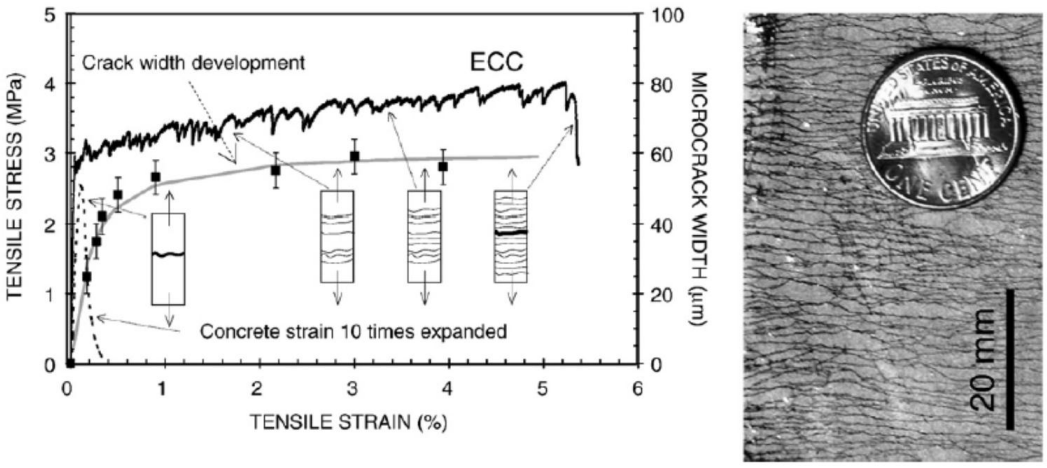

Figure 2.3 Strain-hardening of ECC (Şahmaran and Li, 2009-a)

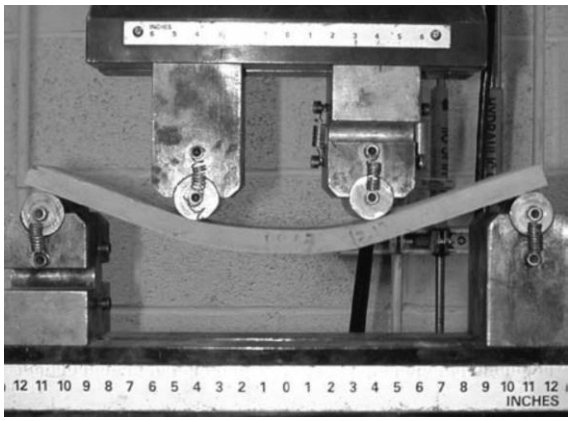

Figure 2.4 ECC under bending (Yang and Li, 2010)

The main reason for the high ductility of ECC is the strain-hardening that it exhibits after the formation of the first crack due its micromechanics based design (Li and Kanda, 1998). During loading, the first crack opens up to average of around 60 μm, and when the loading is continued the number of the cracks are increased instead of the width of the first crack (Figure 2.3). After the formation of the first crack, the material deforms in this way, at the same time it reaches its ultimate strength as the load is increased (Figure 2.3). Even at the maximum deformation that the material exhibits, average crack width is kept constant at 60 μm levels. ECC exhibits self-controlled crack widths under increasing loads.

The behavior mentioned above is possible with micromechanical tailoring of ECC. In micromechanical models, the microstructure of the composite is optimized to obtain the desired mechanical properties. In this way, with the control of the fiber, matrix and interface interaction, high performance composite is obtained (Li, 2003). In micromechanical design phase, the data obtained from the experiments of the mechanical properties of the matrix, the results of single fiber direct pull-out test and the mechanical and physical properties of fibers are used as parameters. To summarize, for ECC to behave as a ductile material and exhibit large number of small cracks instead of small number of large cracks and strain-hardening, the toughness of the matrix should be as low as possible, the bridging (first crack formation) stress should be low, the chemical bond at the fiber matrix interface should be low, and after the breakage of the bond the friction should be sufficient between the fiber and matrix (Li, 1998; Wang and Li, 2007; Li et al.,1995; Li et al., 2002).

ECC is similar to fiber-reinforced concrete from the ingredients point of view. It contains water, cement, sand, fiber, and some commonly used chemical admixtures (Li and Kanda, 1998). Coarse aggregate is not used in order not to affect its homogeneous and ductile behavior. Generally water/cement and sand/cement ratio is about 0.5 (Li and Kanda, 1998). ECC contains very low percentage of fibers as compared to high performance fiber-reinforced concrete. Even in case of structural

usage, it contains usually 2% or less volume of fibers (Schneider, 1991). As a result of micromechanical calculations, for low volume fiber (V_f) (2% level) composites to exhibit strain-hardening, fiber diameters should be lower than (df) 50 μm (Li, 1998). The use of polymeric fibers is preferred in ECC production since 50 μm fiber diameters can be achieved much more easily compared to steel fibers. The differences between ECC, fiber-reinforced concrete (FRC) and high performance fiber-reinforced composites are summarized in Table 2.1 (Li, 2002).

Table 2.1 Comparison of FRC, HPFRC and ECC (Li, 2002)

Parameter/Property	**FRC**	**HPFRC**	**ECC**
Composite design methodology	Not Applicable	Use of high V_f	Micromechanics based, minimize V_f for cost and processibility
Fiber type and amount	Any type, V_f usually <%2; d_f (steel)~500 μm	Mostly steel V_f usually >%8 d_f ~150 μm	Tailored, polymer fibers most suitable; V_f usually <%2; d_f<50 μm
Matrix ingredients	Coarse aggregates used	Fine aggregates used	Controlled for matrix toughness and initial flaw size; fine sand used
Interface	Not controlled	Not controlled	G_d and τ_0 controlled
Tensile behavior	Strain-softening	Strain-hardening	Strain-hardening
Tensile strain capacity	0.1%	<1.5%	>%3 ; 8% demonstrated
Crack width	Unlimited	Typically several hundred μm, unlimited for ε> 1.5%	Typically <100 μm during strain-hardening
Processing	Self-compaction demonstrated; Extrudability demonstrated	Self-compaction impossible due to high V_f, often requires high frequency vibration (e.g. in CRC); Extrudability demonstrated	Self-compaction demonstrated; Extrudability demonstrated

Besides the high ductility of hardened ECC, desired workability properties can also be achieved for fresh ECC mixtures. For instance self-compacting ECC mixtures were successfully produced by Kong et.al. (2003).

The fatigue of ECC under bending loads were also studied and ECC/concrete pavements were found to be 2 times stronger than concrete/concrete pavements and fatigue life is also found to be several times higher (Zhang and Li, 2002).

The damage in the ECC and concrete due to corrosion of reinforcement was also investigated and while the concrete was cracked in a brittle way, ECC behaved in a plastic manner and did not damage due to expansion caused by the corrosion (Miyazato and Hiroishi, 2005; Kanda et al., 2003). In a study related with resistance of reinforced beams to corrosion conducted by Şahmaran et.al. (2008-b), the crack width of control specimens increased continuously (up to 2.0 mm) while the crack widths of ECC specimens were fixed around 0.1 mm. And in the same study it was found out that the service life of reinforced ECC is 15 times more than that of reinforced concrete from corrosion resistance point of view.

In another research by Şahmaran and Li (2007), de-icing salt scaling resistance of mechanically pre-loaded non air entrained standard ECC mixtures was studied. At the end of 50 freezing-thawing cycles, visual inspection and mass loss were found to be inside the limits of ASTM C672. Even in the highly deformed specimens containing lots of microcracks, high durability properties could be achieved according to ASTM C672. After 25 and 50 freezing-thawing cycles, the tensile strength and durability were investigated and the tensile strain capacity was found to be around 3%. The main reason of this behavior was found as the self-healing of thawing cycles. Sahmaran et al. (2008-a) showed that by the use of high volumes of fly ash (up to 55% mass), damage caused by mechanical loading heals in a shorter time and attains the similar strength and durability with that of undamaged specimens within a month.

In addition to corrosion performance, in another study Şahmaran et.al (2007-a) conducted chloride ion penetration tests on cracked and uncracked beams produced with standard ECC mixtures and determined the chloride diffusion coefficients. ECC beam specimens were preloaded in bending to obtain highly damaged

specimens and crack widths were limited to 50μm and much lower chloride ion penetrations (low chloride ion diffusion coefficient) were obtain for ECC than that of similarly loaded reinforced concrete beams. The reason for lower chloride ion diffusion of ECC with respect to concrete was described with the controlled crack width of ECC which is less than 100μm. In addition, the superior performance of ECC was also associated with the self-healing of the specimens observed in ECC specimens exposed to NaCl solution. By the same researchers in another study (Li et al., 2007), the coupon samples prepared with standard ECC mixtures were loaded (damaged) up to different levels under direct tension, afterwards specimens were exposed to salty water for 1, 2 and 3 months and were loaded again. According to results, strain capacities of the reloaded specimens were still more than 3%. It was concluded that self-healing close ups the cracks, high performance of ECC is maintained by self-healing and even if it has cracks ECC is a material resistant to salty water.

In another study, durability of ECC in highly alkaline environment was examined by Şahmaran and Li (2008). Crack development and self-healing of ECC under mechanical and environmental effects were observed. For this purpose, the specimens prepared by deforming ECC mixes under direct tensile stress were exposed to alkaline solution for 3 months at 38 ^{o}C, and afterwards specimens were re-loaded under tension. As a result, ductility and tensile strength of the reloaded specimens exhibited a slight drop and the tensile strain capacity was found to be above 2%. From the microstructural studies, it was found out that self-healing is effective on the results and even after a month self-healing helped to close up the cracks. In the same study Şahmaran and Li (2008) investigated the expansion of ECC bar specimens according to ASTM C1260, and the lengths of bar specimens exhibited no expansion after 30 days at 80^{o}C alkali solution.

Sorptivity and water absorption of damaged ECC specimens were investigated in another study by Şahmaran and Li (2009-b). Depending on the density of the microcracks, sorptivity of the ECC specimens were increased but ECC specimens yielded similar results with undamaged concrete specimens. Nevertheless, the use

of water repellent admixtures decreased the sorptivity and water absorption of the specimens.

The abrasion resistance of ECC used as paving material under traffic loads was investigated and ECC exhibited better wear resistance compared to specifications of State of Michigan (Li and Lepech, 2004). Freezing-thawing resistance of ECC was investigated according to ASTM C666, concrete could not survive after 110 cycles however ECC showed nearly no deterioration. The durability factor calculated according to same standard as 20 for concrete and 100 for ECC. After 300 cycles, the strain capacities of ECC specimens were not changed, wet cured specimens show strain capacity of 3% (Li et al., 2003).

2.1.3 Design of ECC

Behavior of fiber-reinforced cementitious composites in macro level such as a structural member is dependent on its micro level behavior. By the use of micromechanical models, mechanical properties of composites are estimated with the properties of ingredients. Inversely, ingredient properties can be designated by the use of mechanical properties of composites. That is; micromechanical models are employed as a design tool to reach desired mechanical composite properties. The primary mechanical property that is aimed in micromechanical models is composite tensile strain capacity which is achieved by steady state multiple cracking behavior. Fiber, interface and matrix properties are used as input parameters. Micromechanical model is mostly dependent on fiber bridging stress versus crack opening relation and matrix fracture toughness values which are also related with the individual fiber and matrix properties. It is not possible to establish a model that all input parameters can effectively be altered. Even being able to work in industrial level, manufacturing process intervene the input parameters to be assumed independently. Micromechanical modeling starts with the determination of fiber, matrix and interface parameters which are feasible for achieving targeted composite parameters. In this stage, data obtained from previous studies are taken

into consideration; composites potential of strain-hardening is obtained. Next, fundamental material parameters are narrowed for composite strain capacity optimization. Finally, magnitudes of fiber, matrix and interface parameters are selected and ingredient parameters are linked. There are some limitations for constituent parameters for instance; for the fiber point of view fiber strength, diameter, elongation and elastic modulus are all dependent to each other due to fiber manufacturing processes. On the other hand, this relationship provides linkages between these parameters. Likewise, workability issues are in the center of composite production limitations, and it limits the fiber aspect ratio and volumetric fiber content. Besides, sufficient volumetric fiber content is pushed by critical volumetric fraction model to achieve a composite pseudo strain-hardening behavior. Also, there is a cost limitation for the fibers since it is the most expensive ingredient of the composite. When considering the interfacial parameters, strain-hardening model imposes sufficiently low interfacial chemical and frictional bonds which are also effective on volumetric fiber content. For hindering shrinkage cracking, aggregate content should be as high as possible, however high aggregate content increases matrix fracture toughness which inhibits steady state cracking. Also, due to the lack of coarse aggregates in the ECC, binder content is higher which also increases the risk of shrinkage cracking. Therefore, aggregate size and amount is adjusted to attain sufficiently low matrix toughness for steady state cracking and minimizing shrinkage cracking at the same time. High w/c ratio is beneficial for a low matrix fracture toughness value and low frictional bond; it is also advantageous since it provides uniform fiber distribution due to increased consistency. However, due to its negative effect on compressive and tensile strengths there is a requirement for an upper limit of w/c (Li et al., 2001).

2.1.4 Micromechanical Design Principles of ECC

Main objective of micromechanical design theory of ECC is to achieve a pseudo strain-hardening behavior by multiple cracking of brittle matrix with the use of microstructural material parameters. Studies of developing ECC design theory for a

brittle cement matrix with randomly distributed fibers was initiated in the beginning of 90s (Li and Leung, 1992; Li and Wu, 1992; Li, 1993) based on previous studies. Prior, multiple cracking and pseudo strain-hardening was achieved for ceramic matrix with continuous reinforcement and cement matrix with aligned fibers as mentioned by Li and Wu (1992). For continuous aligned fibers, sufficient number and sufficiently high tensile strength of bridging fibers are required to carry the load due to the matrix cracking in order to avoid rupture of fibers that results in a brittle fracture. However, in case of randomly distributed fibers there should be a sufficient number of fibers along with bond strength and embedded length of bridging fibers in order to avoid fiber pull-out which also results in a brittle fracture. Consequently, it can be said that it is harder to achieve pseudo strain-hardening by using randomly distributed fibers compared to continuous aligned reinforcement (Li and Wu, 1992). However, the ease and lower cost of processing and isotropic mechanical properties are the advantages of short random fiber composites that cannot be disregarded over aligned continuous fiber composites. The needs for a random discontinuous fiber composite which both possess the advantages mentioned above and ductile behavior arose (Li and Leung, 1992). Development of micromechanical design theory for a multiple cracking pseudo strain-hardening cementitious material with short random fibers has been implemented since then.

When a composite is loaded with a tensile stress which is higher than composite's cracking strength, a crack initiates from a defect site and extents infinitely. During this extension, crack opens and applied load remains constant and bridging elements sustains passing the loads. If the applied tensile stress is increased, new flat crack propagation starts in another defect site. This type of cracking behavior is called "steady-state cracking". On the contrary, in case of a Griffith type crack extension, applied load is decreased continuously as crack opening widens (Yang and Li, 2007).

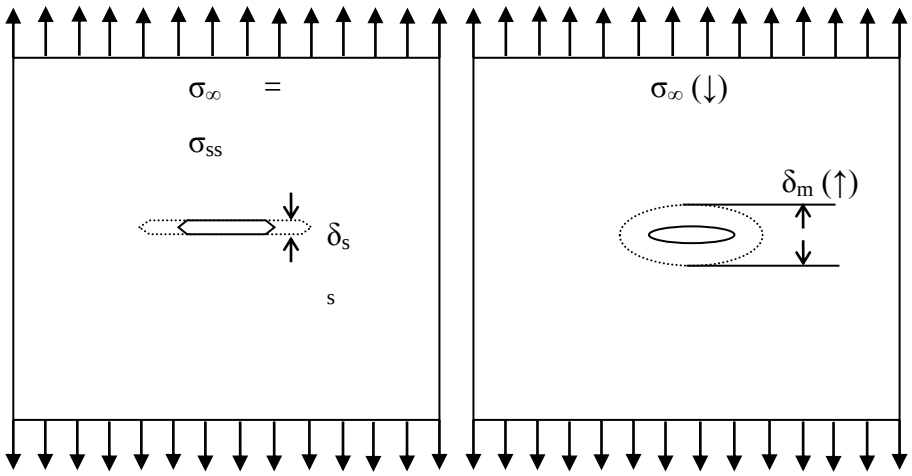

a. Steady-state cracking b. Griffith crack

Figure 2.5 Cracking theories (Yang and Li, 2007)

Fiber bridging property of a fiber-reinforced cementitious composite is defined as tensile stress (σ) that can be transmitted by fibers across a crack having a uniform width (δ) and generally denoted by a (σ-δ) curve (Li, 2003). The composite bridging stress versus crack opening displacement relationship should be known for the application of micromechanical model since it provides links between fiber, matrix and interface properties and the tensile ductility of composite. A formulation for predicting this relationship was proposed by Li et al. (1991) as:

$$\sigma(\delta) = \frac{4V_f}{\pi d_f^2} \int_{\emptyset=0}^{\pi/2} \int_{z=0}^{L_f/2cos\emptyset} P(\delta)p(\emptyset)p(z)dz\, d\emptyset \qquad (2.1)$$

Where V_f, d_f and L_f are volume fraction, diameter and length of fibers, *p(ø)* and *p(z)* are probability density functions of fiber orientation and fibers centroidal distance from the crack plane, respectively. In a three dimensional random fiber distribution p(ø)=sinø and p(z)=2/L_f. P(δ) is pull-out force displacement relationship of a single fiber.

For PVA fibers, tensile strength of the fiber is observed to be decreased due to interaction of fiber with the matrix resulted from the inclination angle between fiber and matrix (Kanda and Li, 1998). A similar effect was observed in the pull-out load called "snubbing effect", and was considered with an exponential expression "$e^{f\emptyset}$". σ(δ) relation was modified by Lin et al. (1999) to take into account the snubbing effect. Therefore:

$$\sigma(\delta) = \frac{4V_f}{\pi d_f^2} \int_{\emptyset=0}^{\pi/2} \int_{z=0}^{L_f/2cos\emptyset} P(\delta) e^{f\emptyset} p(\emptyset) p(z) dz \, d\emptyset \qquad (2.2)$$

Pseudo strain-hardening property of cementitious composite is achieved by multiple cracking in the brittle matrix. For multiple cracking to occur, there are two main criteria namely; strength and energy criteria. Matrix cracking strength (σ_{ss}) must always be lower than the maximum fiber bridging strength (σ_0) which is called the "strength criterion" for multiple cracking.

$$\sigma_{ss} \leq \sigma_0 \qquad (2.3)$$

This criterion provides the initiation of a crack from a flaw site before the tensile stress exceeds the maximum fiber bridging capacity of the composite. If this criterion fails, it yields a crack where the tensile stress cannot be carried by the fiber bridging (Li, 2003).

To be able to understand the "energy criterion" it is better to think of σ-δ curve as a spring law which describes the behavior of non-linear springs connecting the opposite flanks of a crack that describes the forces on bridging fibers against the opening of crack.

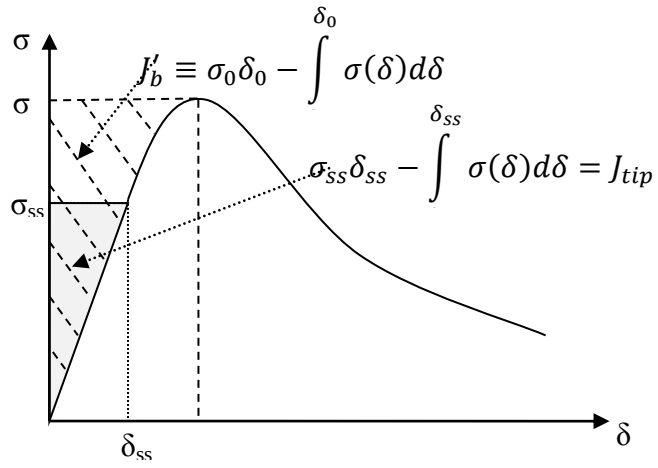

Figure 2.6 Complementary energy concept represented on an σ-δ curve of a steady-state cracking composite (Yang and Li, 2007)

If fiber/matrix interface is too weak, fibers pull-out and peak strength (σ_0) of the σ-δ curve becomes lower. On the contrary, if it is too strong, the spring will not be able to stretch, fibers will rupture and the value of critical opening δ_0 will be small. In both cases complementary energy represented by the hatched area in Figure 2.6 will be small. Steady-state crack analysis conducted by Li and Leung (1992) showed that if the complementary energy is smaller than the energy required for breaking the crack tip material which results in extension of the crack known as "crack tip toughness", the crack will behave as a Griffith crack as depicted in Figure 2.5.b instead of a steady-state crack. During crack propagation, at the middle of the crack as maximum crack opening (δ_m) exceeds critical crack opening (δ_0) springs will start to unload. Crack will expand and the load carrying capacity of the composite will decrease resulting in a tension softening behavior with localized cracking. However if the complementary energy is high, during propagation, crack will remain flat and steady state crack opening ($\delta_{ss}<\delta_0$) will be provided and tensile load carrying capacity will be maintained since the fibers remain intact. Another crack will initiate from a defect site since tensile load can still be transferred from the existing crack. This loop will yield multiple cracking

phenomenon. Hence, shape of the σ-δ curve, thus complementary energy is very effective on the behavior of composite (Li, 2003).

Energy criterion can be formulated as:

$$J_b' \equiv \sigma_0\delta_0 - \int_0^{\delta_0} \sigma(\delta)d\delta \geq J_{tip} \tag{2.4}$$

where:
J_b': Maximum complementary energy,
J_{tip}: Crack tip toughness.

Crack tip toughness can be assumed as cementitious matrix toughness in composites containing small amount of fibers and it is also valid for ECC since it contains less than 3% volumetric fraction of fibers (Li, 2002; Li et al. 2002). Thus:

$$J_b' \equiv \sigma_0\delta_0 - \int_0^{\delta_0} \sigma(\delta)d\delta \geq \frac{K_m^2}{E_m} \tag{2.5}$$

where;
K_m: Matrix fracture toughness,
E_m: Matrix Young's Modulus. (Li, 2002)

as mentioned in Li et al. (2002), Li (2001), Li (2002), Lin et al.(1999), Li (1998), Yang and Li (2007).

The shape of the σ-δ curve thus the amount of complementary energy "J_b'" is dependent on the fiber and interface properties. To be able to maximize the amount of J_b' for achieving a strain-hardening behavior, fiber and interface properties should be tailored. Together with the above equation it is clearly seen that the matrix properties should also be tailored to attain low matrix fracture toughness and relatively high matrix modulus of elasticity to increase the

possibility of multiple cracking. The slope of rising branch of the σ-δ curve is controlled by fiber content V_f, fiber diameter d_f, length L_f and modulus of elasticity E_f and interface frictional bond τ_0 if it is assumed that there is only frictional connection between fibers and matrix. If there is also chemical bond G_d between fibers and matrix, this time the σ-δ curve starts at a point little bit higher on y-axis, instead of origin, without any change in the slope of rising branch of the curve which decreases the amount of complementary energy, J_b'. The peak point of the curve which should be high in terms of strength criterion is controlled by V_f, d_f, L_f and τ_0, for simple friction assumption, and also by G_d for chemical bond assumption. Properties of ultra-high molecular weight polyethylene (PE) fibers are most suitable fibers in terms of fiber and interface properties for strain-hardening cementitious composites production, however due to the high cost of this material as a result of the search for a more attainable fiber, polyvinyl alcohol (PVA) fibers are started to be used successively instead by tailoring the interface properties by using oiling agents. On the other hand, low cost fibers like Nylon, low density PE, and polypropylene (PP) fibers were found to be unsuitable due to their low tensile strength and low modulus of elasticity (Li et al. 2002).

The difference between J_b' and J_{tip} and also the difference between σ_0 and σ_{ss} should be as high as possible to attain multiple cracking because of the random nature of flaw size and fiber distribution in cementitious composites. Pseudo strain-hardening performance index is used for this purpose for strength and energy criteria (Yang and Li, 2010).

$$PSH\ energy = \frac{J_b'}{J_{tip}} \tag{2.6}$$

$$PSH\ strength = \frac{\sigma_0}{\sigma_{ss}} \tag{2.7}$$

Li (1993) proposed a formulation for critical fiber volumetric content that designates the minimum volumetric fraction of fibers for achieving strain-hardening behavior as

$$V_f^{crit} \equiv \frac{12 J_{tip}}{g\tau(L_f/d_f)\delta_0} \tag{2.8}$$

where

$$g = 2(1 + e^{\frac{f\pi}{2}})/(4 + f^2) \tag{2.9}$$

By interference from the above equation, if J_{tip} is small, the amount of fiber required for strain-hardening will be less. It also means that decreasing matrix toughness by decreasing w/c or altering aggregate volume, size and type and microfillers strain-hardening potential can be increased. On the other hand, too low of a matrix toughness leads to low first cracking strength which is not desirable under normal service conditions. Interface bond properties can also be modified for strain-hardening behavior. Increasing the frictional bond provided that the fibers are not broken will be beneficial. Multiple crack density which is the source of pseudo strain-hardening increases with the frictional bond strength. Longer fibers are preferable for strain-hardening; however poor workability limits the fiber length and also rupture and poor post peak behavior is more likely to occur in long fibers (Li, 1998). Effect of chemical bond and frictional bond on critical fiber content was also presented in Figure 2.7. It is obvious that the critical fiber content rises with the increase in chemical bond since the probability of fiber rupture increases due to high chemical bond. On the other hand there is an optimum range for frictional bond which minimizes the critical fiber content by adequate fiber bridging and energy absorption and limiting fiber rupture (Li et al. 2000).

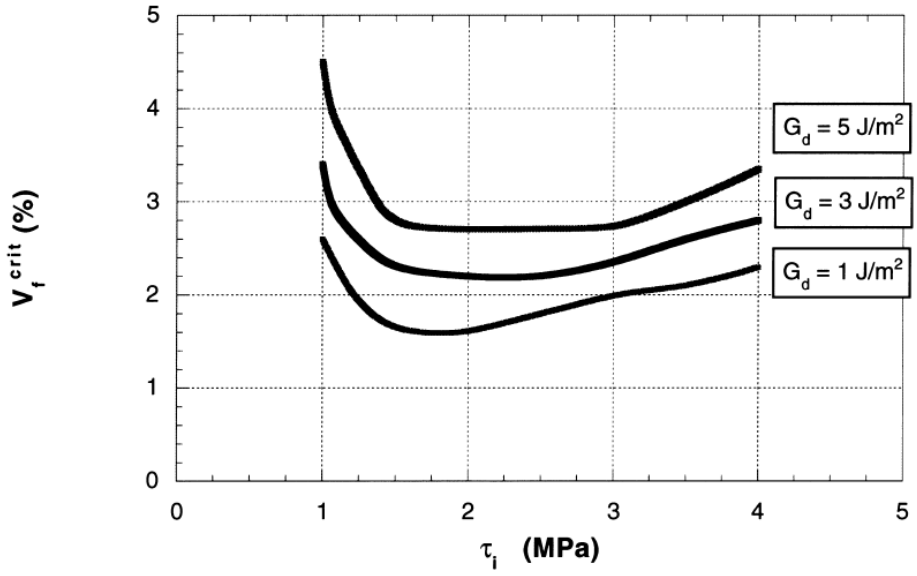

Figure 2.7 Effect of chemical bond and frictional bond on critical fiber content (Li et al. 2000)

2.1.5 ECC Applications Concerning Dimensional Compatibility

Potential applications of ECC generally focus on layered systems or repairs which require the use of ECC together with another material. Lepech and Li (2009) demonstrated the use of self-consolidating ECC in a bridge deck link slab which is replaced with mechanical expansion joints between neighboring simple span bridge decks to suppress the stresses that arise from differential thermal deformations. Main purpose of this replacement was to improve constructability, durability and sustainability since the mechanical expansion joints are prone to durability problems and they are the source of deterioration of the whole structure. Detailed studies on the use of ECC in bridges were presented in the reports prepared by Li et al. (2003) and Li et al. (2005). Likewise, Li and Lepech (2004) used ECC as a patch material for concrete bridge deck repair, and ECC repair performed much

better than commercial patching material in terms of visually observed crack widths 2 days, 4 months and 10 months after casting.

Performance of ECC link slabs was also investigated under monotonic and cyclic loadings and compared with concrete link slabs and usability of ECC for construction of link slabs was shown (Kim et al., 2004-a).

Furthermore, life cycle assessment of ECC bridge deck link slabs was studied by Keoleian et al. (2005) considering the material production, distribution, construction, maintenance, traffic congestion due to construction and end of life management. It was found out that by the use of ECC link slabs, the life cycle energy consumption was 40% less, solid wastes was production was 50% less and consumption of raw materials were 38% less.

One example of using ECC together with steel is stud connections which are used in steel/concrete composite structures to provide steel and concrete to work together. ECC was found to increase the ductility, strength and slip capacity when used in stud connections instead of concrete and improved the performance better than the alternative materials studied (Qian and Li, 2006).

Kim et al. (2004-b) designed an ECC mixture to be used as a repair material that is suitable for wet mix shotcreting, with considering both micromechanical and rheological processes. In that study, it was reported that shotcrete ECC performed better the compared commercial prepackaged mortar repairs.

Lim and Li (1997) studied the effect of using ECC as repair material on an older substrate concrete containing a joint in laboratory conditions. To investigate the trapping mechanism of ECC, an initial notch was provided to initiate cracks during loading and mechanical performance of bi-material system was found to be improved.

Cracking and delamination of layered repair systems due to shrinkage effects with different surface preparations were investigated by Li and Li (2006). They found that ECC can be solution for shrinkage induced failures and the amount of shrinkage is less important, if the required material ductility is satisfied. Surface preparation for improving the interface bond was also effective on interface delamination and surface cracking. Li and Li (2007) also studied the use of high early strength ECC in a layered repair and evaluated the performance of repair under mechanical loading against spalling and interfacial delamination of layers. Furthermore delamination of layers due to shrinkage was also investigated in the same study. High early strength ECC was found to accommodate the surface cracking, spalling and delamination due to both mechanical and environmental effects. In another study by Li and Li (2009), a cracking behavior of ECC/concrete layered repair system was also predicted by a FEM model. Experimental behavior was also confirmed by FEM model and repair material ductility, rather than compressive strength, was reported to be more effective for the durability of repaired system. Cracking potential of ECC was also tried to be predicted in the abovementioned studies by the use of experimental results and estimations.

Li and Li (2011) determined the mechanical properties of high-early strength ECC along with free and restrained shrinkage properties in their study and compared the use of high-early strength ECC as a repair material with high-early strength concrete.

Zhang et al. (2002) proposed a ductile strip made up of ECC for structural members like concrete slabs, bridge decks and pavements in order to localize cracks inside the ductile ECC strip instead of concrete. It was shown that the tensile strain capacity of the system composed of concrete and ECC ductile strip was enhanced.

Performance of ECC as a shear bearing beam element was demonstrated by Kanda et al. (1998), and ECC beam performed well under shear forces. Use of ECC in

retrofit of reinforced concrete structures was also studied in the same study. Precast ECC panels were developed to be placed inside the beam column frames in existing reinforce concrete structures as shear walls to increase the seismic resistance of the structures. ECC panels were assembled by using high tension bolts and steel connecting plates which require ECC panels to bear the concentrated compressive stresses under the bolts. For this reason, in order to evaluate the compressive bearing capacity of the ECC panels, indentation tests were also conducted. Kabele et al. (1997) by numerically simulating the behavior of ECC panels concluded that ECC may successively be used in retrofitting to improve the performance of the frame under shear.

Those applications can be summarized as bridge deck link slabs, patch repairs, layered repair systems or overlays, stud connections, shotcrete repair systems, high early strength repairs and ductile strips. For all of these applications, ECC is required to be used adjacent to another material like concrete or steel. This aspect brings about early restrained cracking problems. To achieve the desired durability of a repair material or a material used in bi-material systems, the most important factor may be the compatibility of repair material with the substrate, repaired material or materials which is in contact with it.

2.2 Dimensional Compatibility

Factors affecting the performance of cementitious materials to be used for repair purposes were investigated by several researchers (Rizzo and Sobelman, 1989; Emberson and Mays, 1990; Emmons et al., 1993; Mangat and Limbachiya, 1995; Morgan, 1996; Decter and Keeley, 1997; Poston et al., 2001; Emmons et al., 2000; Emmons and Vaysburd, 1995).

Rizzo and Sobelman (1989) summarized the basic requirements of a repair material. First one of these requirements is that the repair material should stop the deterioration of structure; especially the corrosion of reinforcement bars. Secondly,

structural integrity should be provided, meaning that the strength properties of the repair material should be similar to that of substrate. And finally, repair material should provide an aesthetically acceptable finish. For evaluation of repair materials, it was suggested that ability of repair material to bond to substrate, relative movement of material with respect to substrate depending on shrinkage, thermal movement and behavior on wetting and drying, permeability, chemical passivation of reinforcing bars, strength, ease of application, and durability characteristics must be considered.

Emberson and Mays (1990) also listed strength, modulus, Poisson's ration, coefficient of thermal expansion, tensile adhesion, short and long term shrinkage and creep properties of different types of repair material to be investigated with the structural incompatibilities with concrete.

Emmons et al. (1993), define compatibility as "a balance of physical, chemical, and electrochemical properties and dimensions between a repair material and existing substrate that will ensure that the repair withstand all stresses induced by volume changes and chemical and electrochemical effects without distress and delamination over a designed period of time." Compatibility of repair material with substrate can be divided into sub groups of chemical, permeability, electrochemical and dimensional compatibility. Dimensional compatibility is affected by material properties governing the deformability characteristics, namely; shrinkage, creep, deformations due to thermal changes and instantaneous elastic deformations. As thermal expansion coefficient and modulus of elasticity are more or less known properties and easier to be obtained, time dependent properties, shrinkage and creep, are more critical in terms of dimensional compatibility (Emmons and Vaysburd, 1995).

Mangat and Limbachiya (1995) compared the properties of various repair materials in terms of water permeability, strength, stiffness, compressive creep and shrinkage under different curing conditions. It was stated that the long term interface cracking

and load sharing capacity of repair patch is mainly dependent on the shrinkage and creep properties although design is based on early age properties like strength, bond and plastic shrinkage or expansion which can only indicate the immediate performance of repair. High strength and high modulus of elasticity increases the load sharing capacity, however at the same time it increases the possibility of cracking and failure. Likewise, high shrinkage experiencing materials are more prone to shrinkage cracking but high creep characteristics lower the probability of cracking.

Decter and Keeley (1997) indicated that performance of a repair material depends not only on the compressive strength and low permeability but also on the compatibility between the repaired concrete and repair material and the level of shrinkage. Thus, considering that the quality of repaired concrete is low; instead of using repair mortars with a high strength and modulus of elasticity they proposed to use repair mortars with low strength and modulus of elasticity in order to provide the compatibility between the materials.

Morgan (1996) dealt with compatibility issues of repair materials and presented several case histories. Dimensional compatibility was also defined in the study as the ability of a repair material to withstand volume changes without any loss in bond and delamination. Dimensional compatibility includes the ability of repair material to carry the subjected load without distress.

Emmons et al. (2000) studied the parameters affecting the durability and serviceability of concrete repairs to establish guidelines for repair material selection with respect to dimensional compatibility. They have suggested preliminary performance criteria in terms of tensile strength at 7 and 28 days, modulus of elasticity, drying shrinkage at 28 days, coefficient of thermal expansion and cracking at 28 days according to Coutinho ring, German angle and SPS plate tests.

Poston et al. (2001) conducted a series of experiments to reveal the factors influencing the dimensional compatibility of repair materials. Conducted experiments were restrained and free shrinkage tests, modulus of elasticity, tensile and compressive creep, coefficient of thermal expansion, flexural, compressive and direct tensile strength tests. It was concluded that to prevent restrained shrinkage cracking, material should exhibit relatively low drying shrinkage. Tentative requirements proposed in the study are as follows: Compressive strength of repair material should not be less than 17.2 and 27.6 MPa for 3 and 28 days respectively; tensile strength should not be less than 8% of the compressive strength, 28 days drying shrinkage should be less than 400 millionths and long term shrinkage should not be more than 2 times 28 day drying shrinkage value, the tip curling should be less than 0.25 mm at 28 days of SPS plate test and no cracking after 28 days of ring test indicates high restrained resistance to restrained cracking.

In light of the abovementioned studies, it can be concluded that dimensional compatibility can be counted as the most important property of a repair material and different material properties were suggested to affect the compatibility of repair material by different researchers. However there is no consensus on which properties of materials affect the dimensional compatibility and how they relate each other. Moreover, there are no commonly accepted performance criteria for repair material selection. What is certain is that, if there is a mismatch between the properties of repair material and substrate material, together with differentiating conditions (temperature, hydration, environmental, loading) and restraining effect of substrate material internal stresses are formed. These stresses result in the formation of tension cracks which further may accelerate failure of repair material.

Li (2004) formulized the criteria for cracking potential of a strain-hardening material under restrained shrinkage conditions. Considering a slab composed of a quasi-brittle material with a strain-softening behavior with length of L and with rigid end constraints, when tensile stress exceeds the tensile strength of material a single crack forms. Hence:

$$E(\varepsilon_{sh} - \varepsilon_{cp}) \geq \sigma_t \tag{2.10}$$

Here, ε_{sh} is the shrinkage strain, $\varepsilon_{cp}$is the tensile creep strain, E is the modulus of elasticity and σ_t is the tensile strength of the material. Noting that $\varepsilon_e = \sigma_t/E$, above formulation can be arranged as:

$$\varepsilon_{sh} \geq \varepsilon_e + \varepsilon_{cp} \tag{2.11}$$

where ε_e is the elastic strain capacity of the quasi brittle material. This equation also satisfies the commonly accepted fact that low shrinkage and low elastic modulus, high elastic and creep strains under tension is in favor of dimensional compatibility. Cracking potential (p) under restrained conditions is defined as excess of shrinkage strains over elastic and creep strains:

$$p = \varepsilon_{sh} - (\varepsilon_e + \varepsilon_{cp}) \tag{2.12}$$

For ductile materials like ECC cracking occurs under condition of:

$$\varepsilon_{sh} \geq \varepsilon_e + \varepsilon_i + \varepsilon_{cp} \tag{2.13}$$

where ε_i is the inelastic tensile strain capacity. Hence cracking potential of ECC can be re-written as:

$$p = \varepsilon_{sh} - (\varepsilon_e + \varepsilon_i + \varepsilon_{cp}) \tag{2.14}$$

Where all values are in percent. It was estimated that the cracking potential is a very small even a negative value for ECC. For instance by assuming ε_{sh} between 0.1 and 0.15, ε_e as 0.015, ε_{cp} of about 0.07 (compressive and tensile creep assumed to be equal) and ε_i between 2 and 5, corresponding value of cracking potential was calculated to be between -4.99 and -1.94 percent. However, inelastic strain-

hardening behavior of ECC is attributed to multiple cracking; hence the main discussion is how large the crack width is (Li, 2004; Li and Stang, 2004).

Cracking potential is a superposition of time dependent strains within the cementitious material. Resultant tensile stress development due to restraining effect is responsible for crack formation which also depends on material properties such as elastic modulus. Cracking potential can be seen as a value which includes the 'drivers' and 'resistors' of cracking. Drivers of cracking potential include shrinkage (autogenous, plastic, drying and carbonation shrinkage, thermal), modulus of elasticity and the resistors are elastic and inelastic strain capacity and creep of the material. Cracking due to the lack of the dimensional compatibility of the material with substrate can be prevented or reduced by altering material parameters that affect cracking potential (Morgan, 1996; Li and Stang, 2004; Li and Li, 2009).

2.3 Factors Affecting Dimensional Compatibility

2.3.1 Shrinkage

Shrinkage is the name given to the process initiated with the loss of water due to evaporation or hydration of cement, and also by carbonation (Neville and Brooks, 1987). The loss of water inside the cementitious material yields volume changes either by moisture movement or by sequential physical or chemical process (Brooks, 2003).

Shrinkage can be considered in two stages as early age and long term (or later ages shrinkage). The first day after casting of concrete while the concrete is in plastic state is generally defined as early age. After the first 24 hours of casting the second stage, long terms or later age, starts. Shrinkage measurements are usually performed after the first day during this later age. Long term shrinkage is the only stage that is generally considered in the literature and also in structural design (Holt, 2001).

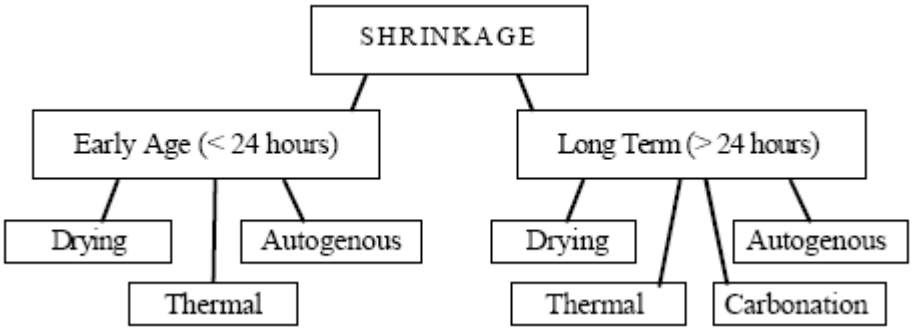

Figure 2.8 Main types of shrinkage in concrete (Holt, 2001)

Plastic (early age) shrinkage is related to the volume changes of concrete during the first hours within the early age reactions, while fresh concrete is still in a liquid form and its skeleton is in formation stage (Holt, 2001). Moisture loss from fresh concrete, unless obviated, can result in cracking. Generally, water is lost by evaporation from the surface of freshly placed concrete which yields surface cracks. Moreover, water can be absorbed by formwork or sub-base material which can also yield surface cracking or potentiate the effect of evaporation. The spaces between the particles of fresh concrete are initially filled with water. Paste volume contracts when the water in the spaces between the fresh concrete particles is removed as a result of negative capillary pressure due to exterior influences like evaporation. Capillary pressure rises till it reaches breakthrough pressure at which the water in the pores is not evenly distributed any more. Most of the plastic shrinkage occurs just before the paste reaches the breakthrough pressure (Mindess et al., 2003). The only reason for plastic shrinkage is not the loss of water by evaporation, since it can be observed in the lack of evaporation. The shrinkage in the absence of evaporation is caused by the settlement due to gravitational and capillary forces. However, the first reason is dominant over the second one (Emmons and Vaysburd, 1995).

In theory, plastic shrinkage is beneficial because it results in a compacted paste volume; however the problem is that the influence of plastic shrinkage is not evenly distributed over the volume since it is more effective near to the surface and the differentiations in the volume change cause cracks as a result of induced tensile stresses (Mindess et al., 2003).

Temperature, relative humidity and wind velocity are the factors affecting the amount of water lost from the concrete surface, hence, the degree of plastic shrinkage. In addition, mixes possessing low w/c and high amount of cement exhibits higher amount of plastic shrinkage. On the contrary, if the bleeding rate is high, surface of the concrete dries slower that reduce cracking due to plastic shrinkage (Neville, 2003).

Drying shrinkage is the type of shrinkage which can be defined as the volumetric change as a result drying of the concrete (Mokarem, 2005). Drying shrinkage is a consequence of storing concrete in unsaturated air which causes withdrawal of water from concrete. The volume of lost water is not equal to the change in volume of concrete subjected to drying. At first, free water is lost which results in no or relatively low shrinkage. Later, as concrete continues to dry, adsorbed water is removed. In this stage, the change in the volume of cement paste is nearly equal to the water layer lost from the surface of all gel particles. It was also suggested that shrinkage may be related to the loss of intracrystalline water (Neville, 2003).

The term of drying shrinkage is generally attributed to hardened concrete and defines the strain resulted by the removal of water from the hardened material. Autogenous shrinkage due to self-dessication and carbonation shrinkage is generally considered as special cases of drying shrinkage (Mindess et al., 2003).

In spite of the commonly accepted fact that 80% of drying shrinkage measured under laboratory conditions occurs within 3 months, drying shrinkage can continue for many years. Since the rate of the water lost during drying is dependent on the

size and shape of concrete, they also control the duration of shrinkage. Shape and size of concrete is generally considered together in terms of volume to surface area ratio. Specimens having larger surface area experience shrinkage longer, but the total amount of shrinkage may be lower (Holt, 2001). This may be due to average length of the diffusion path and there is an inverse relation between the rate of early shrinkage and ultimate amount of shrinkage (Mindess et al., 2003).

As a result of restraining effect of aggregates, drying shrinkage of concrete will be less than cement paste. Also, most aggregates are dimensionally stable under differentiating moisture conditions. Aggregate amount, stiffness and maximum size are the parameters that affect the degree of restraining. Increase in maximum aggregate size results in an increase in stresses at cement paste- aggregate interface which further results in an increment in the cracking of the interface (Mindess et al., 2003).

In case of continuous supply of water to hydrating concrete after setting may cause expansion, also called swelling, as a result of adsorption of water by cement gel due to the water molecules acting against the cohesive forces and forcing gel particles to move away from each other and generating a swelling pressure. However if the concrete is isolated from moisture movements, shrinkage occurs. Autogenous and chemical shrinkage can be dealt together and can be explained as the consequence of withdrawal of water from the capillary pores as a result of hydration of the unhydrated cement, known as self-desiccation. Autogenous shrinkage is hindered by the rigid skeleton of hydrated cement particles and aggregates (Neville, 2003).

Chemical shrinkage is regarded as the reduction in the total absolute volume of solids and liquids in cement paste due to hydration reactions since the absolute volume of hydration products are less than hydration reactants. Chemical shrinkage is considered as microscopic volume change while autogenous shrinkage is considered as shrinkage of hydrating system caused by chemical shrinkage. The

main difference between autogenous shrinkage and chemical shrinkage is that the chemical shrinkage is the driving force behind the autogenous shrinkage and it does not comprise the hydration voids. Chemical shrinkage continues as long as hydration reactions continue, however after initial set paste does not deform as it was in plastic stage, as a result, formation of voids compensates chemical shrinkage (Kosmatka et al., 2003).

Autogenous shrinkage may not be a result of chemical shrinkage after concerete hardens. At later ages autogeous shrinkage can also be a result of self dessication since a rigid skeleton is already formed which resists cehemical shrinkage. Self dessication is drying due to the decrease in the local humidity since the water is consumed in hydration reactions. Self dessication does not start immadiately after casting like chemical shrinkage but occurs longer than chemical shrinkage (Holt, 2001).

Autogenous shrinkage is most significant in high-strength, or high performance concrete with a water to cement ratio less than 0.42 since it increases with a decrease in water to cement ratio and with an increase in the amount of cement paste. It may reach to the half of the drying shrinkage for concretes with water to cement ratio of 0.3 (Kosmatka et al., 2003).

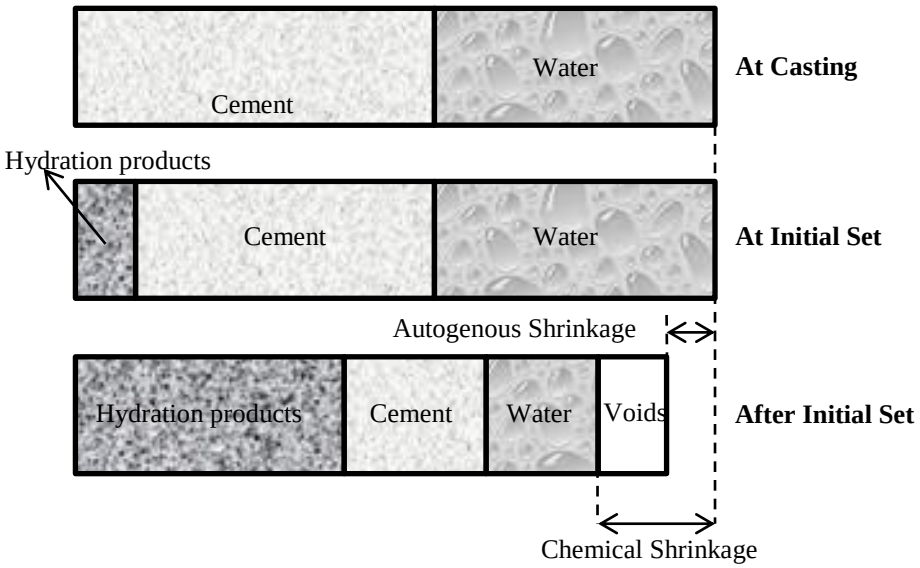

Figure 2.9 Schematic representation of the chemical and autogenous shrinkage (Holt, 2001)

The factors affecting the degree of autogenous shrinkage are not well defined. Properties related to components such as water to cement ratio, cementitious material type and amount and paste volume have the most marked effect on autogenous shrinkage. Autogenous shrinkage cannot be hindered by casting, placing or curing practices, but must be taken into account during concrete mix proportioning (Holt, 2001).

Thermal shrinkage refers to change in the volume of the concrete caused by the fluctuation in temperature. General solids experience expansion when heated and contraction when cooled. The change in volume of a material is dependent to the thermal expansion coefficient of the material along with the degree of temperature fluctuation. Ordinary concrete structures are not influenced by temperature changes unless they are subjected to extreme climatic conditions. On the other hand, heat liberation due to hydration together with the poor heat dissipation develops a large

rise in the temperature of concrete in massive structures in a few days after the concreting process. Following the immediate rise in temperature, cooling of concrete to ambient temperatures results in shrinkage. Since the structural integrity of the mass concrete structures is the main concern, material selection, mixture proportioning, curing and concreting practices should be carefully elaborated to control the temperature rise. In low tensile strength materials like concrete, thermal shrinkage becomes more important since the tensile stresses resulted may be high enough to cause cracking, depending on modulus of elasticity, degree of restraint and stress relaxation due to creep strains (Mehta and Monteiro, 2006).

Carbonation shrinkage is a result of chemical reactions between hydration products and atmospheric carbon dioxide. Reason of carbonation shrinkage may be the dissolving $Ca(OH)_2$ crystals which are under compressive stress imposed by drying shrinkage and the deposition of $CaCO_3$ in spaces without stress afterwards. Hydration products near a pore continuously dissolve to provide Ca^{++} ions to the liquid phase which in turn migrates to $CaCO_3$ nucleation site resulting a crystal growth. As carbonation shrinkage simultaneously occur with drying shrinkage, they cannot be separated and both are denoted as drying shrinkage. Mass of the specimen increases during the carbonation of hydration products. Water is produced as a result of carbonation reactions. It is the drying shrinkage which results in a mass loss due to carbonation (Goodwin, 2006).

In cases where the fly ash addition increases the paste volume, provided that the water content is fixed, drying shrinkage may be slightly increased. If the water content is reduced it may result about the same amount of shrinkage with concrete that does not contain fly ash. Up to 20% fly ash content is reported not to affect the amount of shrinkage. In some studies it was also reported that the increased fly ash content may result in a slightly less shrinkage (ACI Committee 232, 2003).

Mehta and Monteiro claim that the plastic shrinkage of the high volume fly ash concrete is higher if it is not protected; on the other hand it has lower thermal and drying shrinkage (Mehta and Monteiro, 2006).

In most cases shrinkage seems to be lower for concrete containing fly ash with respect to concrete without fly ash. However there are some cases where the shrinkage is equal to or higher than the shrinkage of concrete without fly ash. There is a very limited study about the effect of fly ash on autogenous shrinkage of mortar and concrete. Autogenous shrinkage of mortars and concretes containing fly ash are expected to be lower (Jawed et al., 2005).

Published data on the effect of slag cement on creep and shrinkage indicates conflicting results. It was generally suggested that the drying shrinkages of slag cement concrete and portland cement concrete is similar (ACI Committee 233, 2003).

Bucher (2009) denotes that fly ash containing cemetitious systems experience lower autogenous and drying shrinkage. Mortars containing Class F fly ash were resulted similar autogenous shrinkage with mortars of same water to cement ratio. However Class C fly ash showed higher autogenous shrinkage with respect to control mortar.

Wei (2008) indicates that autogenous shrinkage of pasted containing ground granulated blast furnace slag (BBGFS) experience higher autogenous shrinkage than neat pastes.

2.3.1.1 Methods of Determining the Shrinkage

Plastic shrinkage of restrained fiber-reinforced concrete can be evaluated according to ASTM C 1579 (ASTM, 2006-a). In this method plastic shrinkage cracking behavior of fiber-reinforced concrete under the effect of evaporation, settlement

and early age autogenous shrinkage is observed. In order to maintain environmental conditions an environmental chamber as seen in Figure 2.10, is used. Optical microscopy or automated image analysis techniques can be used for quantifying cracks at the end of 24 hours after mixing. This method can be useful for comparing the plastic shrinkage behavior of fibrous materials. However test setup requires the use of stress risers to force material for cracking, thus it is not possible to evaluate free plastic shrinkage.

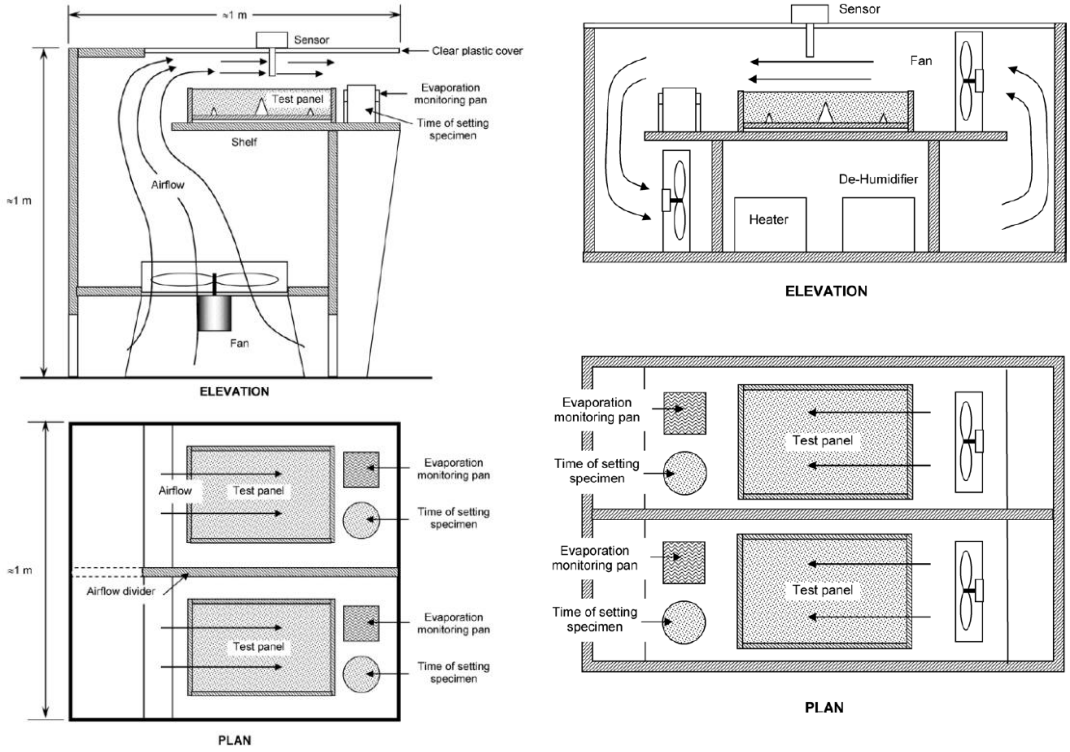

Figure 2.10 Examples of environmental chambers according to ASTM C 1579 (ASTM, 2006-a)

ASTM C 827 (ASTM, 1995) can be used to give an idea about the early age shrinkage properties of cementitious materials. In this method the change in the height of the specimens placed in cylindrical molds (100, 150 or 300 mm in height

according to the maximum aggregate size) are measured by the help of a magnifying lens and projection system as seen in Figure 2.11. An indicator ball is placed on the specimen and projection of the ball on the indicating chart is used for measurement. Even though the method is intended for measuring volume changes in plastic phase, it has an advantage that it can also be used for hardened phases. However, Emmons and Vaysburd (1995) suppose that this method has disadvantages like unrealistic curing conditions, deficiency in precision of zero reading and variation in the test results.

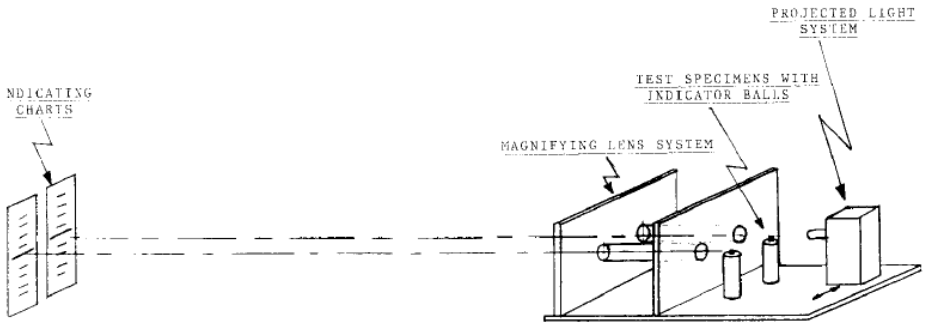

Figure 2.11 ASTM C 827 test setup (ASTM, 1995)

Another early age shrinkage testing method, named slab method, was developed by Technical Research Center of Finland. In this method both vertical and horizontal length changes are measured. Setting time, evaporation, temperature and internal capillary pressure measurements are also simultaneously taken. Generally early age shrinkage within 24 hours is measured by using the apparatus; however test duration can be extended. For measuring autogenous shrinkage the mold can be covered with a stiff plastic hood or a thin sheet plastic. Generally two molds of specimens are used for evaluating drying and autogenous shrinkage at the same time (Holt, 2001).

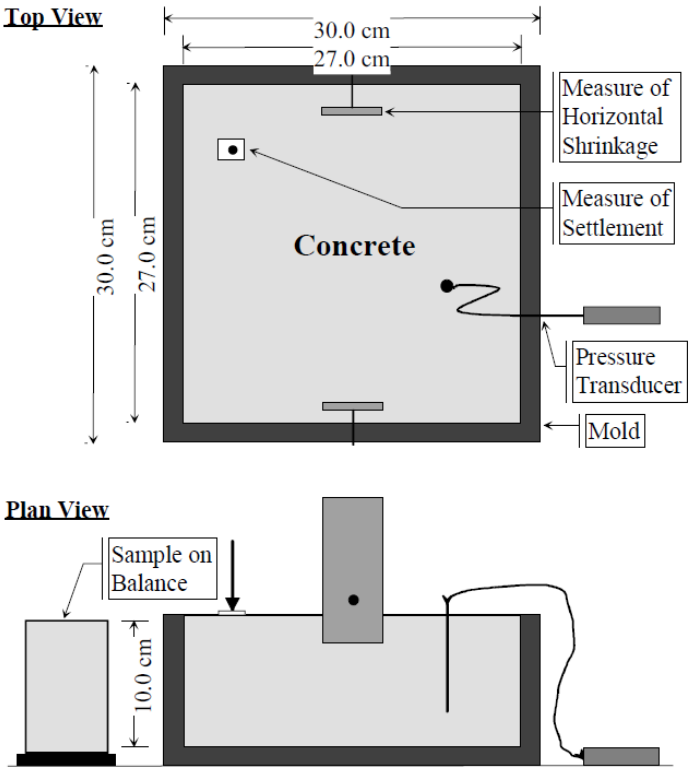

Figure 2.12 Schematic representation of slab test (Holt, 2001)

Plastic shrinkage strains can also be measured by the use of linear prismatic molds, also called shrinkage drain, in which the surface in touch with the specimen are covered with Neoprene sheets or Teflon spray which is applied to avoid friction. The mold allows measurements of shrinkage strains of the specimens by the use of a linear variable differential transformer (LVDT) attached on one end which is free to move while the other end of the mold is fixed. Desired environmental conditions can be generated during measurements. The length of the mold should be long enough to obtain accurate readings. Wongtanakitcharoen and Naaman (2007), in their research, used a similar setup to measure the early age shrinkage of fiber-reinforced concrete. A similar setup was used by Wei et al. (2011) for

autogenous shrinkage measurements. If additionally, the setup is arranged to measure the change in the height of the specimens, it is called “Bending Drain”.

Figure 2.13 Free shrinkage specimens (Wongtanakitcharoen and Naaman, 2007)

There is no standard method for measuring the drying shrinkage of concrete; Generally, concrete or mortar prism specimens are subjected to drying under controlled environmental conditions and the change in the length of the specimens are monitored by using strain gages which are attached on the surface of the specimens or by recording length of the specimens at the axis by using length comparators (Lawrence, 2004). ASTM C157(ASTM, 2006-b) which is a general purpose method for determining the length changes caused by other than applied forces and temperature changes is used for drying shrinkage. ASTM C 157 (ASTM, 2006-b) defines different specimen dimensions for mortar and concrete. 25 x 25 x 285 mm specimens are used for mortars, 100 x 100 x 285 mm are used for concretes having maximum aggregate size of 50 mm and 75 x 75 x 285 mm specimens are used for concretes having maximum aggregate size of 25 mm. After the specimens are demoulded, they are placed in water for 15 or 30 minutes in order to avoid length changes due to temperature variation; the first comparator reading is taken afterwards. For 28 days, specimens are cured under water and after

curing period, subsequent readings are taken at 4, 7, 14, 28 days and 8, 16, 32 and 64 weeks on specimen subjected to drying. This method is particularly useful for comparison of different mixtures of cement based materials. In addition the drying shrinkage for the first 28 days cannot be determined by using this method.

For drying shrinkage measurements of up to 28 days, duration of the methods used for plastic shrinkage measurements can be extended.

Determination of the chemical shrinkage of hydraulic cement paste is standardized in ASTM C 1608 (ASTM, 2007). The chemical shrinkage can be determined per unit weight of cement for 24 hours with two different methods. First method is based on level change of water on a capillary tube inserted to a laboratory vial. A paste is prepared and introduced to vial, then water is added to vial to fill the empty spaces, and then a stopper and capillary tube is attached to the vial. The level of the water increases, paraffin oil is placed over water in order to minimize evaporation. Specimens are placed into constant temperature water bath and time and water level in the capillary tube is recorded for 24 hours. A density bottle is used for the second method. Similarly, a paste is introduced to bottle, then a stopper is placed on bottle and the bottle is filled with water, excess water is removed with absorbent paper. For 24 hours, as the level of water decreases, the bottle is filled with water and the mass of the bottle is recorded.

There is no standardized method for autogenous shrinkage. Sealed specimens where the humidity transfer from the atmosphere is prevented can be used for length measurements to determine the autogenous shrinkage. For sealed specimens, it is important to measure the shrinkage on a constant mass specimen (Şahmaran et al., 2009). Autogenous shrinkage of pastes can be measured by using flexible rubber membrane test. In this method specimens are sealed in a latex membrane and the specimen can be submerged into water, as the reactions progress the volume of the specimen and buoyancy decreases, by the use of a balance the change in mass is determined and the change in volume of the specimen is

calculated. If the test is done on mortars, there is a risk of aggregate particles to break the membrane (Holt, 2001). Loukili et al. (2000) measured the early age deformations caused by autogenous shrinkage and thermal expansion or contraction induced by the cement hydration by a similar test setup on mortars. The thermal and auogenous shrinkages were also separated.

2.3.2 Creep

When concrete is loaded under compression or tension, the total deformation resulted can be divided into two separate parts; an immediately occurred deformation (the term "elastic" is not generally favored since the strain may be in the inelastic range, for this reason the term "instantaneous strain" is generally used) and a time dependent deformation which starts immediately and continues with a decreasing rate with time as loading of concrete continues. This time dependent deformation of concrete is called creep (Kosmatka et al., 2003). Creep is in many ways similar to shrinkage since both the drying shrinkage and creep is caused by the removal of adsorbed water from the hydrated cement paste. The reasons of creep however are more complex (Mehta and Monteiro, 2006).

The creep deformation in reinforced concrete is dependent mainly on (Kosmatka et al., 2003):

- The rate of the applied stress
- The strength and the age concrete when the load is applied
- The duration of loading

And other factors related to concrete quality and exposure conditions such as (Kosmatka et al., 2003):

- Type, amount, and maximum size of aggregate
- Type of cementitious materials
- Cement paste amount
- Size and shape of the concrete

- Volume to surface area ratio of the concrete
- Steel reinforcement amount
- Curing conditions before loading
- Temperature and humidity of environment (Kosmatka et al., 2003).

Shrinkage and creep in concrete exhibit a degree of irreversibility as shown in Figure 2.14 and 2.15. After drying, shrinkage strain cannot be fully recovered on rewetting. Therefore, shrinkage is separated into reversible and irreversible shrinkage. Similarly after loading, when the load is removed, an instantaneous recovery is followed by a creep recovery but the total creep stain cannot be recovered. Similar to shrinkage creep is also separated into reversible and irreversible creep (Mehta and Monteiro, 2006). Creep and stress is proportional under normal stress ranges. Creep in younger concretes is largely unrecoverable; on the other hand in older or drier concretes it is largely recoverable (Kosmatka et al., 2003). Creep data can be presented in different ways such that creep strain per unit stress is specific creep and creep strain per elastic strain is creep coefficient (Mehta and Monteiro, 2006). Creep strains are linearly proportional with the applied stresses up to 50% of ultimate strength of concrete. Specific creep was found to increase with an increase in w/c. Aggregates also act as restraints against deformation as in shrinkage, and decreases the amount of creep. Tensile creep is important in terms of cracking potential estimation. However, it is very difficult to measure tensile creep accurately due to the low tensile strength of concrete; hence it is not possible to compare tensile and compressive creep quantitatively. It is possible that the rate of creep is higher initially in tension, and it is greater in short durations compared to compressive creep, however for longer durations the opposite may be valid for compressive creep. Both compressive and tensile creeps are affected by the same experimental parameters (Mindess et al., 2003).

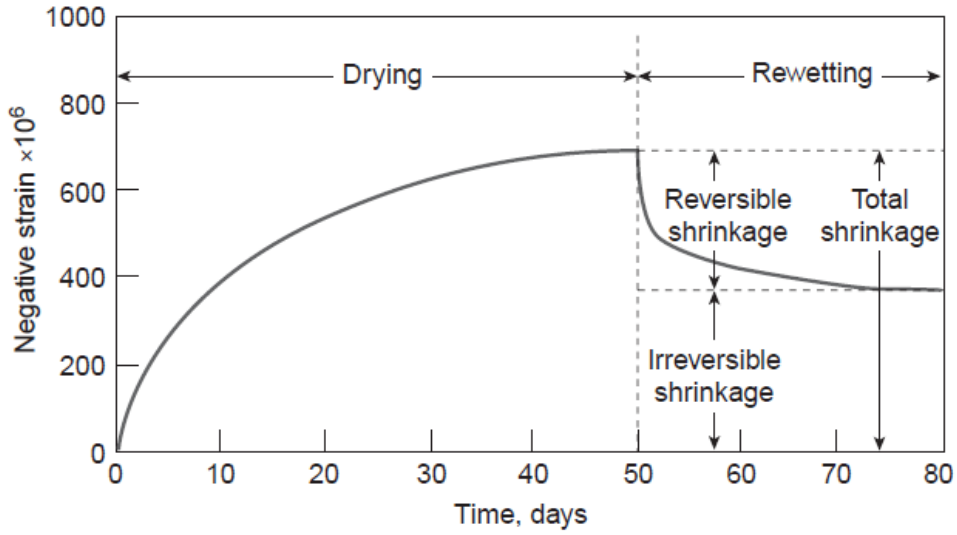

Figure 2.14 Reversibility of shrinkage (Mehta and Monteiro, 2006)

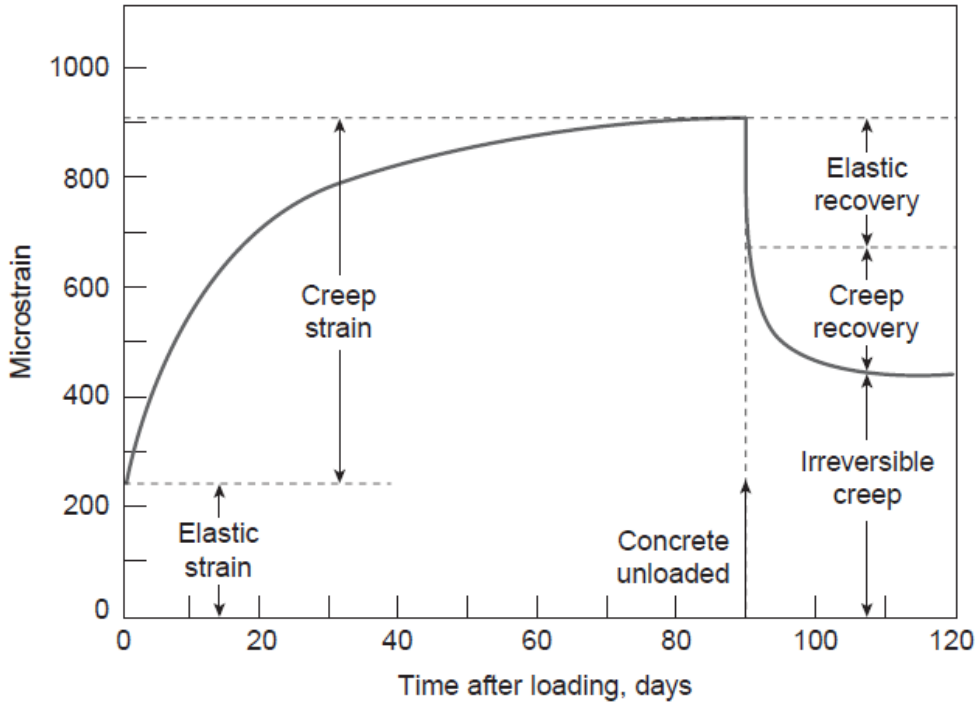

Figure 2.15 Reversibility of creep (Mehta and Monteiro, 2006)

The mechanism of tensile creep was based on microcraking by Ward and Cook (1969). The validity of seepage theory, viscous shear theory and microcracking which are used to describe the mechanism of creep under compression, for describing the mechanism of tensile creep was investigated by Bissonnette et al. (2007). According to the experimental results of that study the following conclusions were drawn:

The seepage theory was found to be convenient to describe tensile creep since some of the free water in the large capillaries is adsorbed by the gel pores as they open up by the effect of tensile load. However tensile creep was found to be higher under drying conditions compared to that of sealed conditions, which cannot be described by seepage theory. Water is moved from the paste as a result of drying which yields contraction, however tensile creep under drying conditions found to increase the expansion due to tensile creep which is the deficiency of seepage theory in describing tensile creep (Bissonnette et al., 2007).

Viscous shear theory was also found to be successful in describing tensile creep. The applied load together with evaporation disturbs the adsorbed water layers and as water is lost, gel particles slide or flow one against the other. If the water movement is prevented, loading causes the disturbance of adsorbed water alone which can also explain that the basic creep is smaller than the drying creep (Bissonnette et al., 2007).

Finally microcracking which was proposed by Ward and Cook (1969) could not be proved to describe the tensile creep as the modulus of elasticity of specimens before and after tensile creep found to be close to each other by Bissonnette et al. (2007) however it was attributed to low tensile stresses applied in their study and further investigation was proposed.

Tensile creep of ECC was studied by Boshoff and Van Zjil (2007), Boshoff et al. (2009-a) and Boshoff et al. (2009-b) by using dumbbell type, flat and thin

specimens. Boshoff and Van Zjil (2007) applied sustained tensile load of up to 50% of the ultimate load and monitored the tensile creep phenomenon for 8 months on unsealed specimens. Drying shrinkages of the specimens were also monitored for the same duration. They have found out that even at a load rate of 50%, time dependent microcraking can be possible. Boshoff et al. (2009-a) conducted tensile creep tests on pre-cracked specimens and also single fiber pull out creep and single fiber creep tests were conducted in order to investigate the effect of fiber on creep behavior. However all the tests were conducted on a single mixture which is different than the mixtures used in this study. Tensile loads were sustained at 30, 50, 70 and 80% of their ultimate tensile strengths and 2 specimens were used for each loading rate. It was concluded that, tensile creep has three sources which are matrix creep, time dependent crack formation and time dependent pull out of the fibers and calculated creep strain due to cracking was found to be 90% of the total strain.

2.3.2.1 Methods of Determining Creep

Creep of concrete under compression, having maximum aggregate size of 50 mm at most, is standardized in ASTM C 512 (ASTM, 1987). Cylindrical specimens with diameters of 150 mm and heights of minimum 292 mm are used in the experiments as can be seen in Figure 2.16. This method allows the determination of creep strains when subjected up to 40% of its compressive stress due to the assumption that the compressive creep is proportional to compressive strength up to this level. Specimens are moist cured at $23\pm1.7^{o}C$ for 7 days. After moist curing, specimens are stored at $23\pm1.1^{o}C$ at a relative humidity of 50±4% until the end of the experiment. Load is sustained by using a loading frame consisting of header plates and a load maintaining element. If basic creep will be determined, then the specimens are sealed to prevent loss by evaporation.

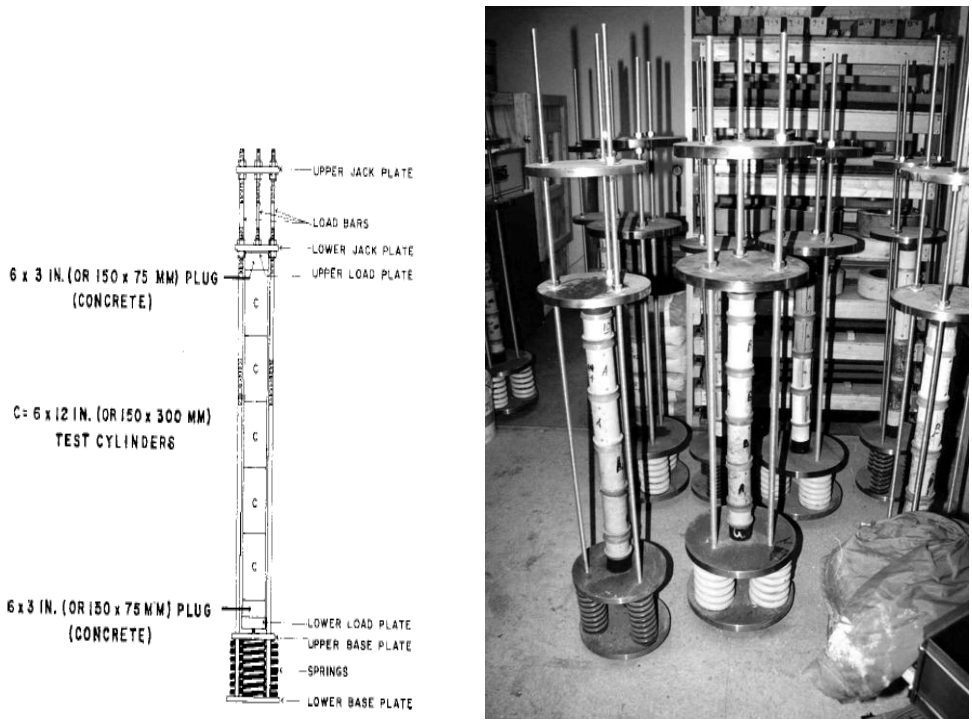

Figure 2.16 ASTM C 512 test setup of creep under compression (ASTM, 1987)

There is no standardized test method for tensile creep determination. However there are several direct tensile creep setups used in literature. Poston et al. (2001) used 76 x 76 x 305 mm specimens and loaded up to 40% of the tensile strength determined at 3, 7 and 28 days by using a tensile creep test frame as seen in Figure 2.17. Initial loading was at 3 days and load is increased at 7 and 28 days and kept constant till the end of the experiment. Mechanical strain gages were used to measure the strains over a gage length of 250 mm. Shrinkage specimens were cast in the same sizes and effect of drying shrinkage is also monitored (Poston et al., 2001).

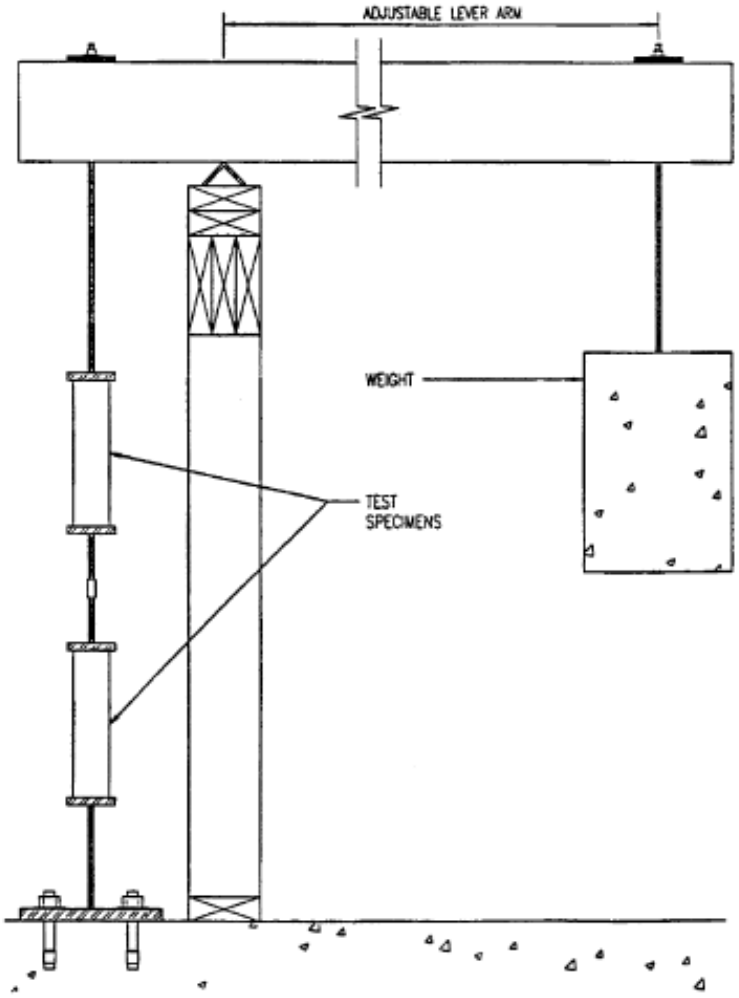

Figure 2.17 Loading frame used for tensile creep measurements (Poston et al., 2001)

Garas et al. (2009) used 100 x 380 mm cylindrical ultra-high performance concrete specimens with a gage length of 250 mm. High strength epoxy was used to fix the specimens to the tensile creep setup. Loading was initiated at the age of 7 days and specimens were loaded 40% and 60% of the tensile strength for duration of 14 days. This setup allows loading at a constant loading rate. Two sets of identical specimens free of load were used for drying shrinkage measurements. The setup which was used in the study can be seen in Figure 2.18.

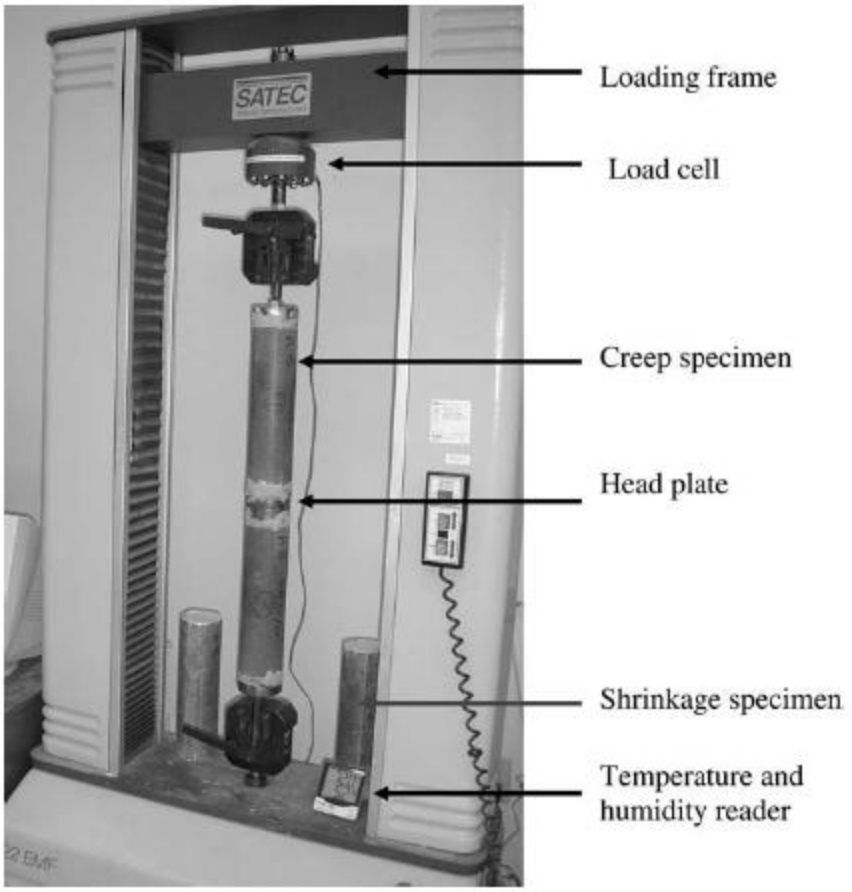

Figure 2.18 Setup for tensile creep test (Garas et al., 2009)

Bissonnette et al. (2007) used 70 x 70 x 400 mm specimens and loaded up to 20% and 40% of the ultimate tensile strength at 7 and 28 days and shrinkage measurement were also taken at the same time. A loading frame as seen in Figure 2.19 with a capacity of three specimens was used. A pneumatic jack and an amplifier were used to generate the load and the load was transmitted to the specimens with hinged steel rods. Extensometers were used for both creep and shrinkage tests. Although tests were continued between 70 to 175 days, most of the time dependent strain were reported to occur in 2 months.

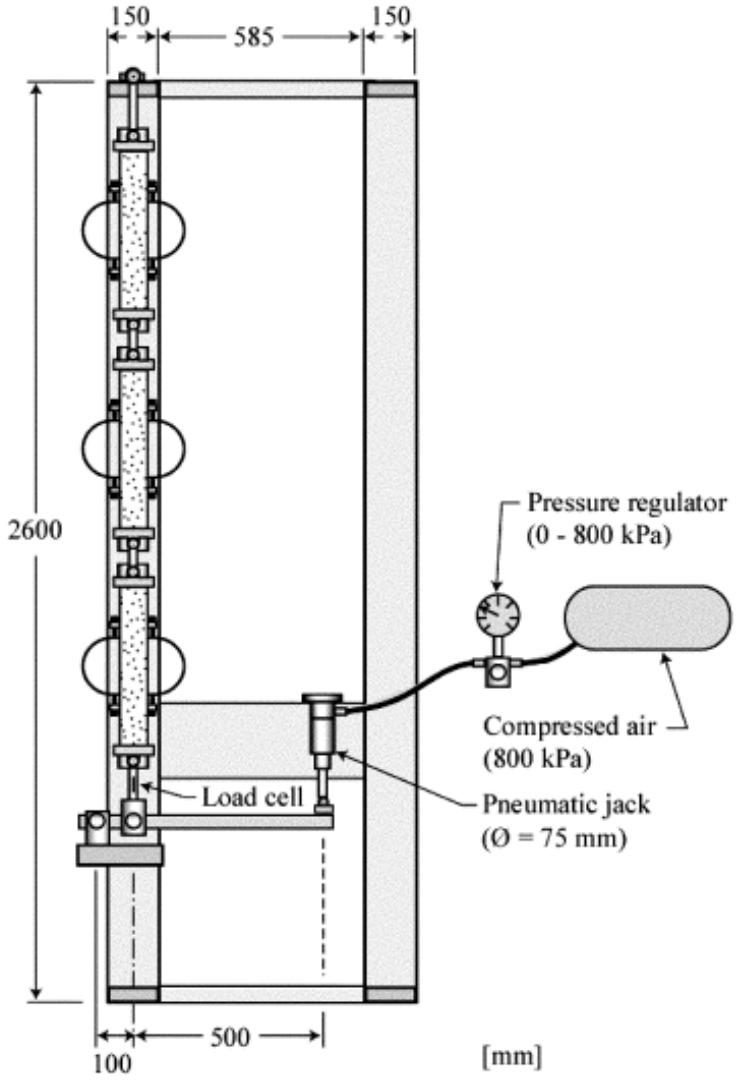

Figure 2.19 Schematic representation of tensile creep apparatus (Bissonnette et al., 2007)

Garas et al. (2012) used 75 x 75 x 483 mm steel fiber-reinforced prism specimens to evaluate the effect of thermal treatment on tensile shrinkage properties. Specimens were loaded 40% of their tensile strengths for duration of 1 year. Setup used in that study is presented in Figure 2.20.

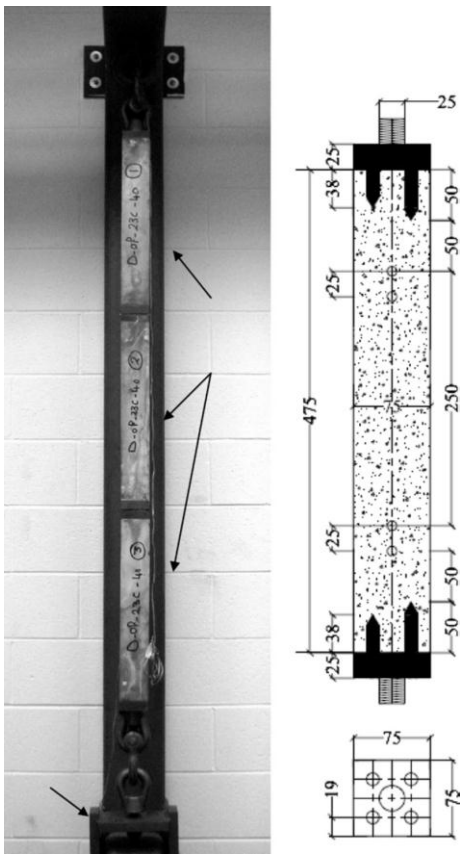

Figure 2.20 Tensile creep test setup and specimen dimensions (Garas et al., 2012)

2.3.3 Restrained Shrinkage

Differential drying of concrete members like partial depth repair, overlay, floor slab or wall, through the thickness yields tensile stresses as a result of internal restraints. Also adjacent structural members can act as an external restraint, again yielding tensile stresses to be built up due to drying. The resulted tensile stresses may be relaxed by the tensile creep and cracking may be prevented or delayed. Time between casting and cracking depends both on the tensile strength and tensile creep characteristics of concrete (See et al., 2003). Determination of cracking behavior from free shrinkage measurements is very questionable because in reality materials are restrained at least by the boundary and/or reinforcement. This is the reason why the restrained shrinkage tests are proposed (Emmons et al., 2000).

2.3.3.1 Methods of Determining the Restrained Shrinkage

For the evaluation of restrained volume change and sensitivity of materials to cracking, restrained shrinkage methods were developed. These methods generally rely on cracking of materials within a given period of time. There are three types of restrained shrinkage tests that are generally used but the most common is the ring test. Several ring tests are defined in the literature, with rings in different dimensions but conducted with a similar procedure. Concrete is poured between two steel cylindrical molds and cured for a day. The outer mold is removed after one day and material is started to be monitored under laboratory conditions for evidence of cracking. Crack widths are measured from three locations along the crack height. The day that the concrete first cracked, average crack with, sum of crack widths are recorded (Emmons et al., 2000). The ring method is standardized in ASTM C 1581 (ASTM, 2009). Schematic description of the mold used in ASTM C 1581(ASTM, 2009) is shown in Figure 2.21. In this standardized method strains of the inner steel ring during drying of the specimen can also be monitored by using strain gages.

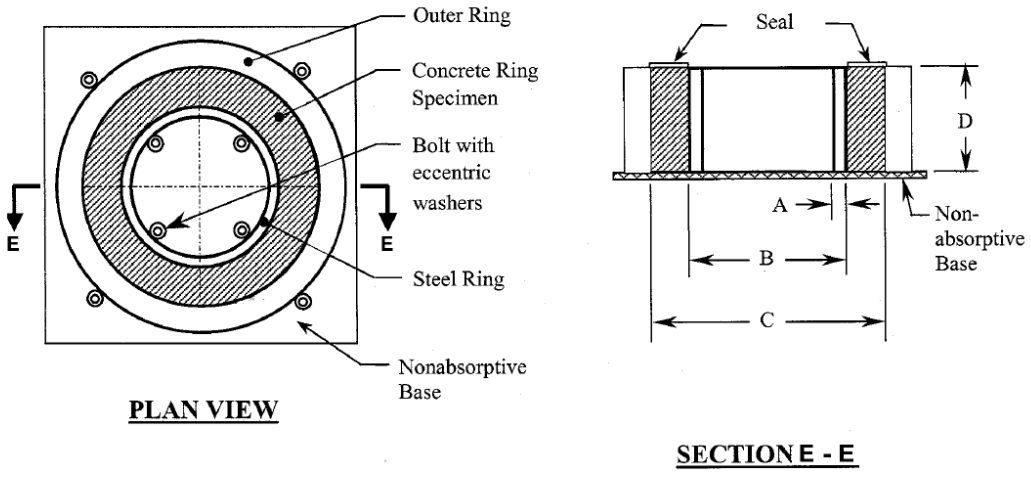

Figure 2.21 Schematic view of restrained shrinkage ring (ASTM, 2009)

In German Angle Test, which is a linear restraint method, concrete or mortar is placed in shrinkage channels and kept uncovered in standard atmospheric conditions and crack formations are monitored continuously. At the end of 90 days, the number of cracks, the average crack width and maximum crack width, along with the time of cracking and large areas where steel mold and specimen detaches are monitored and recorded (Emmons et al., 2000).

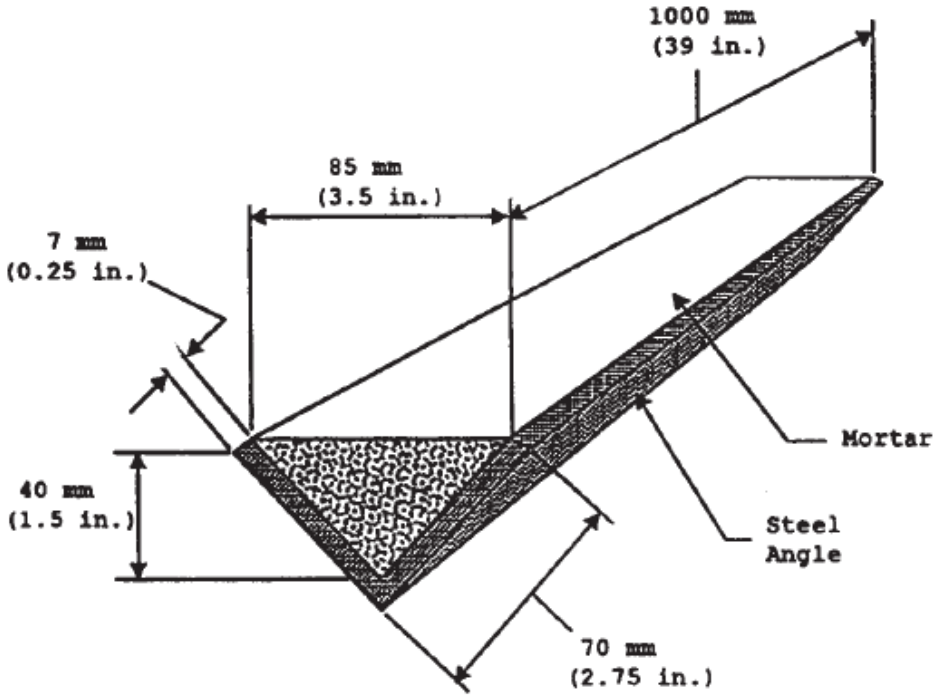

Figure 2.22 German angle test setup (Emmons et al., 2000)

In Structural Preservation Systems (SPS) Plate test, material is cast against a thin steel plate. In order to improve the bond between the plate and the specimen a layer of epoxy and sand grit is used. One end of the specimen is maintained clamped while the other end is left free for measuring the upward deflection of the beam (Poston et al., 2001).

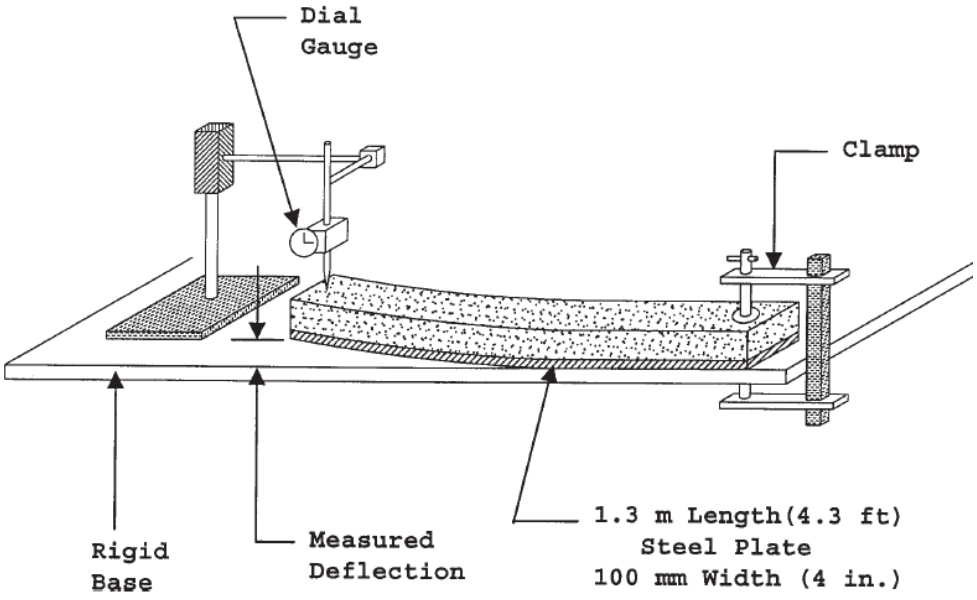

Figure 2.23 SPS plate test setup (Emmons et al., 2000)

CHAPTER 3

EXPERIMENTAL STUDY

3.1 Experimental Program

In order to investigate the dimensional compatibility and mechanical properties of Engineered Cementitious Composites designed with locally available materials, sixteen different mixtures, with varying amounts of cement, fly ash (FA), ground granulated blast furnace slag (GGBFS) and silica sand were prepared. Original ECC mixture that contains fly ash as a pozzolanic material was considered as the control mixture. Half of designed mixtures incorporated GGBFS in order to evaluate its effect on dimensional compatibility and mechanical properties. For all mixtures the volumetric fiber content was fixed at 2%. Mechanical properties determined were; compressive strength, flexural strength, deflection under bending and matrix fracture toughness. For evaluating the dimensional compatibility properties, autogenous shrinkage, drying shrinkage and restrained shrinkage cracking tests were employed. Tensile creep tests were conducted on four different mixtures selected among sixteen mixtures. In addition to the abovementioned tests, to reduce the adverse effect of autogenous shrinkage, effect of internal curing by the use of pre-soaked lightweight aggregates on dimensional compatibility and mechanical properties were also studied. For this purpose three additional ECC mixtures were prepared by using expanded perlite as pre-soaked lightweight aggregate, and evaluated on basis of their dimensional compatibility and mechanical properties.

3.2 Materials

3.2.1 Cementitious Materials

During the experimental study, CEM I 42.5R type ordinary portland cement (corresponding to ASTM Type I) with a specific gravity of 3.06 and Blaine specific surface area of 3250 cm^2/g produced by Adana Cement Factory was used. The fly ash used in the study was obtained from Sugözü Thermal Power Plant and corresponds to Class F according to ASTM C 618. Specific gravity and Blaine fineness of fly ash were determined as 2.61 and 2900 cm^2/g, respectively. In addition, ground granulated blast furnace slag (GGBFS) was also used. The GGBFS used, was an industrial waste of İsdemir Iron and Steel Plant, and ground to a Blaine fineness of 4250 cm^2/g by Oysa İskenderun Cement Factory. Specific gravity of GGBFS was determined as 2.79. Chemical composition and particle size distribution as determined by laser diffraction technique, of cementitious materials are presented in Table 3.1 and Figure 3.1, respectively.

Table 3.1 Chemical composition of the cementitious materials

Chemical Composition	**Portland Cement**	**FA**	**GGBFS**
CaO (%)	61.43	1.64	34.48
SiO_2 (%)	20.77	56.22	38.4
Al_2O_3 (%)	5.55	25.34	10.96
Fe_2O_3 (%)	3.35	7.65	0.81
MgO (%)	2.49	1.8	7.14
SO_3 (%)	2.49	0.32	1.48
K_2O (%)	0.77	1.88	0.86
Na_2O (%)	0.19	1.13	0.18
Loss on Ignition (%)	2.2	2.1	3.0
$SiO_2+Al_2O_3+Fe_2O_3$	29.37	89.21	50.17

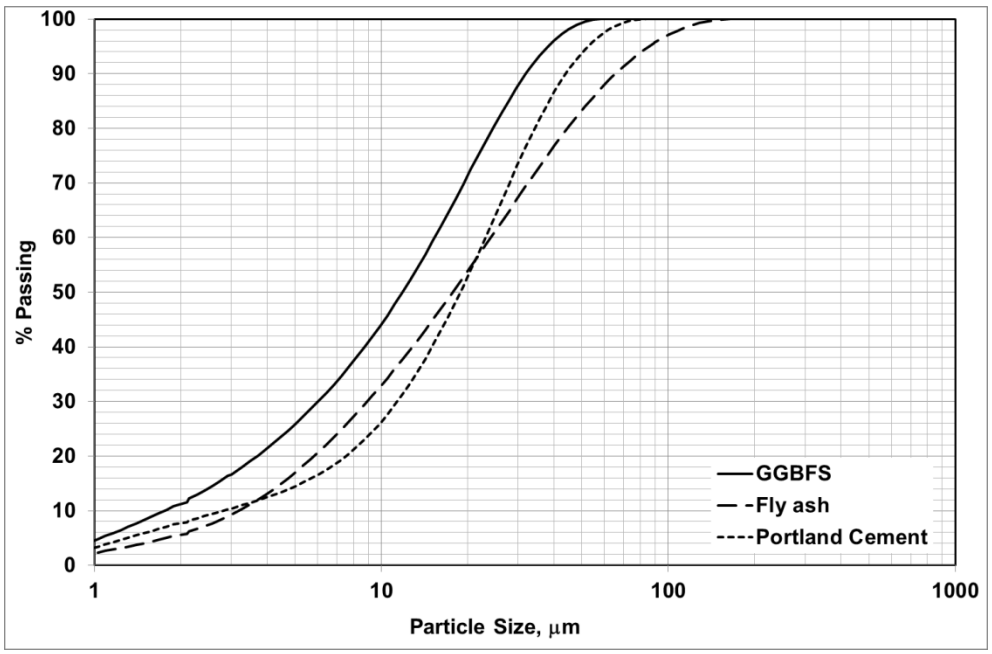

Figure 3.1 Particle size distribution of the cementitious materials

In order to determine the morphology of the ingredients, scanning electron microscopy (SEM) images of portland cement, FA and GGBFS are also determined as provided in Figure 3.2, Figure 3.3 and Figure 3.4, respectively.

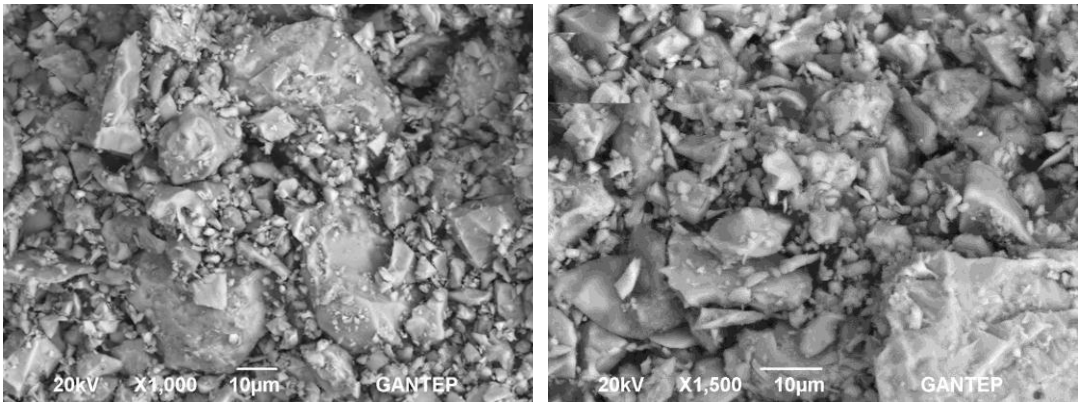

Figure 3.2 Particle morphology of portland cement

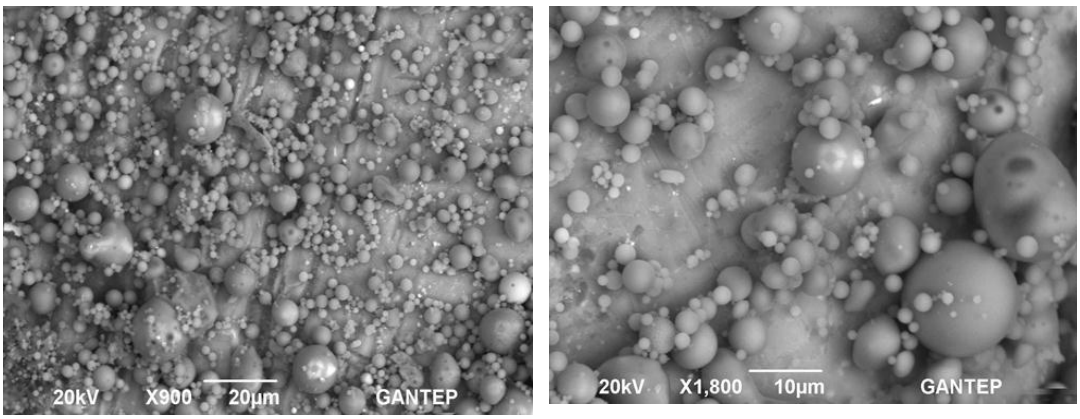

Figure 3.3 Particle morphology of FA

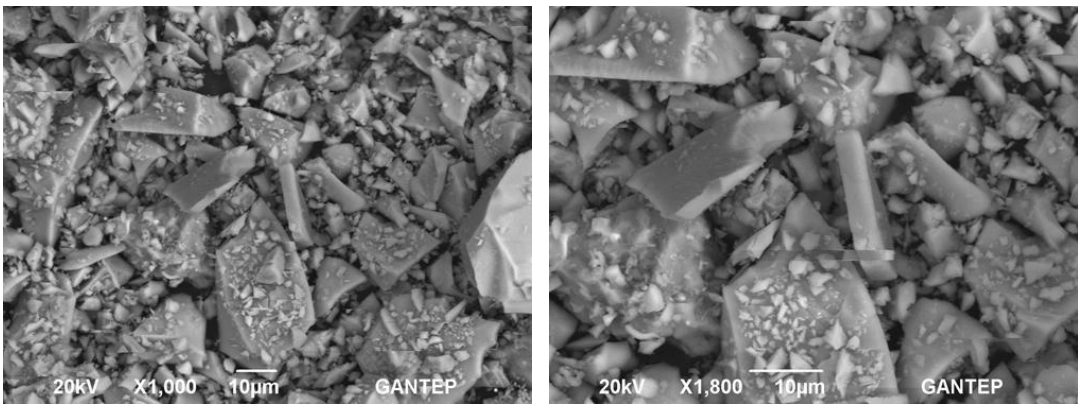

Figure 3.4 Particle morphology of GGBFS

3.2.2 Fibers

As mentioned earlier in the literature review, ductile behavior of ECC is attained by strain-hardening after the first crack formation. In order to achieve strain-hardening behavior, ECC requires tight and dense multiple cracking to occur. This can only be possible when fiber, matrix and interface properties are tailored together according to micromechanical design principles of ECC. Till the end of the 90s, ECC could only be successfully produced by using high molecular weight polyethylene (PE) fibers. However high cost of PE fibers resulted in a search for

incorporating other available fibers to achieve high ductility. Polyvinyl alcohol (PVA) fibers appeared appropriate for this aim; however high chemical bond between the fiber and matrix resulted in rupture of the fiber hence poor ductility. To overcome this problem, PVA fibers were oil coated and started to be used intensively in ECC production (Wang and Li, 2003). In this study, PVA fibers coated with 1.2% hydrophobic oiling agent by mass were used. These fibers are readily provided by the manufacturer in oil coated form and directly used in the mixtures without any preprocessing. The properties of PVA fibers are presented in Table 3.2 as provided by the manufacturer.

Table 3.2 Properties of PVA fibers as provided by the manufacturer

Property	**Value**
Nominal strength, MPa	1620
Apparent strength, MPa	1092
Diameter, μm	39
Length, mm	8
Young's modulus, GPa	42.8
Elongation, %	6
Density, kg/m^3	1300
Melting temperature, °C	230

3.2.3 Aggregates

In design of ECC mixtures, aggregate selection is a much more important concern, with respect to conventional concrete, since the effect of aggregate on matrix toughness is more marked. According to the energy criteria of ECC design theory; complementary energy determined by σ-δ curve should be higher than the matrix fracture toughness which restricts the maximum aggregate size and amount since higher amount and higher maximum size of aggregate increase the matrix toughness and decrease the possibility of achieving multiple cracking and strain-

hardening hence ductile behavior. In the production of standard ECC mixtures, silica sand with maximum and average aggregate sizes of 200 μm and 110 μm, respectively are used. However, in this study locally available silica sand with a SiO_2 content of 99.79%, with a specific gravity of 2.60 and an absorption capacity of 0.3% was used. The maximum and average aggregate sizes were about 400 μm and 200 μm, respectively. In addition to the fine silica sand, coarser silica sand with maximum and average aggregate sizes of about 1000 μm and 330 μm was also used to evaluate the effect of aggregate fineness. In twelve of the ECC mixtures, fine silica sand was directly used as aggregate; in the other four mixtures fine and coarse silica sand were used together by combining 0.65 parts of fine silica with 0.35 parts of coarse silica sand.

In addition to silica sand, expanded perlite aggregate was also used in additional three mixtures intended for investigating the effect of pre-soaked lightweight aggregate as an internal curing agent on autogenous shrinkage, drying shrinkage and mechanical properties. The expanded perlite aggregate used in the study has absorption capacities of 80% and 144% after immersing 1 hour and 24 hours in water, respectively. The term “pre-soaked” is preferred instead of “saturated” since the aggregate used in the study was immersed into water for a duration of 24 hours before using it in the mixtures and it is known that higher durations lead to higher absorption capacities and 24 hours is not a sufficient duration to bring expanded perlite to saturated surface dry (SSD) state. The specific gravity of the expanded perlite used in the study is 0.85 in SSD state.

Particle size distribution of fine silica sand with maximum aggregate size of 400 μm, combined silica sand with maximum aggregate size of 1000 μm and sieve analysis of perlite aggregate are provided in Figure 3.4.

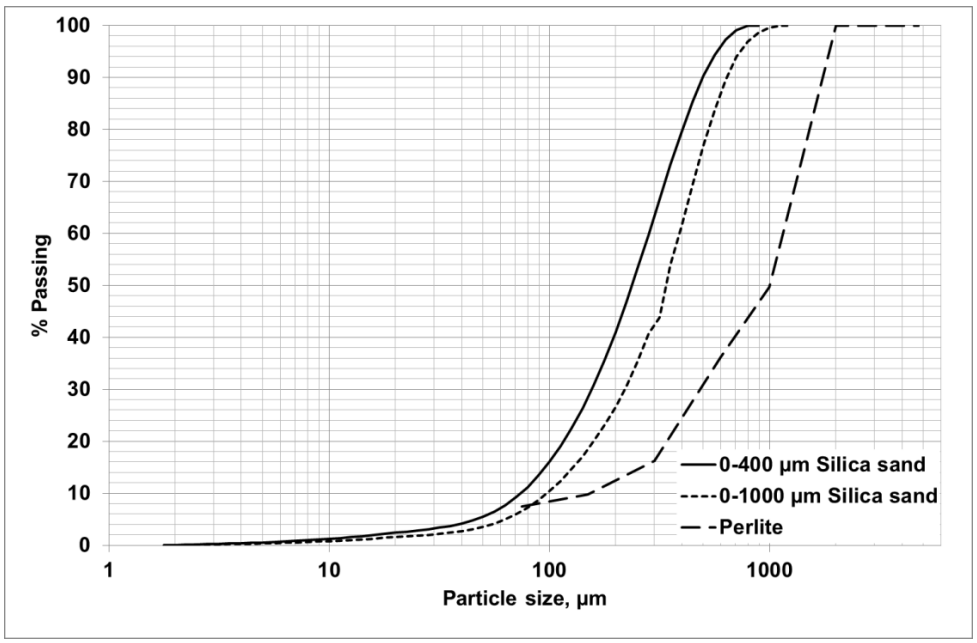

Figure 3.5 Particle size distribution of silica sand and sieve analysis of expanded perlite

3.2.4 Chemical Admixture

In ECC production, in addition to workability issues it is important to prepare a fresh mixture with sufficient consistency to provide uniform fiber distribution without bundling of fibers. As the water to cementitious materials ratio of ECC is quite low (0.27), it requires using water reducing admixtures to satisfy the required consistency. Polycarboxylate ether type high range water reducing admixture (HRWR) produced by BASF chemical company with a commercial name of Glenium 51 and solid content of 40%, specific gravity of 1.1 was used in the study.

3.3 Production of ECC Mixtures

In order to investigate the effect of ingredients of ECC on the dimensional compatibility and mechanical properties of ECC, sixteen ECC mixtures were

designed with varying amounts of cement, fly ash, GGBFS, silica sand and water. These mixtures were decided in basis of ECC mixture proportions widely presented in the literature, also called M45 which is the same as "F1" mixture in this study. Designation and proportions of ECC mixture ingredients are given in Table 3.3.

As mentioned previously, effect of internal curing by using expanded perlite as pre-soaked lightweight aggregate was also studied. For this purpose three additional ECC mixtures were designed by replacing 10%, 20% and 30% of the silica sand with expanded perlite by weight which was pre-soaked for 24 hours before using in the production. The mixture proportions of the additional mixtures are presented in Table 3.4.

Table 3.3 ECC mixture proportions by weight

Mixture Identity	**MA Type**	**C**	**W/CM**	**MA**	**S/CM**	**MAS (μm)**	**HRWR (kg/m^3)**
F 1	FA	1	0.27	1.2	0.36	400	5.1
F 2		1	0.27	1.2	0.45	400	5.1
F 3		1	0.27	1.2	0.55	400	5.0
F 4		1	0.27	1.2	0.36	1000	4.9
F 5		1	0.27	2.2	0.36	400	3.0
F 6		1	0.27	2.2	0.45	400	3.0
F 7		1	0.27	2.2	0.55	400	3.0
F 8		1	0.27	2.2	0.36	1000	3.0
S 1	GGFS	1	0.27	1.2	0.36	400	5.8
S 2		1	0.27	1.2	0.45	400	5.9
S 3		1	0.27	1.2	0.55	400	6.0
S 4		1	0.27	1.2	0.36	1000	4.9
S 5		1	0.27	2.2	0.36	400	4.7
S 6		1	0.27	2.2	0.45	400	4.1
S 7		1	0.27	2.2	0.55	400	4.3
S 8		1	0.27	2.2	0.36	1000	3.5

All mixtures contain 2% of PVA fibers in volumetric basis.
MA: Mineral admixture, C: Cement, W: Water, CM: Cementitious material, S: Sand, MAS: Maximum aggregate size, HRWR: High-range water reducing admixture

Table 3.4 Additional mixtures designed for internal curing

Mixture Identitity	C	W/CM	FA	Silica Sand	Expanded Perlite	Additional Curing Water	Total W/CM	HRWR kg/m3
F1	1	0.27	1.2	0.8	0	0	0.27	4.00
P1	1	0.27	1.2	0.71	0.08	0.02	0.29	4.00
P2	1	0.27	1.2	0.63	0.16	0.04	0.31	3.90
P3	1	0.27	1.2	0.55	0.24	0.06	0.33	3.70

All mixtures contain 2% of PVA fibers in volumetric basis.
C: Cement, W: Water, CM: Cementitious material, FA: Fly ash
HRWR: High-range water reducing admixture

Production of ECC involves selecting mixture proportions and mixing selected amount of ingredients with a planetary mixer of 25 L capacity in a mixing sequence designated to attain the best fiber distribution. ECC mixing sequence starts with placing solid materials in the bowl. All solid materials are blended in the bowl and water is added to the mixture afterwards. Then following the preparation of stiff mixture of cementitious materials and water, HRWR is added and mixing continues until obtaining a mixture with high consistency. Finally, fibers are added and mixing operation is ended after ensuring a uniform fiber distribution.

3.4 Determination of Mechanical Properties

In order to evaluate the mechanical performance of produced ECC mixtures, compressive and flexural strengths at 7, 28 and 90 days and matrix fracture toughnesses at 28 and 90 days were determined for mixtures produced for evaluating the mixture proportions on mechanical properties. For internally cured materials compressive and flexural strength tests were conducted at 28 and 90 days and matrix fracture toughness tests were conducted only at 28 days. For compressive strength tests, six 50 x 50 x 50 mm cubic specimens were prepared for each testing age. Flexural strengths were determined by four point bending test procedure. During flexural strength tests, mid-span beam deflections were also

measured. For flexural strength tests six 360 x 75 x 50 mm beam specimens were prepared. Similarly another six specimens made up with ECC matrix (ECC without fibers) were also produced for matrix fracture toughness determination. All specimens were demolded 24 hours after casting and stored in plastic bags with 95±5% relative humidity (RH) at 23±2 ^{o}C to avoid moisture transfer for the first 7 days, and stored at 50±5% RH at 23±2 ^{o}C afterwards till the day of testing. For flexural strength test specimens were placed symmetrically on two supports 304 mm away each other and load was applied from two points which are 101 mm apart with a loading rate of 0.005 mm/s on a deformation controlled closed-loop testing machine. An LVDT was attached to each flexural strength specimen so that the load and mid-span deflection data of the beams were recorded simultaneously during loading.

Matrix fracture toughness tests were also conducted on the beams, having the same dimensions, which were produced with the same mix proportions excluding the PVA fibers. Unfortunately, there is no standard method for determining fracture toughness of cementitious materials. To overcome this, ASTM E 399 (ASTM, 2003) "Linear-Elastic Plane-Strain Fracture Toughness K_{IC} of Metallic Materials" was adopted for fracture toughness determination. This method was previously used by Li et al. (1995) and feasibility of the method was shown for cementitious materials with maximum aggregate size of less than 1 mm. Before testing, a notch with a depth of 30 mm was opened with a diamond saw at the bottom of the mid-span of each beam specimen. Then, specimens were placed on two supports 304 mm apart from each other and subjected to three point bending test with a loading rate 0.002 mm/s. The following formula was used to calculate the fracture toughness of the specimens:

$$K_Q = \frac{P_Q S}{BW^{\frac{3}{2}}} f\left(\frac{a}{W}\right) \tag{3.1}$$

where P_Q: Ultimate load applied, *S*: Span length of the beam, *B*: Height of the beam, *W*: Depth of the beam, *a*: Depth of the notch, and $f(\frac{a}{W})$: geometric calibration factor (a value between 1.91 and 2.18 according to the exact depth of the specimens) (Li et al. 1995).

3.5 Determination of Drying Shrinkage

Drying shrinkage of the specimens were determined in accordance with ASTM C 157 (ASTM, 2006-b) standard test method. For each ECC mixture three 285 x 25 x 25 mm bar specimens were prepared. As indicated in the relevant standard, all specimens were cured under lime saturated water for 28 days after 24 hours following the casting of specimens. After curing 28 days under water, initial length measurement were taken with a length comparator. Specimens were kept under laboratory conditions at 23±2 ^{o}C and 50±4% RH during the rest of the test up to 180 days. For internal curing specimens test duration was 116 days.

3.6 Determination of Autogenous Shrinkage

Free autogenous shrinkage of ECC mixtures were measured by using special molds called "shrinkage drains" which allow the determination of length change of specimens continuously. As discussed in the previous chapter, this type of molds was used by Wongtanakitcharoen and Naaman (2007) for early age shrinkage and Wei et al. (2011) for autogenous shrinkage measurements. Similar molds were designed and manufactured for autogenous shrinkage measurements. Shrinkage drains are linear prismatic molds consisting of an inner mold having dimensions of 1000 x 60 x 90 mm which is located inside an outer mold. 1000 x 90 mm upper surface and 60 x 90 mm side surface of the inner mold are left open for casting of material and shrinkage measurements, respectively as depicted in Figure 3.6. All inside surfaces of the inner mold are covered with Teflon sheets where the mold is in touch with the specimen to avoid restraining effect due to friction. An LVDT is

attached to the free end of the specimens for continuous acquisition of length data, also under the bottom of each shrinkage drain a thermocouple was located for continuous monitoring of temperature data. Four shrinkage drains were connected to an eight channel data acquisition system and length changes of the specimens and temperature variations measured under the specimens were monitored simultaneously during the test. Before placing freshly mixed ECC to drains, to further reduce friction aerosol Teflon was sprayed over the Teflon sheets and all inside surfaces of the inner mold were covered with thin plastic which in turn is used to cover the surfaces of the specimen to avoid moisture transfer between the specimen and environment. Finally a layer of Teflon spray was applied on the plastic sheet. This sequence which is not originally included in the literature was found to yield best results in terms of repeatability and compatibility.

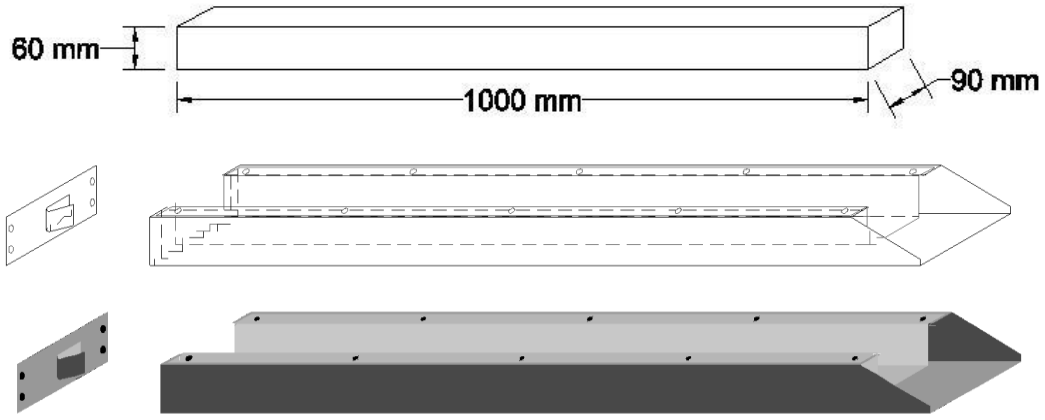

Figure 3.6 Inner and outer molds of shrinkage drain

The open end of the mold was closed with Styrofoam before casting to prevent the loss of fresh material and bleed water as fresh ECC mixtures possess high consistency and low viscosity. Before the length measurements a small plate is embedded inside the fresh material and it was brought in touch with the rod

surrounded with a spring which is connected to the LVDT during the test as can be seen in Figure 3.7 and Figure 3.8.

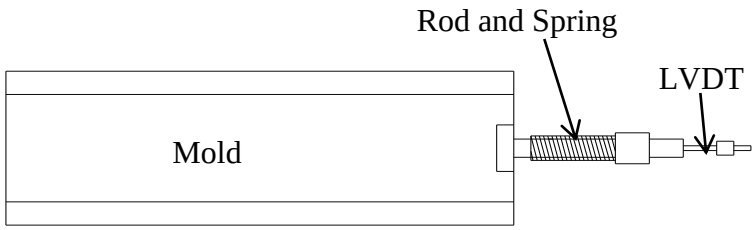

Figure 3.7 Setup for length measurements with LVDT

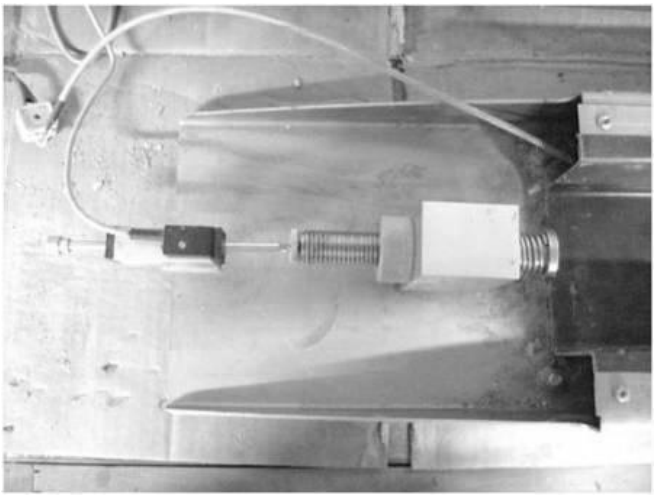

Figure 3.8 Top view of the LVDT and mold

After casting fresh ECC mixtures, all open surfaces of the specimens were encased with the plastic sheet which was placed over the Teflon sheet before casting. Finally, top surfaces of specimens were covered with another piece of Teflon sheet. For the first 12 hours of testing, only temperature measurements were recorded and length measurements were started afterwards, as the setting time of fibrous

cementitious materials cannot be determined accurately by using conventional methods. After 12 hours, the Styrofoam which was placed to hold the fresh material was removed and length measurements were started. Shrinkage drains can be seen in Figure 3.9 and 3.10 before and during the test, respectively.

Figure 3.9 Preparation for the test

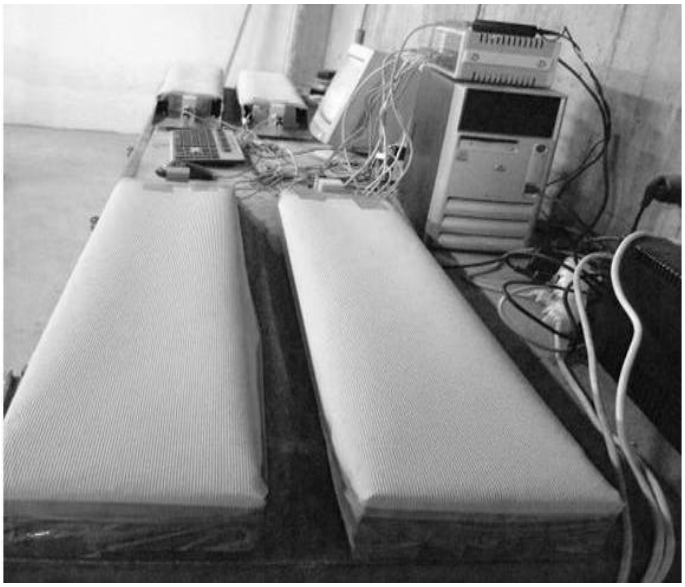

Figure 3.10 A view of the setup during the test

Before starting the measurement, all LVDTs were calibrated and brought in touch with the metal plate. In order to calculate the length change of the specimens, the maximum temperature recorded on a specimen, which is about 16 hours after placing fresh mixtures to drains, was taken as initial length reading of the specimens. During the first 28 days, LVDT readings were taken at every 10 minutes by the data acquisition system. All shrinkage drains were kept in an isolated room equipped with an air conditioning system fixed at an ambient temperature of 23±2 ^{o}C. For ach ECC mixture, two replicates of specimens were cast for autogenous shrinkage measurements.

3.7 Determination of Tensile Creep

A tensile creep setup was designed and manufactured based on the available information provided in the literature. Tensile creep test setup was designed in form of a lever arm and steel I beams were used to form the tensile creep test frame. Four of these frames were produced, each capable of testing three specimens at the same time. Total height of the loading frames is 1.7 m and the total length of the lever is 2.5 m with a load ratio of about 1/7 (ratio of the weight placed on the frame to the applied load) with a maximum weight of 250 kg that can be placed on the frame which corresponds to about 2000 kgf applicable load. 5 and 10 kg masses in form of steel plates which provides sensitivity about 35 kgf are used for loading. Specimens can be loaded without any eccentricity as hinge connections are used in the joints between the frame and the specimens. Tensile creep loading frame and connection details can be seen in Figure 3.11 and Figure 3.12, respectively. All tensile creep test frames were calibrated by using a load cell, after they were assembled in the laboratory and calibration charts were prepared for each frame. A sample calibration chart is given in Figure 3.13.

Figure 3.11 Tensile creep loading frame

For tensile creep test, prismatic specimens are prepared and steel plates with bolts at one face mounted to the bottom and top surfaces of the specimens by using quick setting epoxy resin. This operation requires great care in order to be able to align specimens without excessive eccentricity that may lead additional stresses inside the specimens. Three specimens are connected to each other and to the frame by the use of steel plates and nuts. 75 x 75 x 320 mm prismatic specimens were used at first; however specimens, actually the epoxy resin, failed at locations close to the steel plates due to insufficient bonding between epoxy resin, steel and specimen. To decrease the amount of tensile stress acting on the connections, a special mold was designed with an area of 75 x 75 mm at the connections and 55 x 55 mm in the middle of the specimen as shown in Figure 3.14 and 3.15. Two steel discs were located 250 mm apart on all four faces of tensile creep specimens. Length change measurements were conducted by using a DEMEC digital mechanical strain gage capable of measuring 250 mm with a sensitivity of 0.001 mm as seen from the

Figure 3.16. Although drying shrinkages of all ECC mixtures were determined, considering the size effect, two additional specimens were prepared, having the same dimensions with tensile creep specimens, for drying shrinkage measurements and stored under same conditions with tensile creep specimens. Calculated drying shrinkage of the specimens were used for determination of the tensile creep as creep specimens are inevitably subjected to both creep loading and drying shrinkage at the same time.

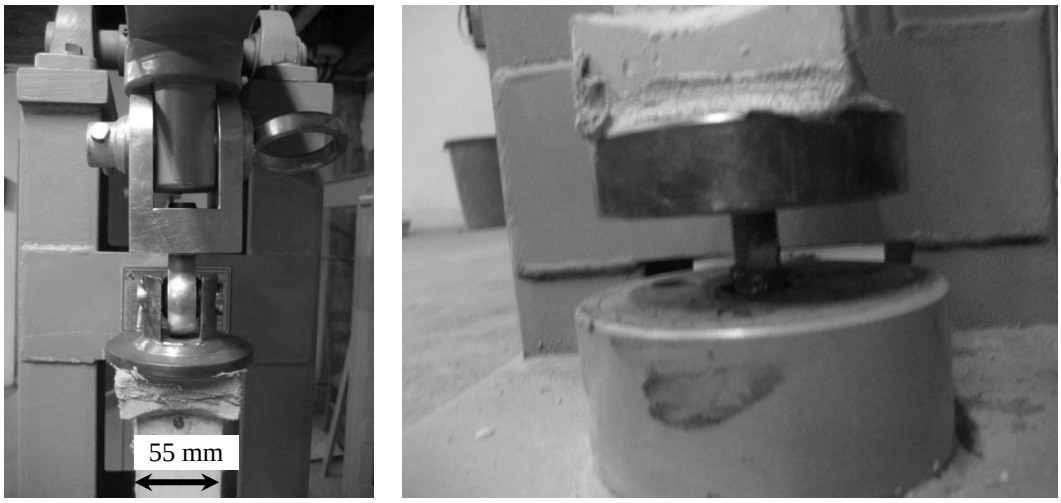

Figure 3.12 Views of top and bottom connections of tensile creep loading frame

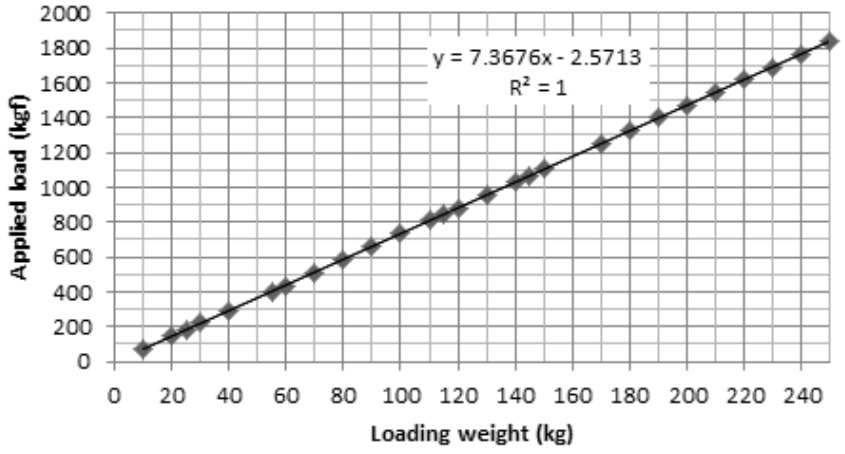

Figure 3.13 Sample calibration chart

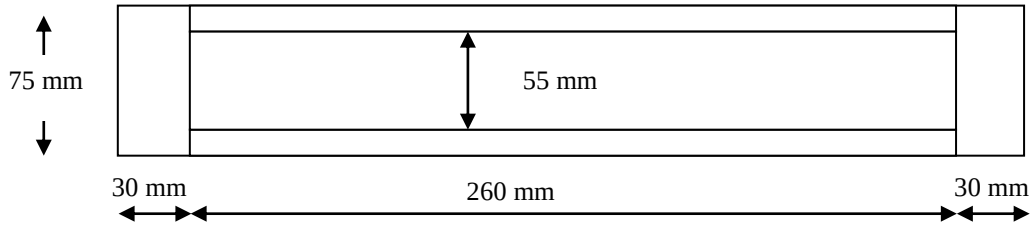

a. Top view

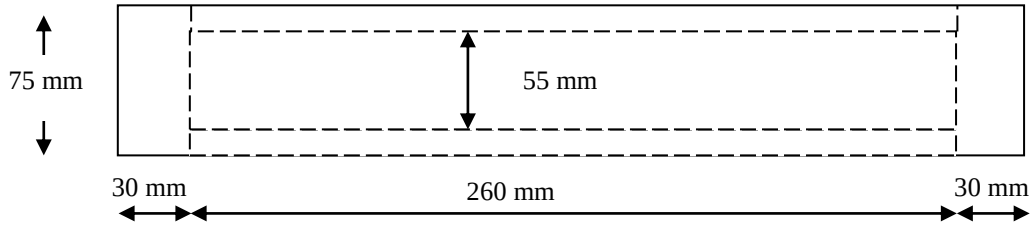

b. Side view

Figure 3.14 Top and side view of tensile creep specimen molds

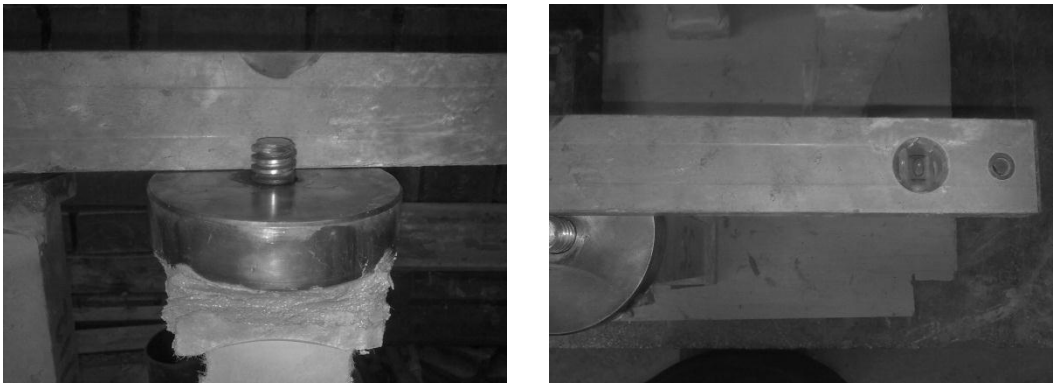

Figure 3.15 Checking for eccentricity before tensile creep test

Figure 3.16 Measurement with DEMEC digital mechanical strain gage

Two sets of experimental program one for the early age, one with standard age, were carried out to study the behavior of selected ECC mixtures under sustained direct tensile stresses. Four of the ECC mixtures, designated with F1, F5, S1 and S5 were selected for tensile creep tests because of the limited capacity and long testing duration. F1 is the mixture that possesses the standard ECC mixture properties; F5 is the mixture with increased amount of fly ash with respect to F1 with a fly ash cement ratio of 2.2 which is 1.2 for F1. S1 is similar to F1 except that the mineral admixture used in the mixture is GGBFS instead of fly ash and finally S5 possesses a GGBFS to cement ratio of 2.2. These four mixtures were selected to evaluate the effect of mineral admixture type and amount.

In the first set of experiments, to evaluate the early age creep, specimens were demolded 24 hours after casting and stored in lime saturated water for 2 days. At the end of 2 days, they were removed from the water and left for drying in

laboratory conditions since the specimen surfaces should be dry in order to achieve sufficient bond strength between epoxy, steel and specimen. After one day of drying, steel plates were mounted to one end of the specimens with epoxy resin and left for epoxy resin to set for one day, the opposite end of the specimens were mounted to steel plates in the same manner and specimens were left for drying and setting till the age of 7 days. At the age of 7 days, specimens were placed into the tensile creep loading frame and loaded to 30% of the ultimate tensile strength of the material determined by direct tensile strength test conducted on briquet specimens. At the ages of 14 and 28 days, tensile strengths of the specimens were determined in the same manner and tensile creep loads were modified to sustain a tensile load of 30% of ultimate tensile strength until the end of 90 days. Tests were conducted in an isolated room and temperature and humidity were fixed at at 23±2 ^{o}C and 50±4% RH by an air conditioning system.

In the second set of tensile creep experiments, one day after casting, specimens were demolded and placed in lime saturated water for 21 days. After 21 days, specimens were processed for tensile creep test as described in the first set. At the age of 28 days, all specimens were placed in loading frame and loaded with a tensile stress of 1.5 MPa for a testing duration of 90 days. For all tensile creep measurements the initial readings were taken immediately after loading.

3.8 Determination of Restrained Shrinkage

Restrained shrinkage tests were performed in accordance with ASTM C 1581 (ASTM, 2009) standard test method. In order to perform the test as described in the standard four restrained shrinkage molds were locally manufactured. Each mold consists of two concentric steel rings with a height of 150 mm located on non-absorbent steel base. Inner ring has a thickness of 13 mm and an outer diameter of 330 mm. Outer ring has an inner diameter of 405 mm that allows casting fresh materials with a thickness of 37.5 mm between two rings. Also four electrical resistance strain gages, wired in a quarter-bridge configuration, were placed inside

the inner ring for measuring the loop strain development those occur as a result of circumferential shrinkage that the test material experience. 32 channel data acquisition system was used to collect the strain data continuously for every 10 minute interval. In order to maintain uniform thickness of test material, inner and outer rings are fixed to the steel base by the use of eccentric bolts which can easily be loosened after casting of material.

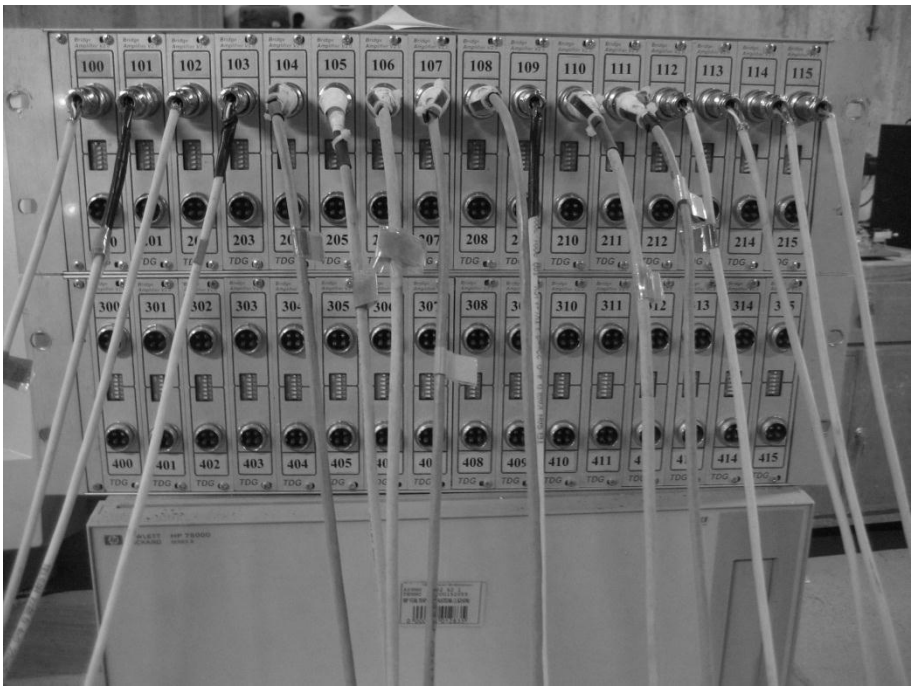

Figure 3.17 Data acquisition system used for strain development measurements

Before casting fresh material, outer surface of the inner mold was coated with aerosol Teflon to minimize the restrain from that end. Immediately after casting the fresh material between the rings, eccentric bolts were loosened and the top surface of the test material was covered with a wet burlap. 24 hours after casting, outer mold was removed and top surface of the test material was sealed with a silicon based sealant. Test material was subjected to drying from the outer surface at an

ambient temperature of 23±2 ^{o}C and 50±4% RH. In addition to the strain development, crack formations were also monitored daily and average crack widths, measured from three locations along the crack length were recorded. According to ASTM C 1581 (ASTM, 2009), restrained shrinkage test is terminated when a crack formation is observed and if cracking does not occur, it is suggested to keep recording and monitoring the strains at least 28 days. Although almost all of the specimens cracked earlier, restrained shrinkage tests were continued up to 14 days for specimens containing GGBFS and 28 days for specimens containing fly ash.

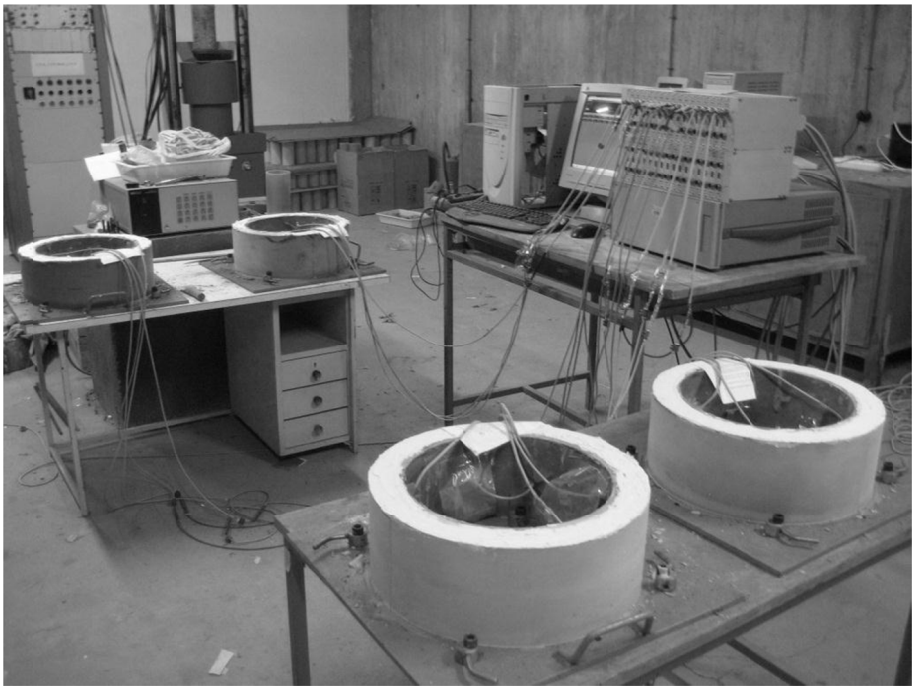

Figure 3.18 A view of restrained shrinkage test setup during the test

In addition to the restrained shrinkage test described above, another restrained shrinkage test setup was employed to evaluate the cracking potential of ECC. Appearance of the molds and procedure of the test is similar to that of ASTM C

1581 (ASTM, 2009) with some minor differences. Firstly no strain gages are used in this setup; hence strain development is not monitored. Secondly, dimensions of the mold differ; height of the mold is 140 mm, outer diameter of the inner ring is 305 mm and the inner diameter of the outer ring is 355 mm maintaining a test material thickness of 25 mm. In addition, outer surface of the inner mold is not sealed that results bonding between ECC and steel which may also affect the results. Specimens are cured in the same conditions with ASTM C 1581 (ASTM, 2009) test. Crack formation and average crack widths measured as an average of three measurements taken along the length of a crack were monitored daily for duration of 28 days. Two replicates of specimens were prepared for each mixture.

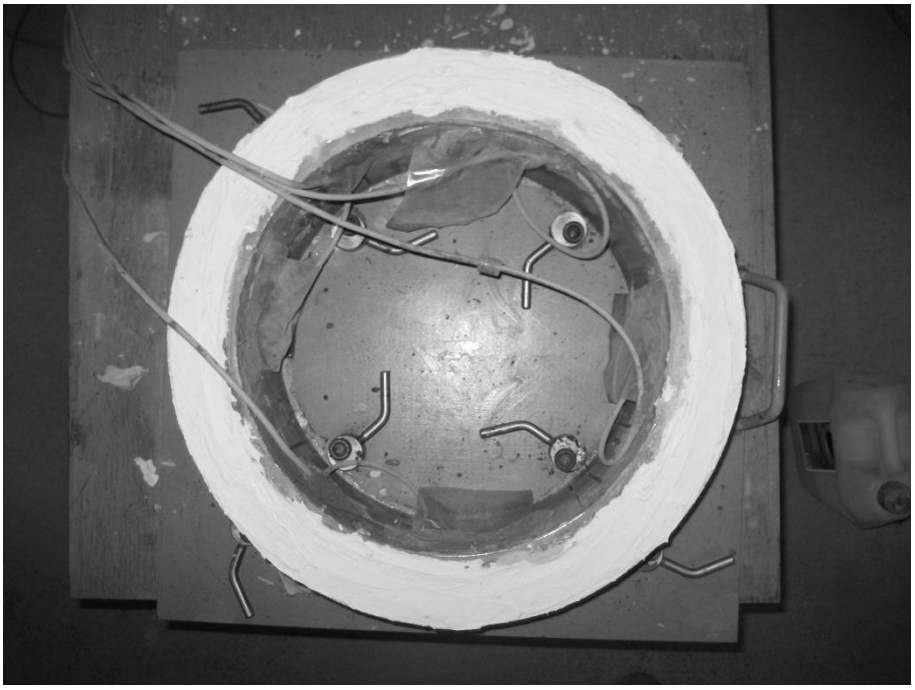

Figure 3.19 A close view of restrained shrinkage ring during the test

CHAPTER 4

RESULTS AND DISCUSSION

4.1 General

In this chapter, the results of mechanical and dimensional compatibility tests are provided. Mechanical tests include; compressive strength, flexural strength, mid-span beam deflection at 7, 28 and 90 days and matrix fracture toughness at 28 and 90 days, and tests conducted for determining the dimensional compatibility properties include; monitoring the drying shrinkage for 180 days, restrained shrinkage for 28 days, autogenous shrinkage for 28 days and tensile creep tests for 90 days. In order to evaluate the effect of internal curing on mechanical and dimensional compatibility properties, similar tests were also conducted on ECC mixtures with expanded perlite except that mechanical tests at 7 days and matrix fracture tests at 90 days and also tensile creep tests were not conducted.

Throughout the experimental test program, initially the experiments were conducted to evaluate the effect of mixture proportions. Therefore the results of the two experimental sets; one for evaluation of mineral admixture type and amount, aggregate size and amount and the other for evaluation of internal curing provided by expanded perlite aggregate as pre-soaked lightweight aggregate were evaluated separately.

4.2 Effect of Mixture Proportioning on Mechanical and Dimensional Compatibility Properties

The experimental test program for evaluation of mix proportioning involves sixteen mixtures with two different amounts and types of mineral admixtures, varying amounts and maximum sizes of aggregates as depicted in Table 4.1.

Table 4.1 Mixture identification

		Mineral admixture/Cement				Maximum aggregate size
		1.2		2.2		
Sand / Cementitious	0.36	**F1**	**S1**	**F5**	**S5**	400µm
	0.45	**F2**	**S2**	**F6**	**S6**	
	0.55	**F3**	**S3**	**F7**	**S7**	
	0.36	**F4**	**S4**	**F8**	**S8**	1000µm
F: FA containing mixtures; **S:** GGBFS containing mixtures.						

4.2.1 Compressive Strength

Results of the compressive strength tests conducted on ECC mixtures at 7, 28 and 90 days are presented in Table 4.2, as average of six 50 mm cubic specimens. In order to visually examine the effects of sand to cementitious material ratio and mineral admixture to cement ratio on compressive strengths of mixtures the data on Table 4.2 is provided in Figure 4.1.

It is obvious that mixtures containing GGBFS possess higher compressive strength values than mixtures containing FA. This is more marked at early ages as mixtures

with GGBFS have compressive strengths about 62% higher than mixtures with FA at 7 days while it is about 48% for 28 days and 39% for 90 days, considering the overall average compressive strengths of mixtures containing FA and GGBFS. The observed high early strength of GGBFS mixtures may have several reasons: i) The high specific surface area (4250 cm^2/g) of GGBFS results in higher reactivity at early ages which is also effective on early age compressive strength ii) As GGBFS contain more SiO_2 and less CaO, compared to portland cement, hydration of GGBFS portland cement mixes produces higher amount of C-S-H gel and lower amount of lime with respect to portland cement hydration alone, which yields a denser microstructure (Neville, 2003) iii) GGBFS show hydraulic binding properties in addition to pozzolanic binding property iv) A consequence of reactions between alkali hydroxides of the cement and GGBFS before the production of calcium hydroxide by hydration of cement (Roy and Idorn, 1983). Moreover, mixtures containing more cement have higher compressive strengths, as compressive strength of the mixtures with mineral admixture to cement ratio of 1.2 are higher than that of mixtures with 2.2, at all ages.

The effects of mineral admixture to cement ratio and maximum aggregate size on compressive strength developments of the mixtures can also be seen in Figures 4.2 for fly ash (FA) and ground granulated blast furnace slag (GGBFS) containing mixtures.

As can be seen in Figure 4.1, and 4.2, effects of sand to cementitious ratio hence aggregate content and maximum aggregate size on the compressive strength are not consistent. Thus, no correlation could be gathered between the strength development and aggregate content of the mixes. Although, the amount of aggregate in the mixtures varies, water to binder ratio of the mixtures is fixed at 0.27 and together with the high amount of binders (>1100 kg/m^3 for all mixtures) some of binder particles remains unhydrated which suppress the effect of aggregate and binder content on compressive strength for ECC mixtures. In spite of the fact that aggregate size is effective on the compressive strength of concrete (Cetin and

Carrasquillo, 1998; Mehta and Monteiro, 2006), maximum aggregate size did not seem to affect the compressive strength of the ECC mixtures dealt in this study which is in contrast with existing literature. This may be attributed to the limited replacement level and maximum aggregate size of coarser silica used in this study.

Table 4.2 Compressive strength of ECC mixtures

Mix ID	**Compressive Strength (MPa)**		
	7 day	**28 day**	**90 day**
F1	40.1	69.3	75.8
F2	40.9	69.8	72.5
F3	37.4	62.6	67.6
F4	37.5	60.8	65.5
F5	30.2	46.1	54.7
F6	29.0	45.8	56.8
F7	30.3	47.9	58.7
F8	27.9	48.7	57.7
S1	59.9	88.5	91.2
S2	58.0	90.0	93.2
S3	56.9	86.5	90.7
S4	60.0	89.6	92.2
S5	51.8	76.3	80.3
S6	50.6	78.5	88.7
S7	52.8	81.5	86.6
S8	52.9	79.4	84.2

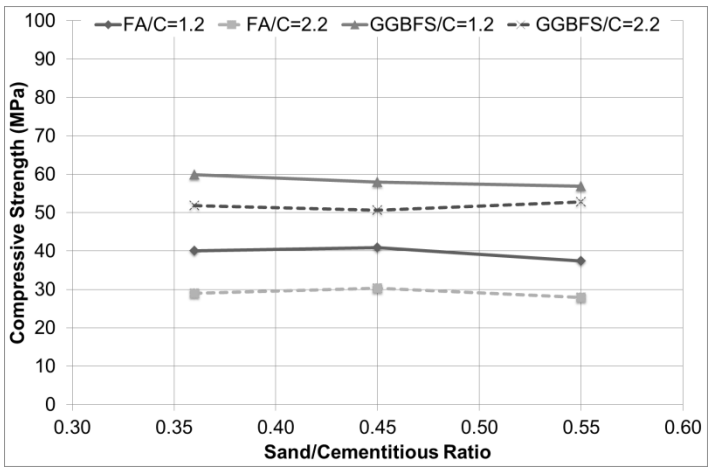

a. 7 days

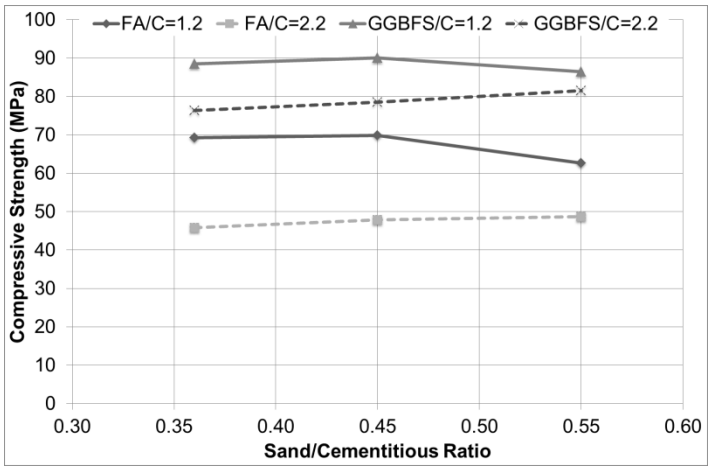

b. 28 days

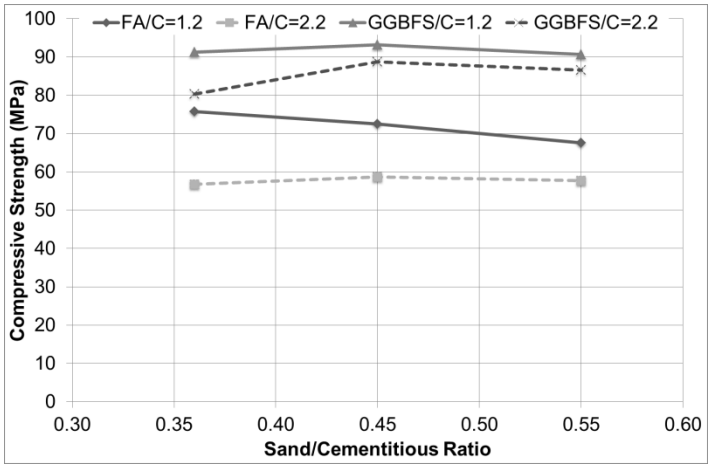

c. 90 days

Figure 4.1 Compressive strengths of ECC mixtures

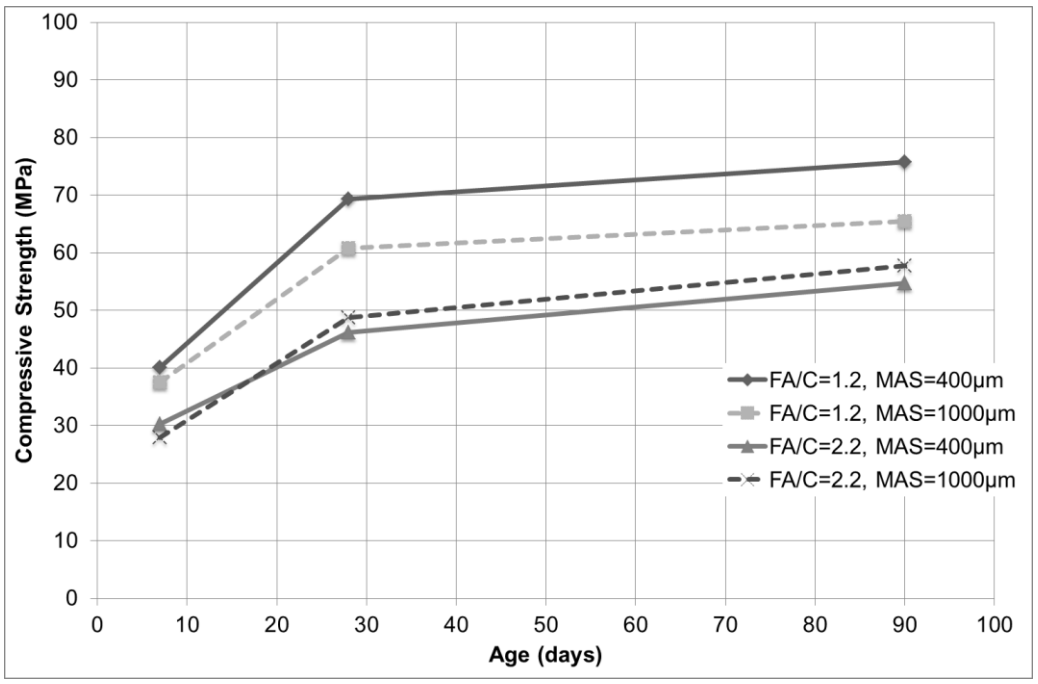

a. FA mixtures

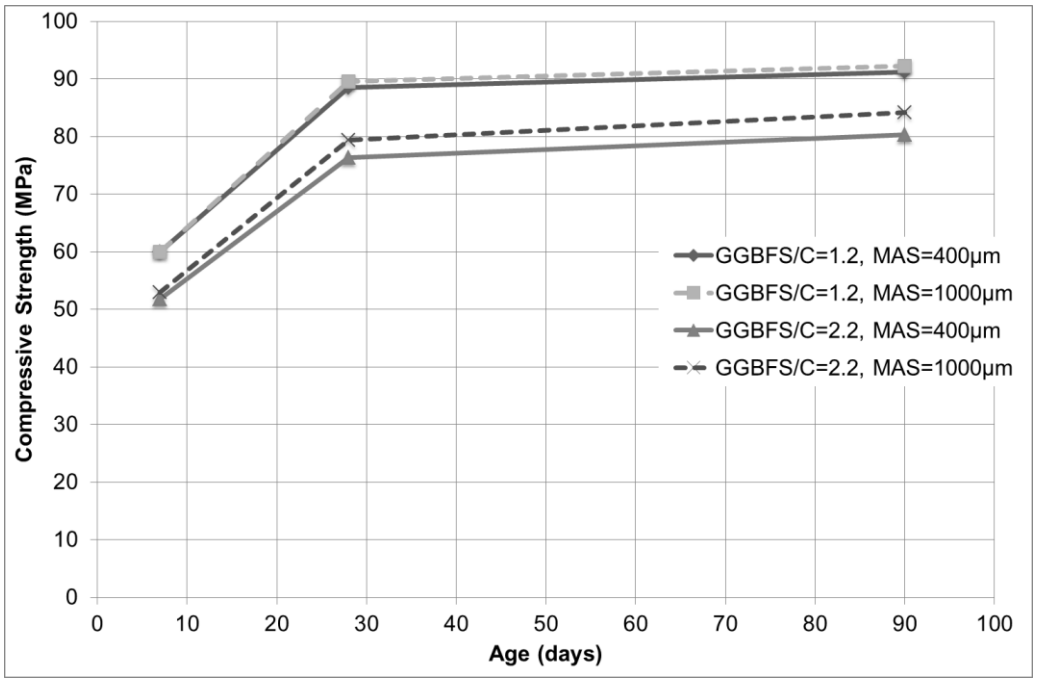

b. GGBFS mixtures

Figure 4.2 Effect of MAS on compressive strength development of mixtures with sand to cementitious ratio of 0.36

With respect to 7 day compressive strength values, considering the mineral admixture mass per cement mass, specimens with FA to cement ratio of 2.2 have the highest rate of average increase in compressive strength which is about 94%, at 90 days which is followed by FA to cement ratio of 1.2 with an average increase of about 80% (Figure 4.3). GGBFS to cement ratio of 2.2 and 1.2 exhibited average increases in compressive strength of 63% and 57% respectively for 90 days. Again, with respect to compressive strength values at 7 days, there is an increase in compressive strength about 33% for mixes with a FA to cement ratio of 2.2 between 28 and 90 days which is followed by FA to cement ratio of 1.2 with an average increase of 12%. Compressive strength of the mixtures with GGBFS to cement ratios of 2.2 have an average increases of 12%, followed by the mixtures with GGBFS to cement ratio of 1.2 with an increase of 5%. Considering the descending nature of strength development by time, it can be concluded that mixtures with fly ash to cement ratio of 2.2 will continue to gain compressive strength more than other mixtures. Hence mixes with GGBFS to cement ratio of 1.2 will have the lowest gain in compressive strength for further ages. These results may be attributed to early reaction of GGBFS with respect to FA, since compressive strength development of FA mixtures are slower especially at early ages due to delayed pozzolanic reactions with $CaOH_2$. It can also be seen that as the FA to cement ratio increases, rate of strength gain becomes slower up to 28 days, but higher between 28 and 90 days.

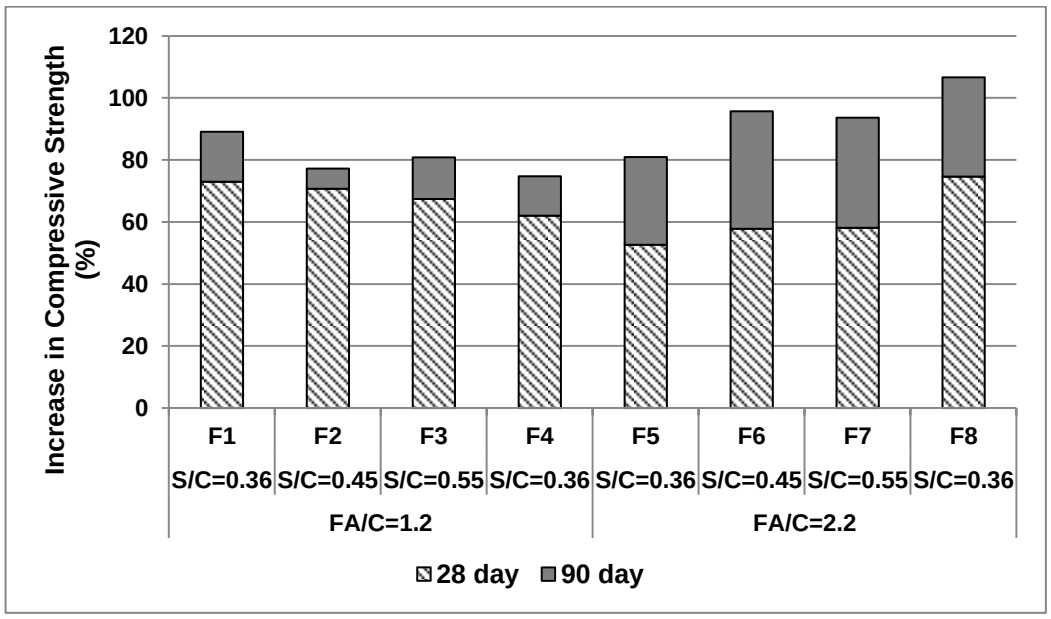

a. FA mixtures

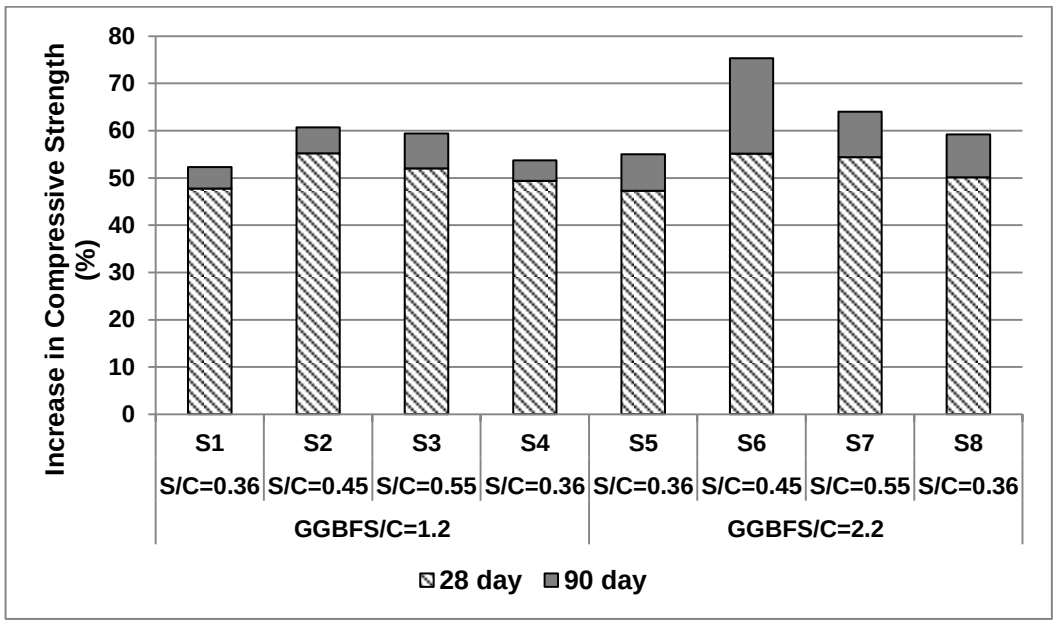

b. GGBFS mixtures

Figure 4.3 Increase in compressive strength of mixtures with respect to 7 day compressive strength

4.2.2 Flexural Performance

The direct tensile test is considered to be the most accurate and effective test method to confirm the tensile strain-hardening behavior of a composite, as quasi-brittle fiber-reinforced composites can potentially show deflection-hardening behavior under flexural loading, depending on the specimen geometry. However, one of the principle concern in designing concrete pavement structures is the flexural performance of the concrete. Flexural strength test of ECC is also an indirect measure of direct tensile performance. Therefore it was decided to use four-point bending test to investigate the flexural strength and ductility by measuring mid-span beam deflection capacity of ECC mixtures. During four point bending test, load deflection curves were obtained and the first inflection point on the curve corresponds to first cracking, maximum load on the curve corresponds to flexural strength or modulus of rupture (MOR) and corresponding deflection is defined as the mid-span deflection capacity of the beam specimen. Qian and Li (2007) demonstrated that the deflection capacity under bending can be correlated to tensile strain capacity directly for strain-hardening materials. In light of this observation it can be concluded that all materials produced in this study exhibited strain-hardening behavior. Flexural strengths and mid-span beam deflections of the mixtures are presented in Table 4.3, as average of six specimens.

As can be seen in Figure 4.4, it is clear that mixtures with GGBFS have slightly higher flexural strengths compared to mixtures with similar proportions containing FA, at early ages. This difference vanishes at 28 and 90 days and flexural strength values become closer. This behavior is very different than what is observed in compressive strength test results since there is always a visible difference in compressive strengths of the FA and GGBFS mixtures at all ages. The most probable reason for this trend may be attributed to the fact that flexural strength is governed by more complex material properties, such as tensile first cracking strength, ultimate tensile strength and tensile strain capacity, particularly in the case of strain-hardening cementitious materials (Qian et. al. 2009).

Table 4.3 Flexural strength and mid-span beam deflection of ECC mixtures

Mix ID	Flexural Strength (MPa)			Mid-span Beam Deflection (mm)		
	7 day	28 day	90 day	7 day	28 day	90 day
F1	8.48	12.73	12.8	5.68	4.83	4.49
F2	7.51	11.92	12.19	4.52	4.23	3.99
F3	7.69	11.41	12.42	4.09	3.97	3.84
F4	7.88	11.63	12.04	5.11	4.59	4.12
F5	7.36	10.19	11.58	7.02	5.89	5.29
F6	7.04	10.79	11.23	6.25	5.56	4.85
F7	7.26	10.14	10.03	5.4	4.99	4.88
F8	6.59	9.39	10.59	5.55	4.72	4.5
S1	9.92	12.58	12.63	3.73	3.1	3.04
S2	9.89	12.38	12.7	3.24	2.71	2.62
S3	9.23	12.19	12.24	2.62	2.44	2.42
S4	9.78	12.04	12.36	3.6	2.94	2.74
S5	8.44	11.5	11.78	4.31	3.98	3.44
S6	8.69	11.89	11.73	3.66	3.22	3.18
S7	8.45	11.42	11.35	3.23	2.55	2.21
S8	8.63	11.29	11.15	4.14	3.35	3.06

Furthermore, the increase in flexural strength of specimens with age is more gradual when compared to compressive strength test results as depicted in Figure 4.5. Aggregate content does not have a consistent effect on flexural strength as discussed in compressive strength test results. However, there is a slight decrease in flexural strength of mixtures with MAS of 1000 μm as seen in Figure 4.5. Average reduction of flexural strength is of about 8.2 and 7.2% for FA mixtures and 3.1 and 3.7% for GGBFS mixtures, at 28 and 90 days, respectively.

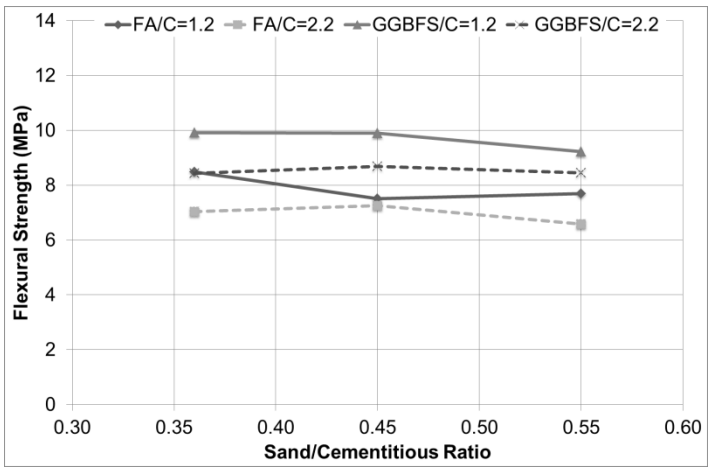

a. 7 days

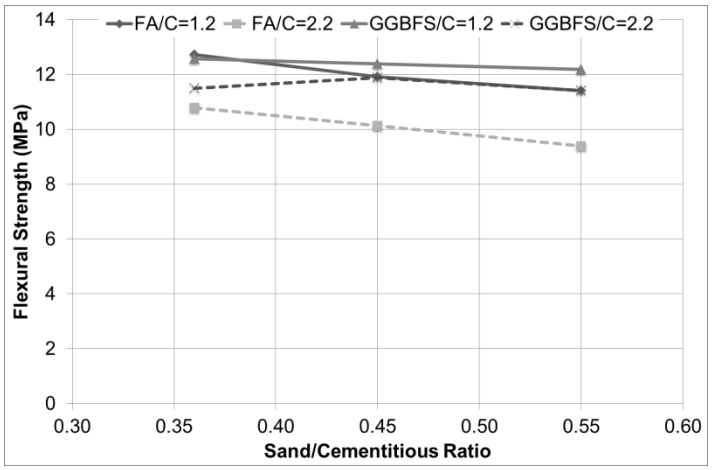

b. 28 days

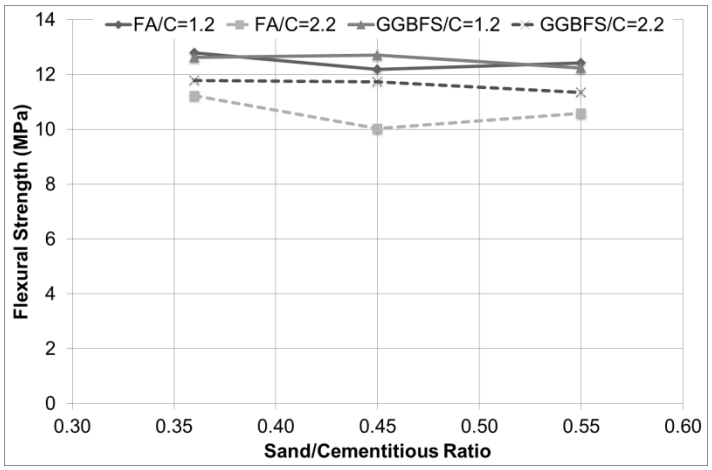

c. 90 days

Figure 4.4 Flexural strengths of ECC mixtures

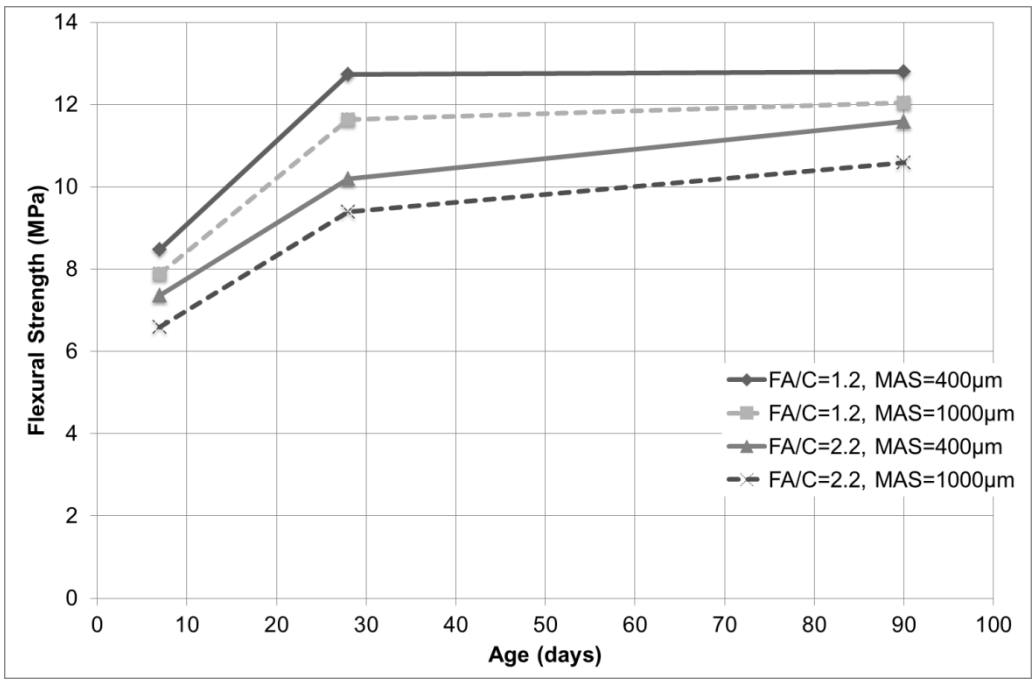

a. FA mixtures

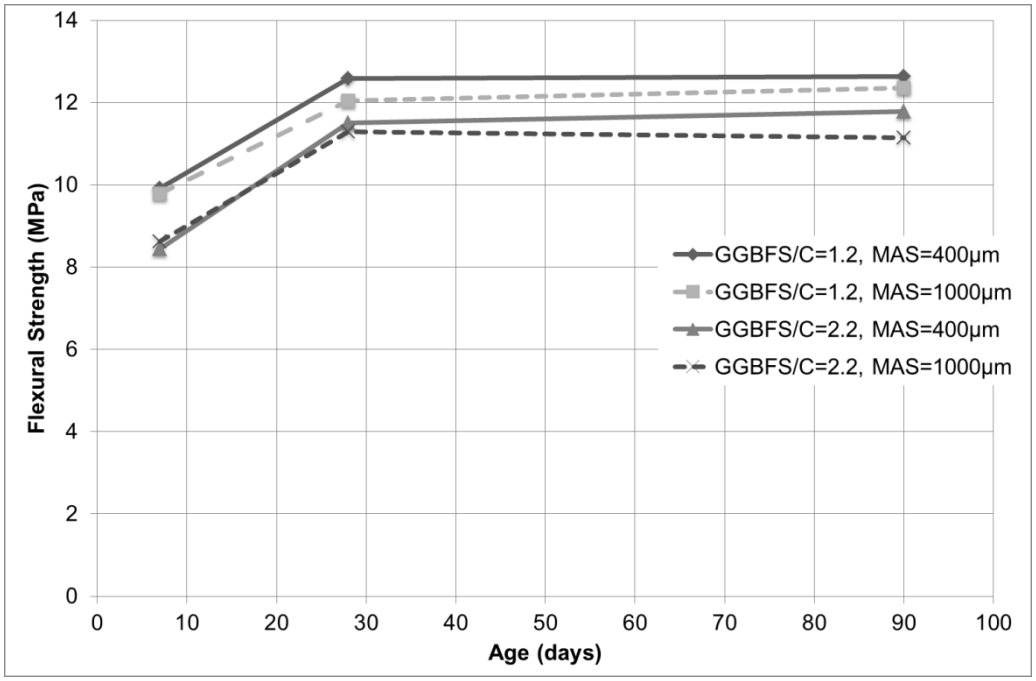

b. GGBFS mixtures

Figure 4.5 Effect of MAS on flexural strength development of mixtures with sand to cementitious ratio of 0.36

As can be seen in Table 4.3, mid-span beam deflections as a measure of material ductility are dependent on type and amount of mineral admixture and also to aggregate amount and maximum size. Specimens containing GGBFS have significantly lower mid-span beam deflections compared to the ones containing FA as seen in Figure 4.6. The low ductility of GGBFS containing mixtures can be a result of high matrix fracture toughness and high bond strength between matrix and fibers with respect to FA mixtures. This can be validated by the SEM images of the fibers' fracture surfaces after a bending test, as shown in Figure 4.7 for FA mixture and Figure 4.8 for a GGBFS mixture. It is clearly seen that as a result of high bond strength and chemical bond between fiber and matrix in GGBFS containing mixtures, there is a visual abrasion on the surface of the fiber in Figure 4.8. While in Figure 4.7, fiber surface is relatively smooth and intact which indicates a satisfactory pullout performance without fiber deterioration. On the other hand, minimum value of mid-span deflection for GGBFS containing mixtures is 2.21 mm, which is still significantly high compared to conventional concrete. It can also be concluded that as the amount of mineral admixture increases, mid-span deflections, hence the ductility of the specimens increases especially for mixtures containing FA. Also for all mixtures, deformation capacity decreases with age, but this drop is slight between 28 and 90 days and stabilizes with time. This behavior is a known fact and attributed to strengthening of fiber-matrix interface and increase in matrix fracture toughness as a result of continuous hydration of cementitious materials (Wang and Li, 2007; Şahmaran and Li, 2009-a).

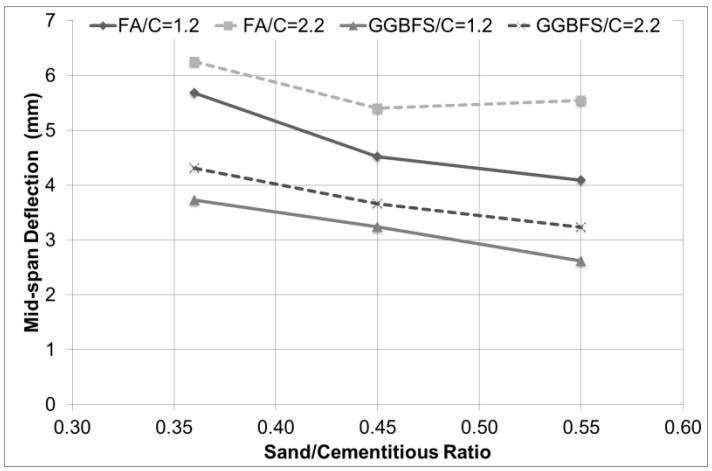

a. 7 days

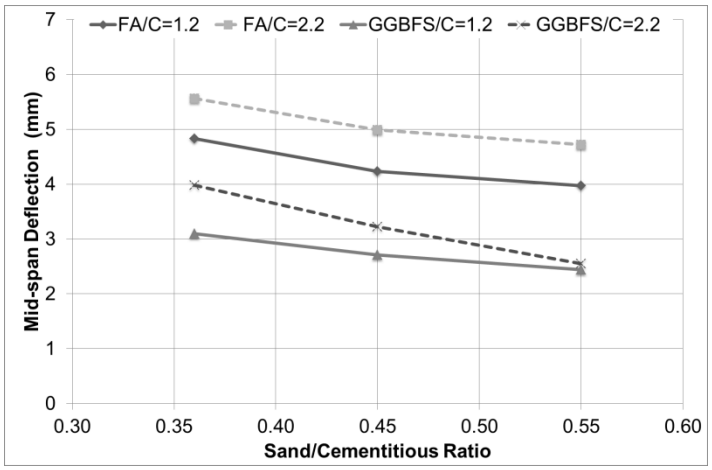

b. 28 days

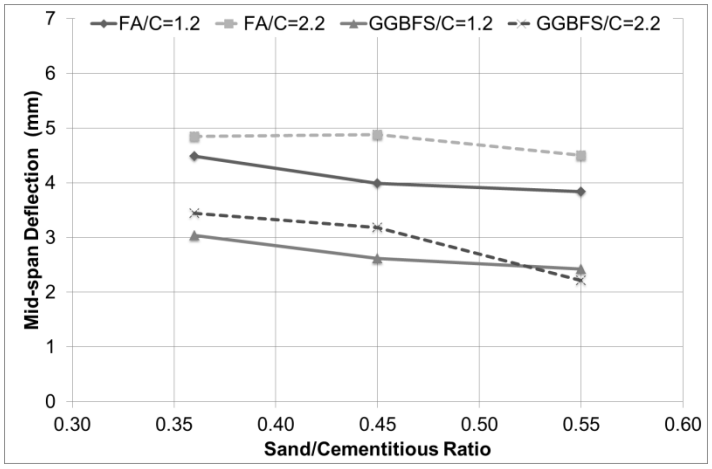

c. 90 days

Figure 4.6 Mid-span deflections of ECC mixtures

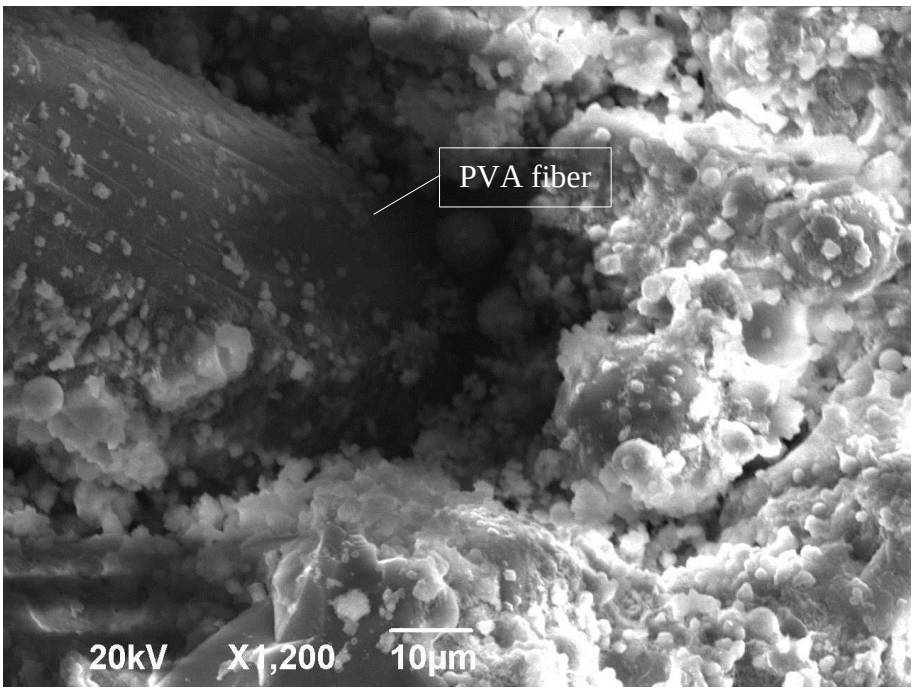

Figure 4.7 SEM image of a fiber in a FA containing specimen

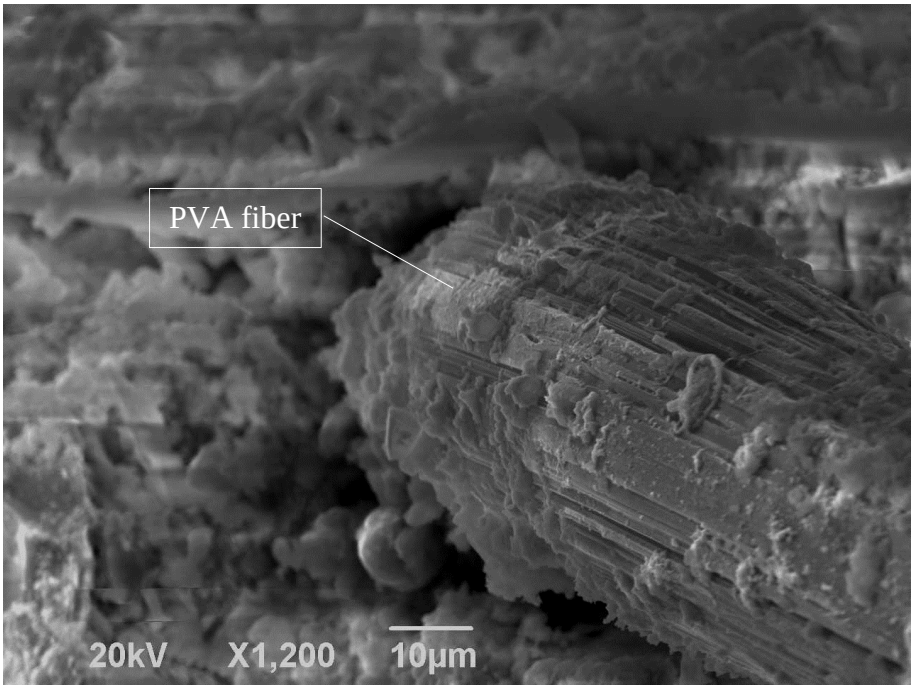

Figure 4.8 SEM image of a fiber in a GGBFS containing specimen

Amount and maximum size of aggregates have an adverse effect on the deformation capacity of mixtures as can be seen in Figure 4.6 and 4.9. Increase in aggregate size may result in poor fiber distribution which may prevent sufficient coating of fibers by the matrix and reduce the effective fiber content which subsequently decreases the ductility (Soroushian et al., 1992). As the amount and maximum size of aggregate increases, matrix fracture toughness increases which lowers the possibility of multiple cracking to attain strain-hardening behavior (Li, 1998; Li et al., 1995).

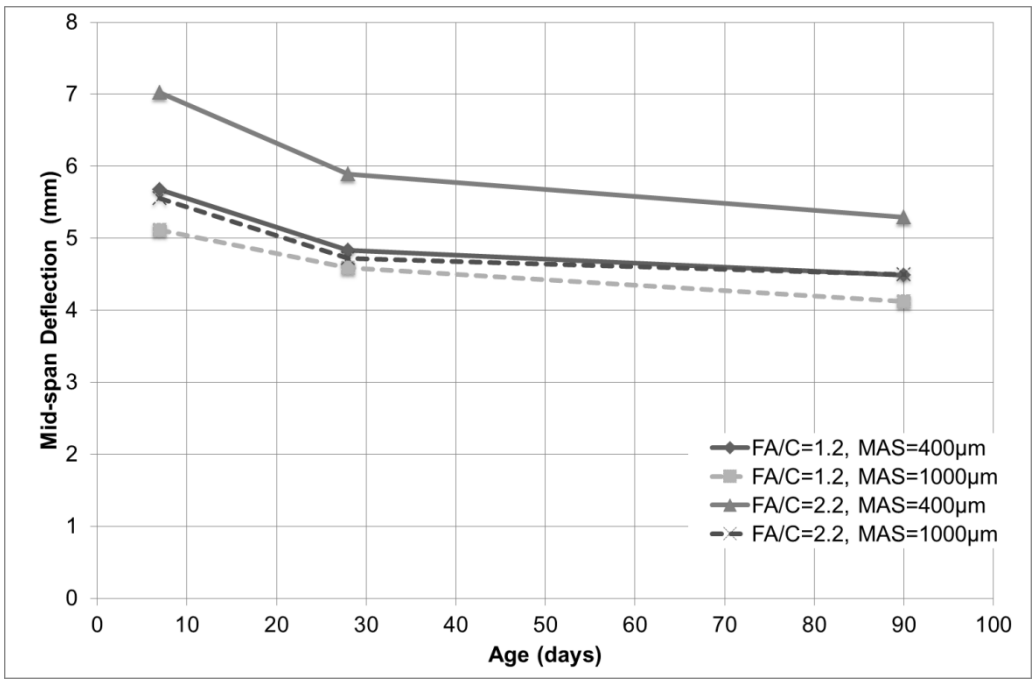

a. FA mixtures

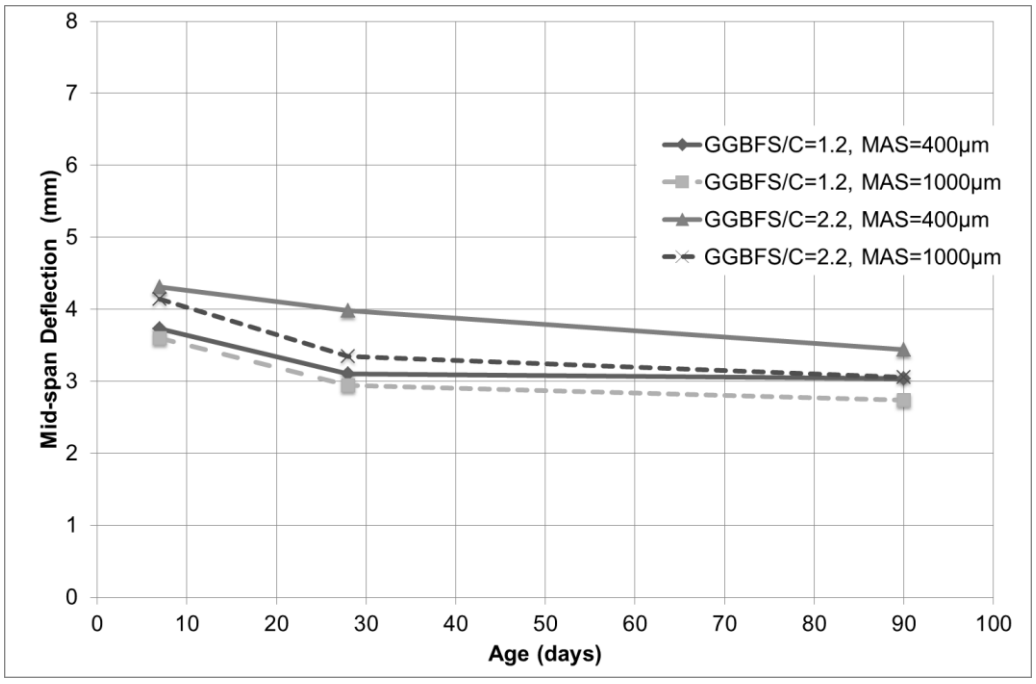

b. GGBFS mixtures

Figure 4.9 Effect of MAS on mid-span deflection of mixtures with sand to cementitious ratio of 0.36

4.2.3 Crack Characterization

After unloading at the end of flexural strength tests, cracks on the specimens were investigated in terms of crack widths and numbers. All tested specimens exhibited multiple microcracks with a small average crack width, fine crack spacing and different number under flexural loading (Figure 4.10).

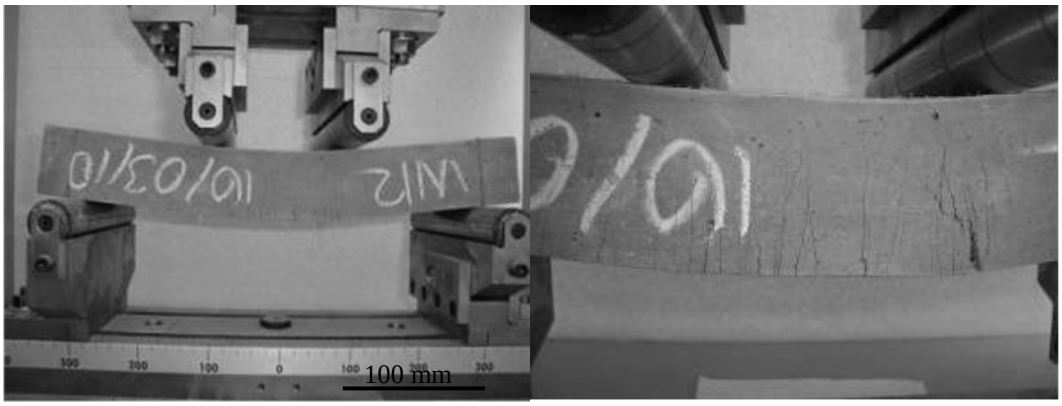

Figure 4.10 Typical cracking patterns of ECC beam specimen after flexural loading

With crack width measurement on the surface of the specimens, it has been indicated that average crack width was lower than 90 μm in average for GGBFS containing mixtures and 70 μm on average for FA containing mixtures. It was also found that the crack width reduces significantly as FA content increased, at all ages. The reason for this is not exactly known, but is probably associated with the enhanced fiber slippage due to spherical shaped FA particles along the fiber-matrix interface and more uniform distribution of fibers throughout the matrix. However, the use of aggregate up to 1000 μm MAS and 0.55 aggregate/binder ratio did not influence the average residual crack width. For many reinforced concrete applications, crack width control is of primary importance, since it is believed that there is a close relationship between the mean or maximum crack widths and the

durability of the structure (Lepech and Li, 2005; Şahmaran and Li, 2009-a). Water flow, or permeability, is proportional to crack width cubed, which means ECC with multiple number of cracks with small crack widths is less permeable than that with one large crack width. Moreover, the lower magnitude of the crack width is expected to promote the self-healing behavior, and thus the transport properties in cracked composites (Yang et al., 2005; Lepech and Li, 2005; Şahmaran et al., 2007-a; Şahmaran and Li, 2009-b). Consequently, in the serviceability limit state a mean or maximum crack width less than about 100 μm is usually prescribed (Evardsen, 1999; Reinhardt and Jooss, 2003).

4.2.3 Matrix Fracture Toughness

Matrix fracture toughness tests were conducted on specimens prepared without fibers and determined by three point bending test as described in Chapter 3. Results are tabulated in Table 4.14. Matrix fracture toughness of mixtures containing GGBFS are higher than those containing FA as seen in Figure 4.11. This is a result of low porosity and pore size, as shown in Figure 4.12, attained by GGBFS hydration, activated by portland cement hydration products, even at early ages. The pores in ECC matrix may act as stress concentrators and the size of their stress intensity field will reduce with a reduction in the pore size. Therefore fracture toughness can be controlled by the total porosity and pore size distribution of the hardened ECC matrix. Correlation between higher fracture toughness and lower porosity in cement mortar was shown by Mai and Cotterell (1985) which is in compliance with the results of this study. In order to provide sufficiently low matrix toughness values for mixtures containing GGBFS, aggregate size and amount should be limited since they increase the fracture toughness as seen in Figure 4.11 and 4.13. Chance of mixtures containing FA to achieve strain-hardening behavior is higher as those mixtures possess lower matrix fracture toughness.

Test results also indicate that the FA particles should be helpful for achieving strain-hardening behavior, as a lower fracture toughness value increases the opportunity for multiple cracking in the composite.

Table 4.4 Matrix fracture toughness of ECC mixtures at 28 days

Mix ID	**Matrix Fracture Toughness ($MPa \times m^{1/2}$)**	
	28 day	**90 day**
F1	0.536	0.662
F2	0.580	0.712
F3	0.627	0.788
F4	0.624	0.700
F5	0.356	0.534
F6	0.424	0.551
F7	0.522	0.647
F8	0.452	0.575
S1	0.795	0.801
S2	0.827	0.839
S3	0.840	0.898
S4	0.778	0.817
S5	0.712	0.728
S6	0.715	0.756
S7	0.747	0.795
S8	0.726	0.799

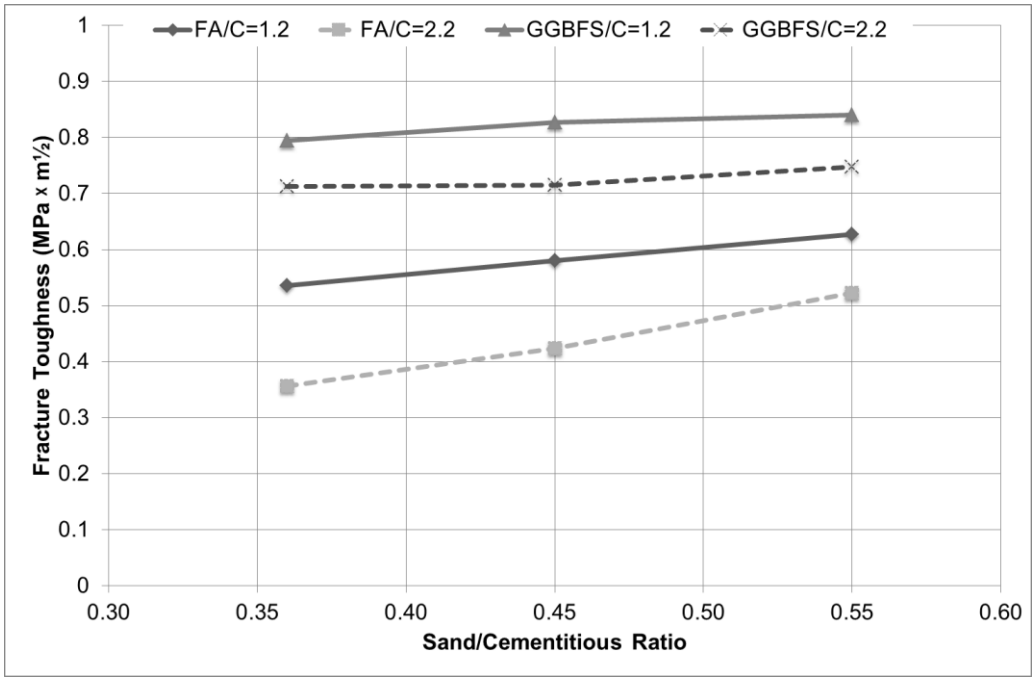

a. 28 days

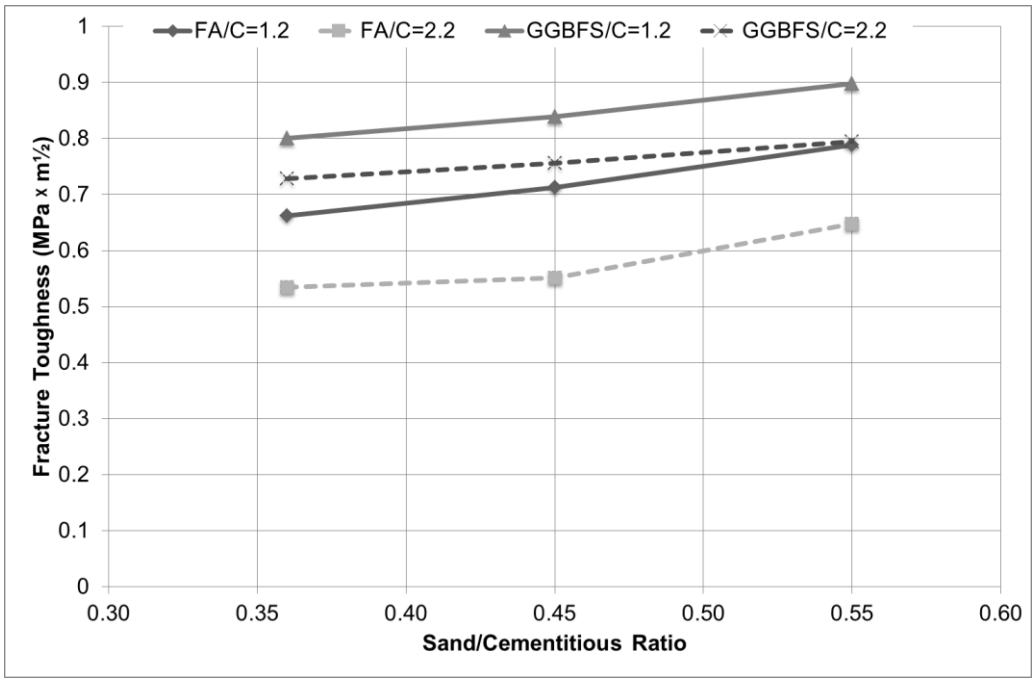

b. 90 days

Figure 4.11 Fracture toughnesses of ECC matrixes

Use of higher amount and maximum size of aggregate increase the fracture energy of the matrix significantly since cracks prefer to propagate along the weaker ITZ instead of passing through the strong aggregates. Therefore cracks deflect and travel around aggregate particles and as the amount and size of aggregates increase, crack path becomes more tortuous that requires higher energy for cracking hence yields higher fracture toughness (Davis and Alexander, 1989; Davis and Alexander, 1992; De Larrard and Belloc, 1997; Chen and Liu, 2004).

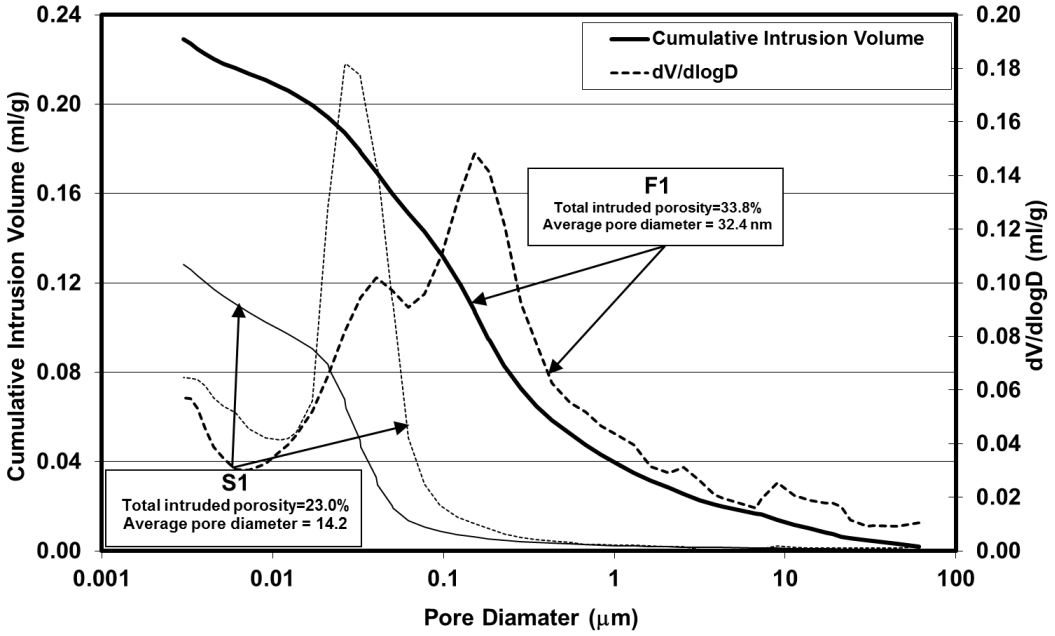

Figure 4.12 Pore size distribution of ECC mixtures with fly ash and GGBFS at 28 days

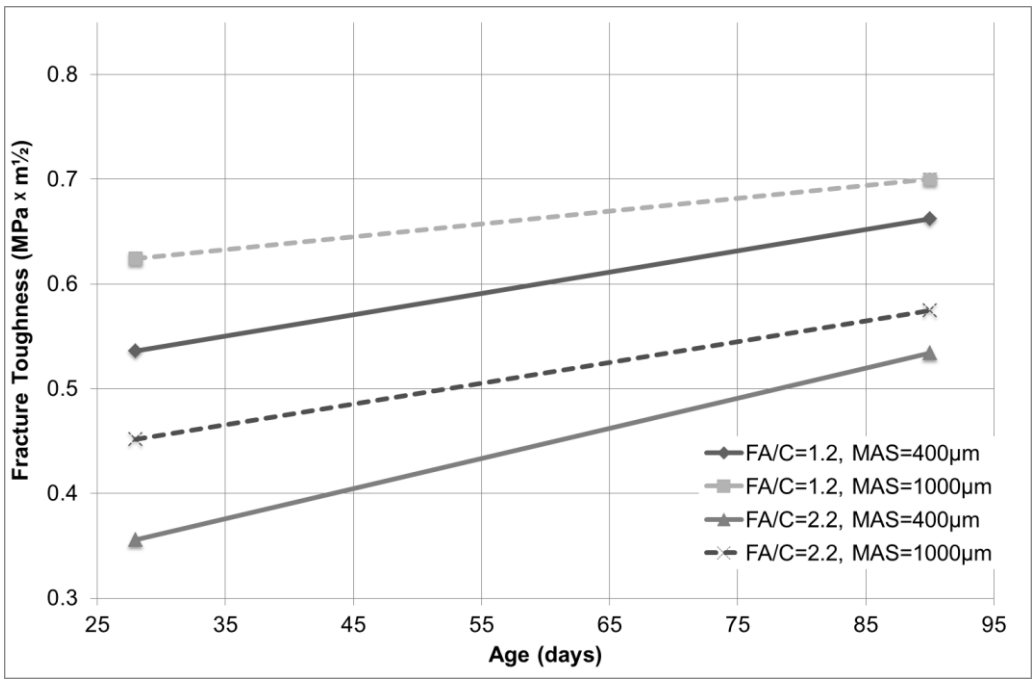

a. FA mixtures

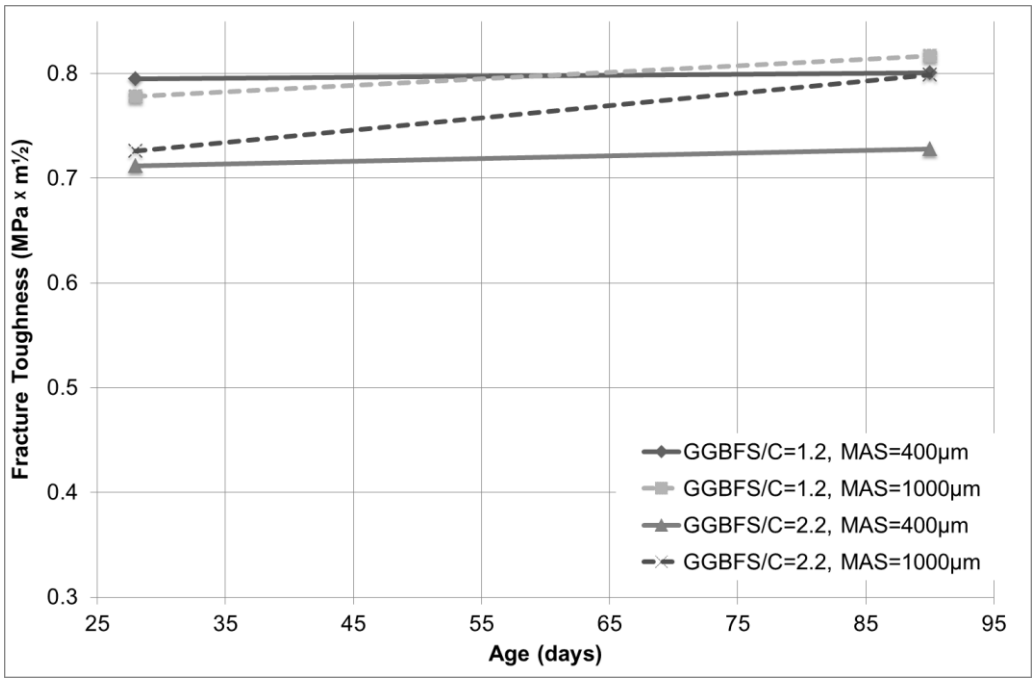

b. GGBFS mixtures

Figure 4.13 Effect of MAS on fracture toughness of ECC matrixes with sand to cementitious ratio of 0.36

According to micromechanical design principles of steady state cracking which is vital to attain strain-hardening behavior, if the matrix fracture toughness is high, the margin to develop multiple cracking reduces (Li et al., 1995; Li, 1998). In Figure 4.14, the relation between the matrix fracture toughness and mid-span beam deflection values obtained from four point bending test is shown. As can be seen clearly there is an almost inverse proportion between mid-span beam deflection and matrix fracture toughness with an inverse linear correlation of 0.85.

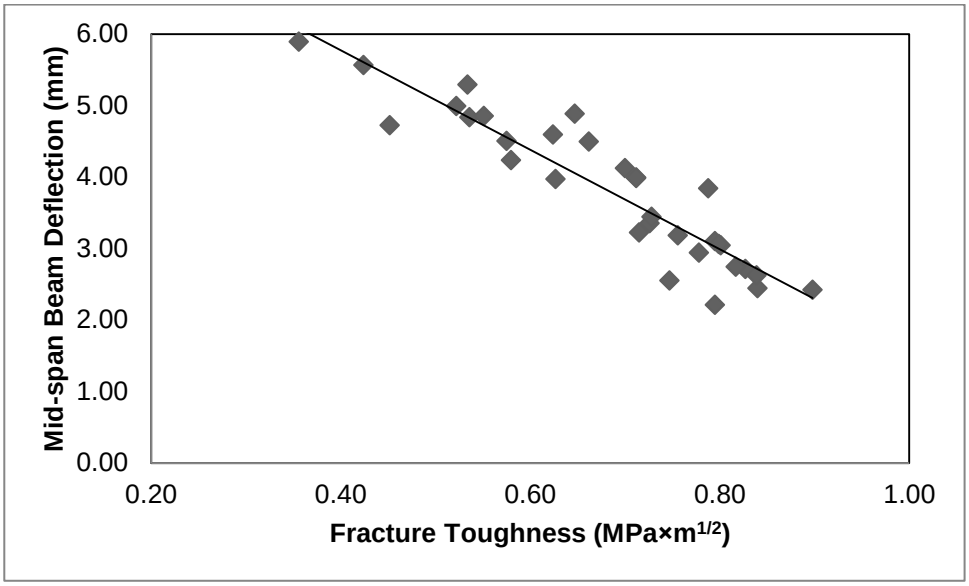

Figure 4.14 Correlation between fracture toughness and mid-span beam deflection

4.2.4 Drying Shrinkage

In Table 4.5, drying shrinkage test results are presented up to 180 days of drying after 28 days of moisture curing. The percent change in drying shrinkage with respect to mixtures with mineral admixture to cement ratio of 1.2, sand to cementitious material ratio of 0.36 and MAS of 400 μm are given in Figure 4.15. The results revealed that the use of additional mineral admixture (regardless of type

of mineral admixture) reduced the drying shrinkage. There is about 12% reduction in drying shrinkage when FA to cement ratio is increased to 2.2 from 1.2 at the age of 180 days. This difference is about 33% for 7 days and 16% for 28 days. This can be attributed to denser matrix due to FA usage which prevents internal moisture loss (Maslehuddin et al., 1987). Alternatively, as the amount of unhydrated particles acting like aggregates in mixtures with higher FA content is larger, they provide restraints for drying shrinkage and also yield coarser pore structures that result in lower surface tension due to menisci formation hence lower shrinkage (Şahmaran et al., 2007-b; Zhang, 1995; Bisaillon et al., 1994).

Table 4.5 Drying shrinkage of ECC mixtures

Mix ID	**Drying shrinkage (με)**			
	1 day	**7 day**	**28 day**	**180 day**
F1	353	692	1157	1527
F2	317	616	1010	1373
F3	305	581	951	1218
F4	297	651	1150	1469
F5	244	466	968	1349
F6	206	402	897	1217
F7	145	335	771	1079
F8	238	445	934	1288
S1	427	991	1477	1761
S2	449	918	1347	1596
S3	250	870	1273	1447
S4	409	1008	1442	1727
S5	416	986	1337	1662
S6	325	868	1250	1529
S7	298	747	1108	1397
S8	407	923	1275	1630

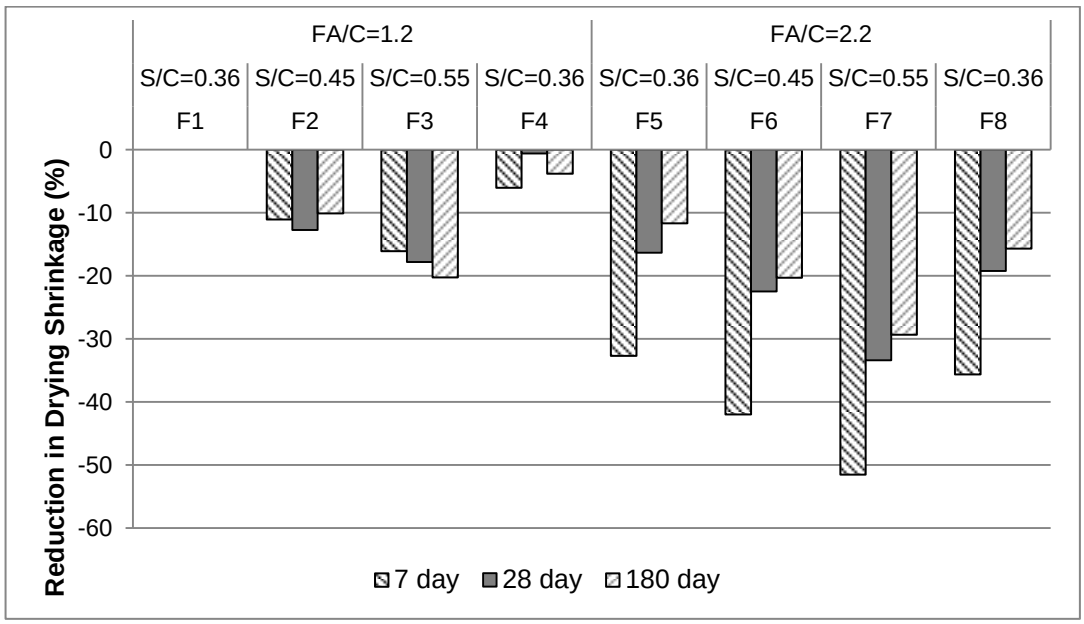

a. FA mixtures

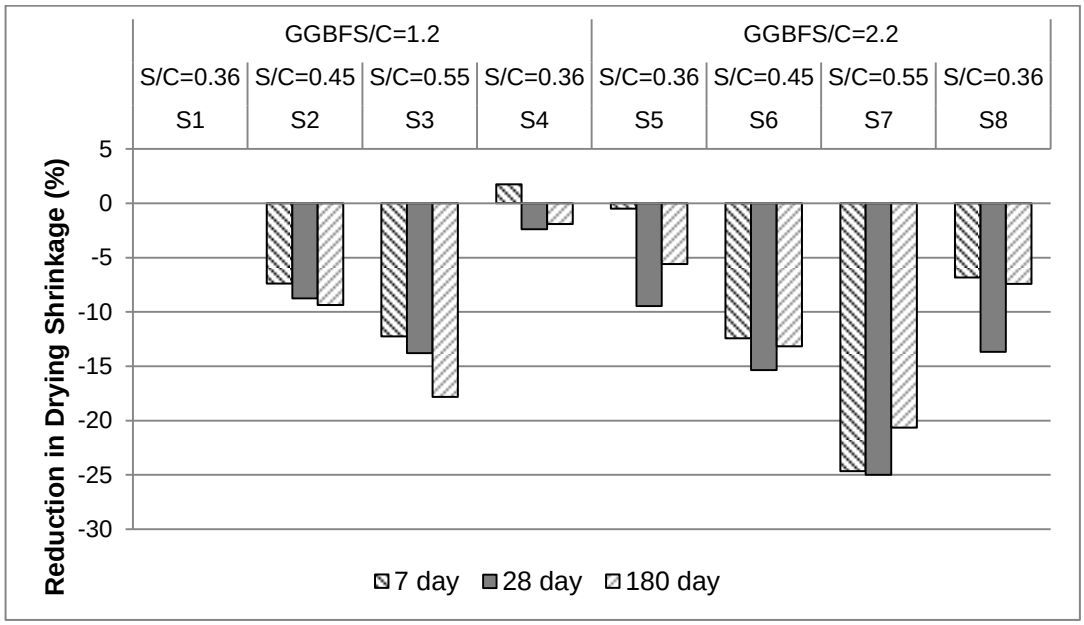

b. GGBFS mixtures

Figure 4.15 Percent change in drying shrinkage of mixtures with respect to control mixtures

ECC mixtures containing GGBFS tend to have higher ultimate drying shrinkage compared with similar mixtures containing FA as seen in Figure 4.16. For instance, free drying shrinkage of the mixture with GGBFS to cement ratio of 1.2, experience about an average 17% higher shrinkage than mixtures with FA to cement ratio of 1.2. This difference is about 26% on average for mixtures with mineral admixture to cement ratio of 2.2. It is clearly seen that increase in GGBFS content results in a higher difference in drying shrinkage of specimens with respect to similar mixtures containing FA.

This increase can be attributed to enhanced pore size refinement mechanism of GGBFS. As seen in Figure 4.11, the porosity of hardened ECC mixtures with GGBFS is much lower and has finer pore sizes than mixtures with FA, which may proportionately increase drying shrinkage (Rao, 2001). Another reason may be the higher autogenous shrinkage of GGBFS containing mixtures, since some of drying shrinkage measured is actually due to autogenous shrinkage. As the mineral admixture replacement level increases, the total porosity and average pore diameter also increase. For a given aggregate content and size, a reduction up to 6% of drying shrinkage is observed when the GGBFS to cement ratio is increased from 1.2 to 2.2.

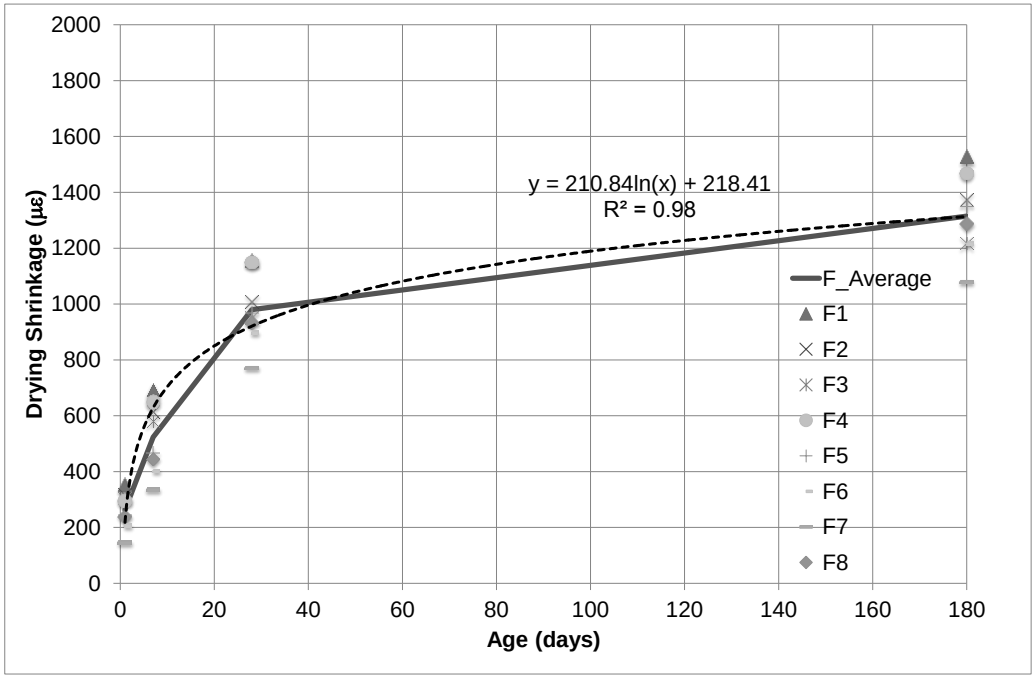

a. FA mixtures

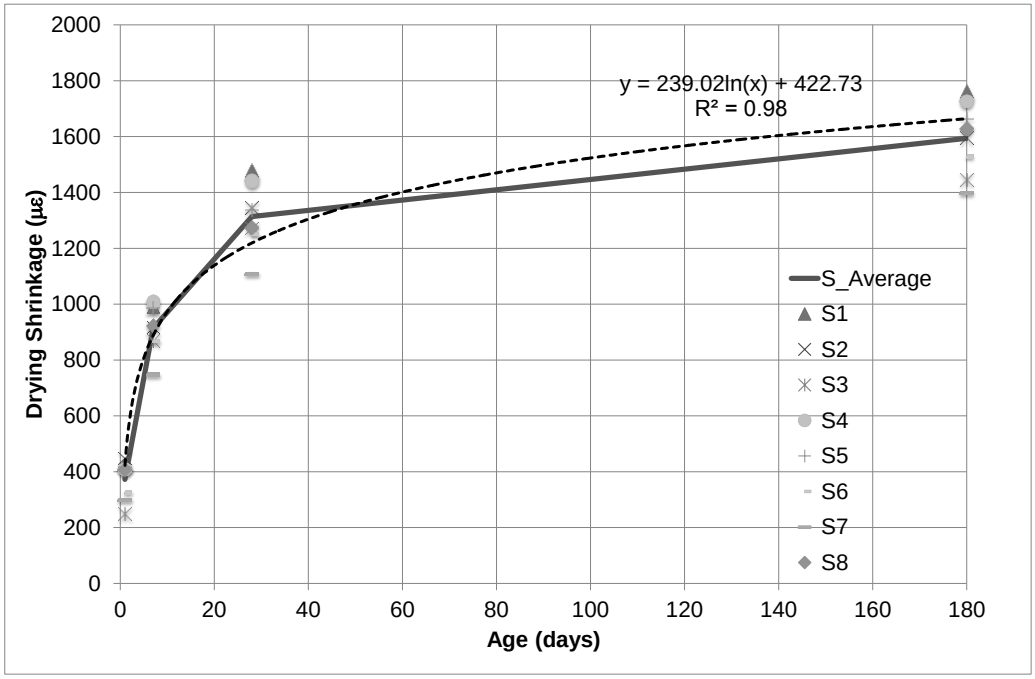

b. GGBFS mixtures

Figure 4.16 Drying shrinkage strain development of ECC mixtures

Even though both aggregate amount and size are both effective on drying shrinkage, aggregate amount has a more pronounce effect compared to the effect of maximum aggregate size which is more visible at long term as seen in Figure 4.17 and 4.18. This is a result of restraining effect of aggregates and coarser pore structure provided by them as discussed earlier.

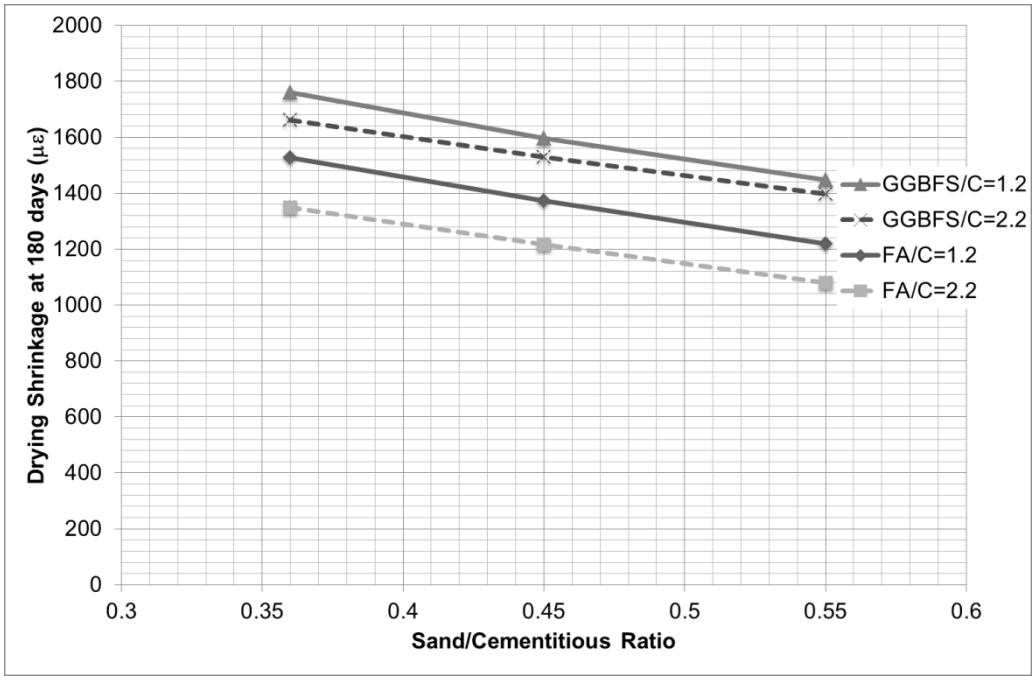

Figure 4.17 Effect of sand to cementitious material ratio on drying shrinkage

It can be concluded that within the used aggregate size in the range of this study, restraining effect of the silica sand in the ECC mixtures was too small to contribute significantly to drying shrinkage.

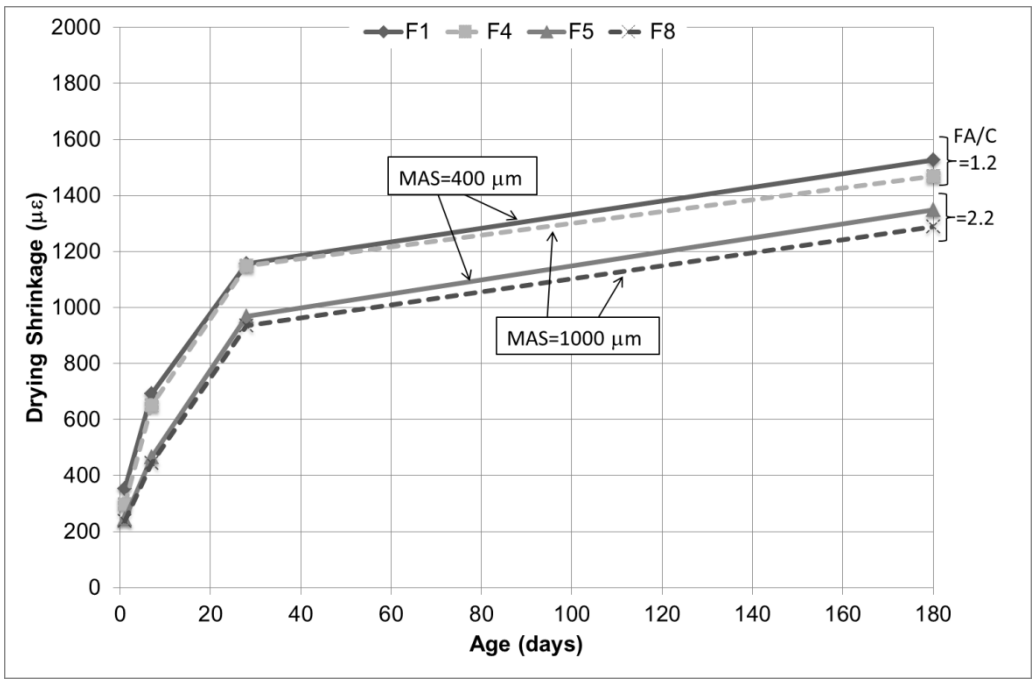

a. FA mixtures

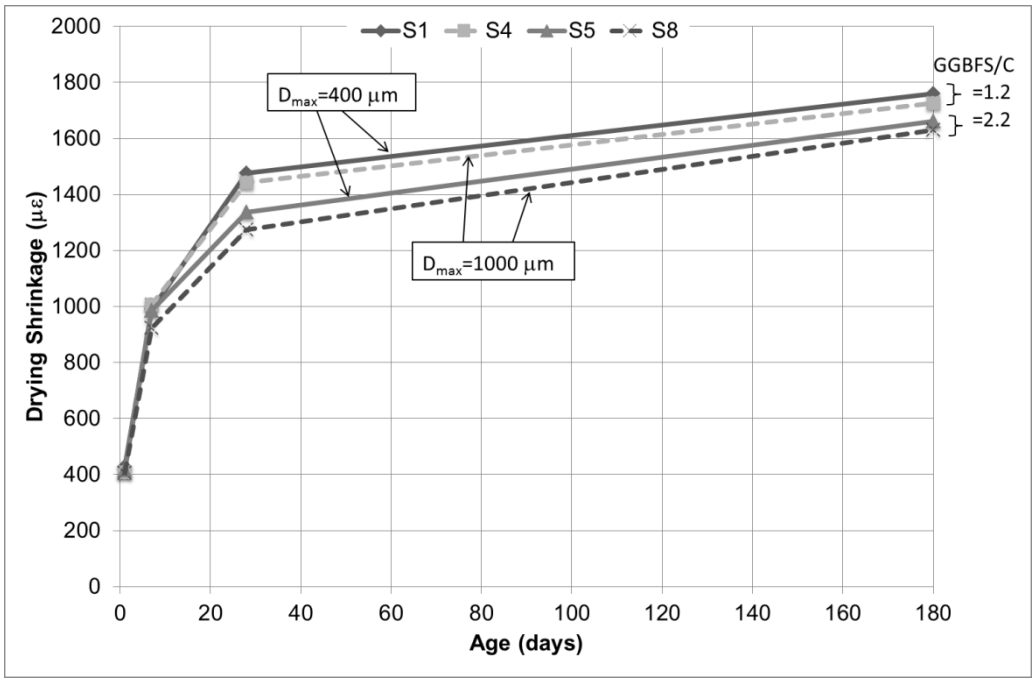

b. GGBFS mixtures

Figure 4.18 Effect of MAS on drying shrinkage strain development

4.2.5 Autogenous Shrinkage

Total autogenous shrinkages of the ECC mixtures at 28 days are summarized in Table 4.6. In the literature, data on the autogenous shrinkage of ECC mixtures is quiet limited. The only data that was available was measured by Sahmaran et al. (2009) using a different test procedure. The 28 day autogenous shrinkage values obtained in this study are significantly lower than those obtained by Şahmaran et al. (2009) mainly due to difference in the methods used to measure the autogenous shrinkage. Autogenous shrinkage developments of FA and GGBFS containing ECC mixtures up to 28 days are presented in Figure 4.19 and 4.20, respectively. As seen from Figure 4.19-a, FA specimens with FA to cement ratio of 1.2 experienced an instant autogenous shrinkage within a couple of days after initiation of the test and reached about 25% of their 28 day measured autogenous shrinkage value. Even though there are differences in trends of autogenous shrinkage strain development of FA and GGBFS mixtures which will be explained further in detail, GGBFS mixtures also exhibit high autogenous shrinkage. Thus, early age autogenous shrinkage should not be overlooked, since the specimens are more prone to cracking especially at early ages due to their lower tensile strength and lower fiber matrix frictional bond.

Table 4.6 Autogenous shrinkage of ECC mixtures

Mix ID	Autogenous Shrinkage (με)	Mix ID	Autogenous Shrinkage (με)
	28 day		28 day
F 1	442	S 1	680
F 2	386	S 2	599
F 3	334	S 3	542
F 4	419	S 4	644
F 5	300	S 5	660
F 6	252	S 6	582
F 7	216	S 7	510
F 8	296	S 8	630

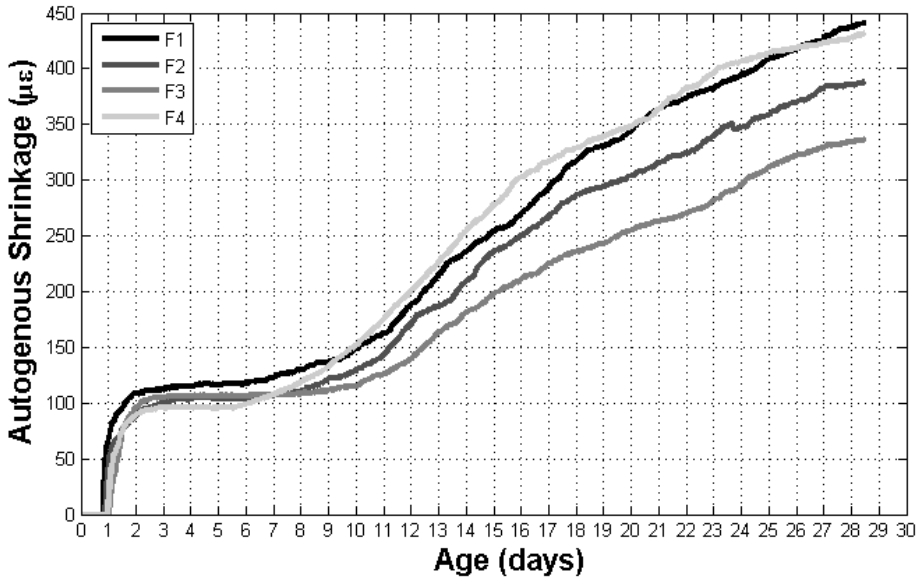

a. FA/C=1.2

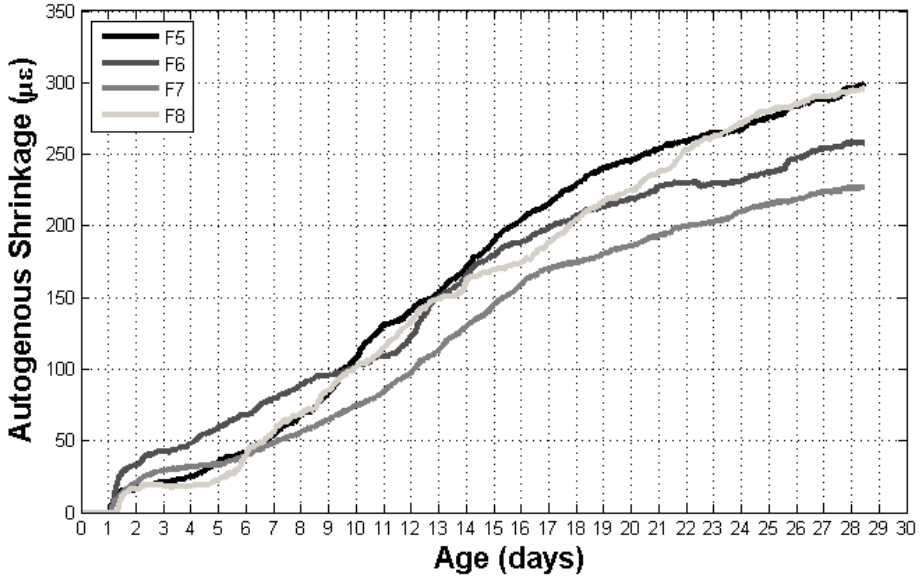

b. FA/C=2.2

Figure 4.19 Autogenous shrinkages of mixtures with FA

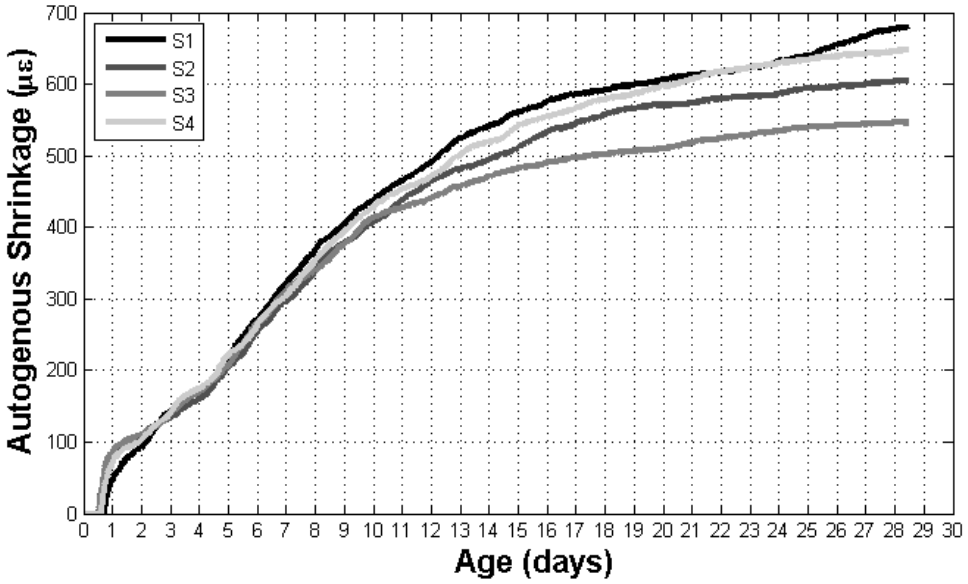

a. GGBFS/C=1.2

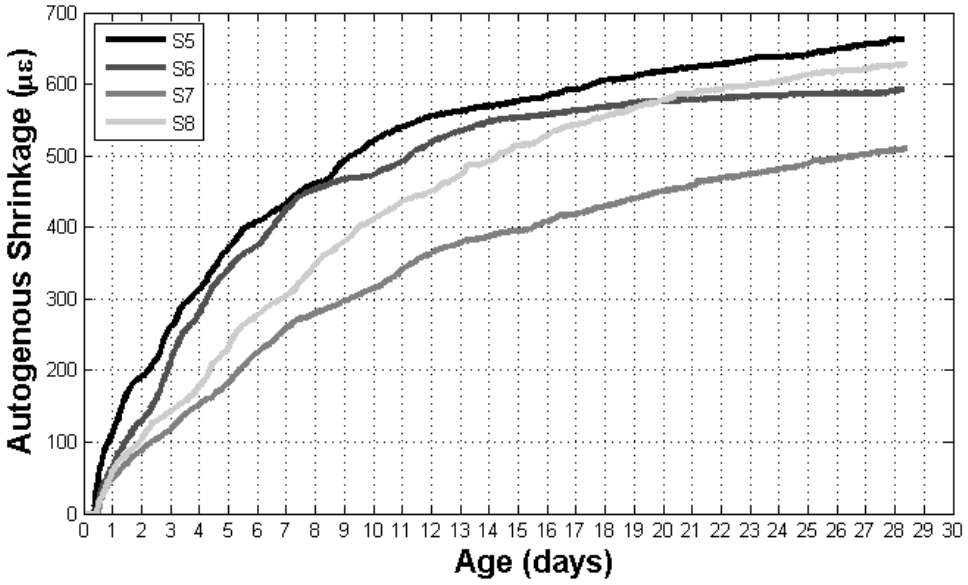

b. GGBFS/C=2.2

Figure 4.20 Autogenous shrinkages of mixtures with GGBFS

Autogenous shrinkage of a cementitious material should be considered in two separate stages. At all stages of hydration (both early and later ages) the volumetric difference between reactants and products of hydration reaction also referred to chemical shrinkage occurs. The amount of chemical and autogenous shrinkage is equal till the formation of solid skeleton which corresponds nearly to final setting time. After the formation of solid skeleton, a mechanism similar to drying shrinkage which is called self-desiccation is dominant on autogenous shrinkage. Self-desiccation is the internal drying of cementitious material as the water is consumed in the hydration reaction. Since there is always available water in the system at the early ages of hydration, self-desiccation does not occur at the early ages.

As in the drying shrinkage, capillary porosity and pore size have great importance on the amount and development on autogenous shrinkage strains. The relationship between the pore size and shrinkage is described by three mechanisms known as capillary tension, surface tension and disjoining pressure. Capillary pores which are formed during the hydration are filled with water and as the water is consumed for further hydration, the humidity of the pores decrease. As the humidity drops, a meniscus forms together with surface tension inside capillary pores. As a result, capillary tensile pressure develops which is balanced by compressive stress in neighboring particles that result in volumetric reduction. Solids in touch with other materials have surface tension in their interfaces. The amount of surface tension is dependent on the thickness of adsorbed water. As the water is removed, surface tension increases yielding compressive stresses on solids which results in shrinkage. C-S-H particles have large surface area which attracts water at the interfaces, resulting repulsion between layers called disjoining pressure. Disjoining pressure decreases with the decrease in the thickness of adsorbed water. During drying, as disjoining pressure decreases, shrinkage occurs. It is clear that relative humidity plays a fundamental role in the mechanism of shrinkage. As the pore diameter decreases, internal relative humidity drops quickly as shown in Figure 4.21 (Mindess et al., 2003; Wei, 2008; Holt, 2001).

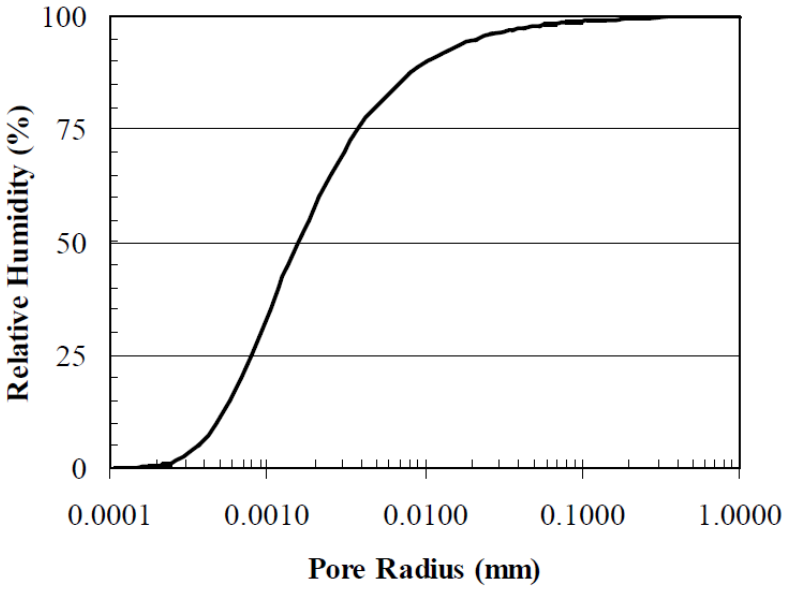

Figure 4.21 Relation between pore size and relative humidity (Holt, 2001)

During an autogenous shrinkage test, the temperature of the sample also changes and sample temperature variation measured under a specimen is also given in Figure 4.22. Temperature of the specimen increases and reaches to a maximum value about 16 hours after casting and drops until it reaches equilibrium with ambient temperature which corresponds to about 4 days after casting. While measuring the autogenous shrinkage, LVDT measurements were started 12 hours after casting while the temperature is in ascending branch. As the duration and amount of the temperature rise may vary among specimens, it is not accurate to start autogenous shrinkage calculations at 12 hours after casting. On the other hand if the calculations are started after the temperature of the specimen reaches equilibrium, early age autogenous shrinkage could not be monitored. As the temperature is recorded under the inside mold of the shrinkage drain, it may not reflect the actual temperature inside the specimen. For these reasons time corresponding to maximum temperature recorded by the thermocouple located under a specimen was taken as origin for autogenous shrinkage measurements.

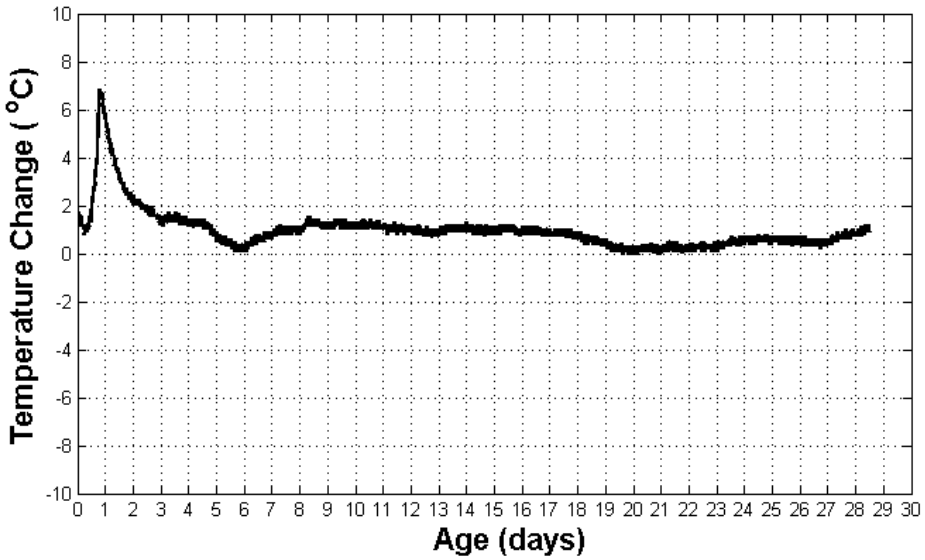

Figure 4.22 Sample temperature variation plot during autogenous shrinkages test

As can be seen in Figure 4.19, autogenous shrinkage strains of FA containing ECC mixtures develop rapidly and then stabilize for a duration about 5 days. This may be attributed to slow reaction of FA particles which does not participate in the development of autogenous shrinkage strains. It may be thought that cement hydration should result in an increase of autogenous shrinkage. However, the autogenous shrinkage due to cement hydration may be compensated by the expansion due to ettringite formation as a result of early C_3A and C_4AF hydration as mentioned by Wei (2008). As seen in Figure 4.23, total autogenous shrinkage is lower in FA containing mixtures compared to GGBFS containing ones. This may be attributed to higher porosity and larger pore sizes of FA mixtures (Figure 4.12) hence higher relative humidity in the pores. Higher relative humidity results in lower capillary stresses and thus lower autogenous shrinkage.

In the case of ECC mixtures containing GGBFS, there is no visible plateau since hydration of GGBFS starts earlier as it reacts with alkali hydroxides in the pore solution before the formation of calcium hydroxide by portland cement hydration

as discussed in compressive strength results. Expansion due to ettringite formation may be much lower than the shrinkage due to GGBFS reactions which is a possible reason for absence of a dormant period in autogenous shrinkage strains.

As seen in Figure 4.23, for all sand to cementitious material ratios total autogenous shrinkage of GGBFS containing ECC mixtures at 28 days are higher than that of FA containing mixtures which can be attributed to lower pore sizes of GGBFS containing mixtures. Smaller pores have lower relative humidity hence higher capillary stresses which results in higher autogenous shrinkage due to self-desiccation.

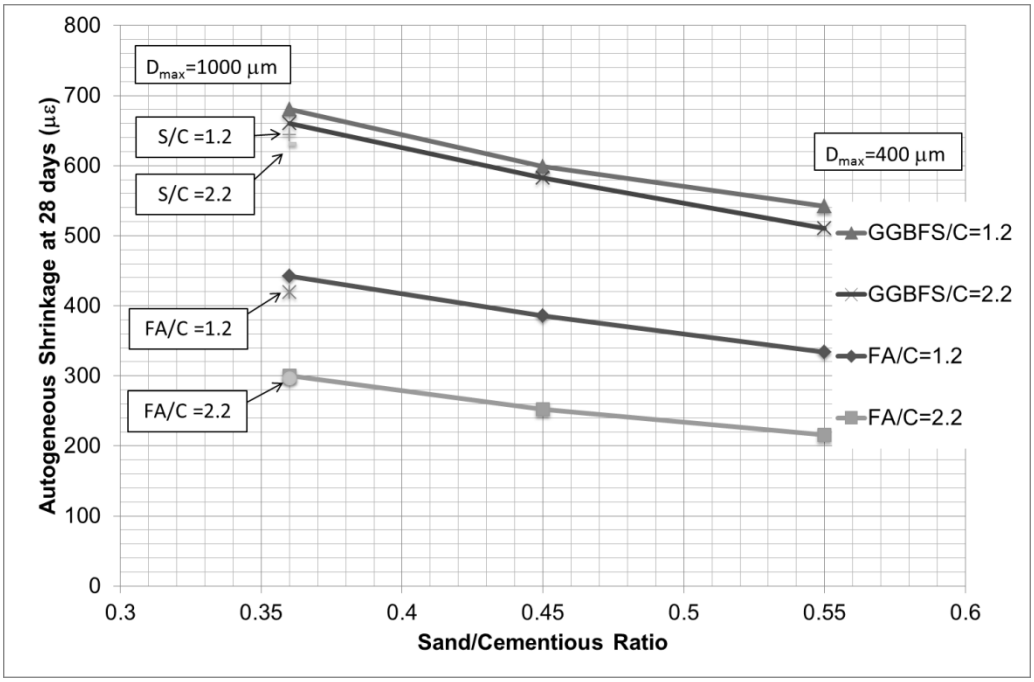

Figure 4.23 Effect of sand to cementitious ratio and MAS on autogenous shrinkage

Increase in aggregate content results in a reduction in autogenous shrinkage strains for all mixtures as they act as restraints for shrinkage and they provide a coarser

pore structure. Also, amount of binder is decreased as the amount of aggregate increases. As in the drying shrinkage test results, maximum aggregate size also reduces autogenous shrinkage as can be seen in Figure 4.23.

Test results of all ECC mixtures also indicate that autogenous shrinkage phenomenon has not stabilized after 28 days which may be attributed to the secondary hydration caused by pozzolanic reaction of FA and GGBFS.

4.2.6 Restrained Shrinkage

In order to evaluate the cracking potential of the ECC mixtures, restrained shrinkage test was conducted by using two separate setups with two different rings with different dimensions. One of the setups was designed in accordance with ASTM C 1581 (ASTM, 2009) , although this setup was intended for measuring the induced tensile strains inside the steel ring to evaluate the cracking potential, the strain data obtained were not plausible to be used in evaluation of induced tensile stresses. Also the mold described in ASTM C1581 (ASTM, 2009) provides a material thickness of 37.5 mm while the material thickness is 25 mm for the second mold. Therefore, the amount of tensile stress developed in the specimens subjected to restrained shrinkage test according to ASTM C 1581 (ASTM, 2009) is lower. Hence, time of first cracking was shifted, and limited number of cracking, even no cracking, was observed for some of the specimens. For this reason only the second setup was used for evaluation of cracking potential of mixtures. Development of average crack width with time is presented in Figure 4.25 and 4.26. Also typical crack pattern of a restrained shrinkage specimen is given in Figure 4.24.

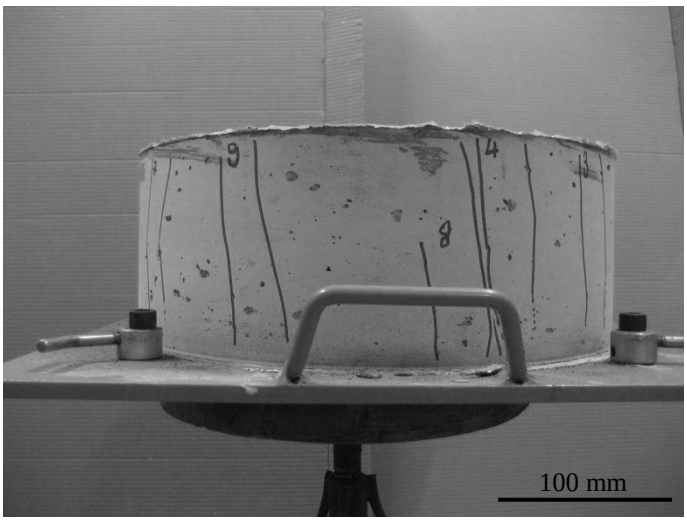

Figure 4.24 Typical crack pattern on restraining a shrinkage specimen

As can be seen from Figure 4.25 and 4.26, all mixtures exhibited a degree of multiple cracking under tensile stresses induced by restrained shrinkage. In general when a crack forms within several days crack width increases quickly and stabilizes to a constant value with time. It can be seen that for the mixtures containing GGBFS the first crack occurs between 2 to 3 days. On the other hand, for FA mixtures the first crack occurs between 4 to 8 days depending on the amount of mineral admixture and aggregate. It is very clear that FA usage shifted the age of first cracking. Also aggregate amount has the same effect with FA as the aggregate amount increases the age of the first crack formation delays proportionally for FA containing mixtures due to the restraining effect of aggregates. In addition, the average crack widths of the mixtures with FA are lower than that of mixtures with GGBFS. The use of GGBFS significantly accelerated the onset of first crack, independent of the amount of aggregate. The adverse effect of GGBFS usage can be attributed to high drying shrinkage hence high tensile stresses inside the specimens. As discussed earlier, low tensile strain capacity and low tensile creep together with high matrix toughness resulted in a dimensionally incompatible mixture compared to FA containing mixtures which performed better under restrained shrinkage conditions.

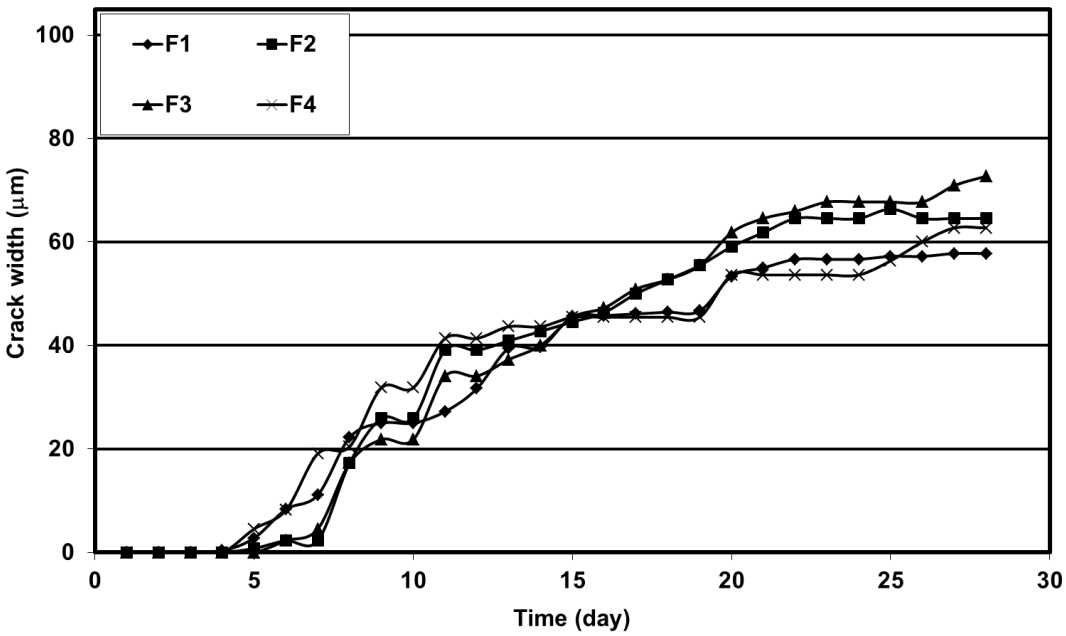

a. FA/C=1.2

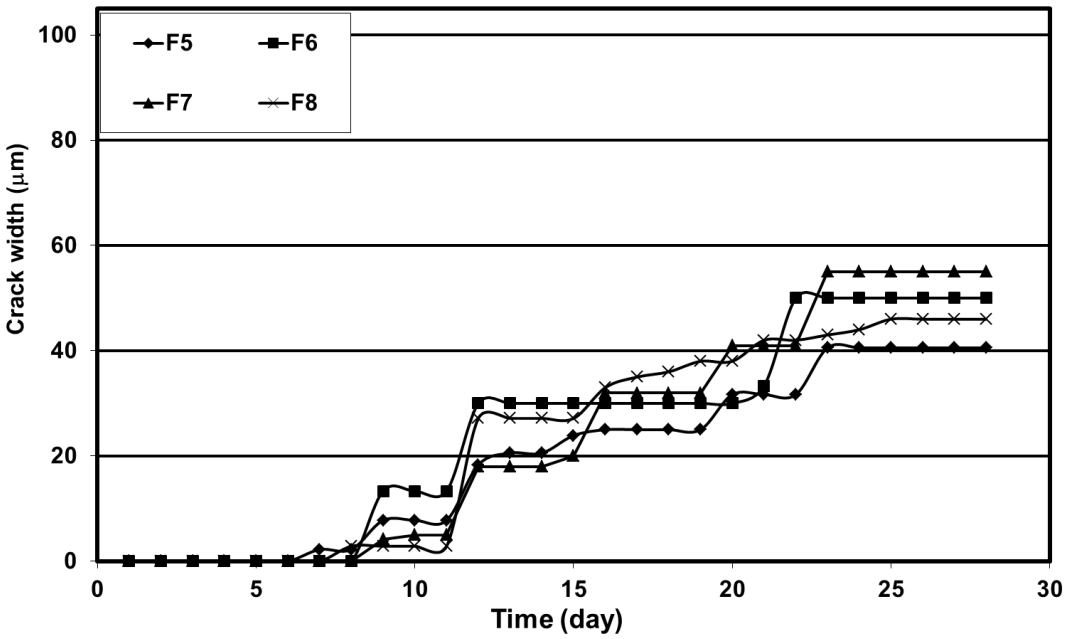

b. FA/C=2.2

Figure 4.25 Crack width development in restrained shrinkage specimens with FA

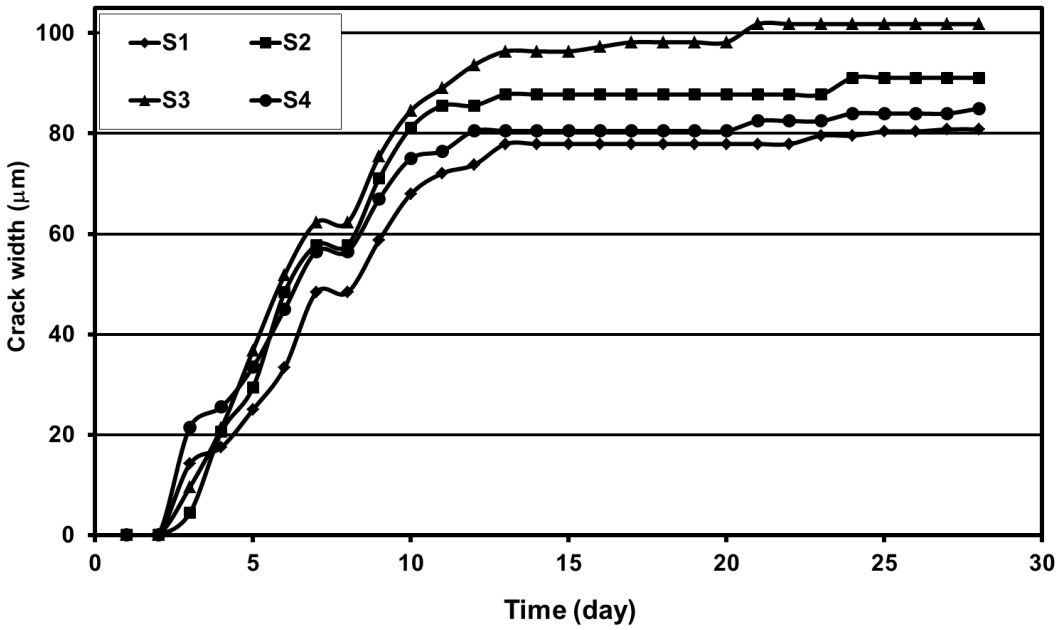

a. GGBFS/C=1.2

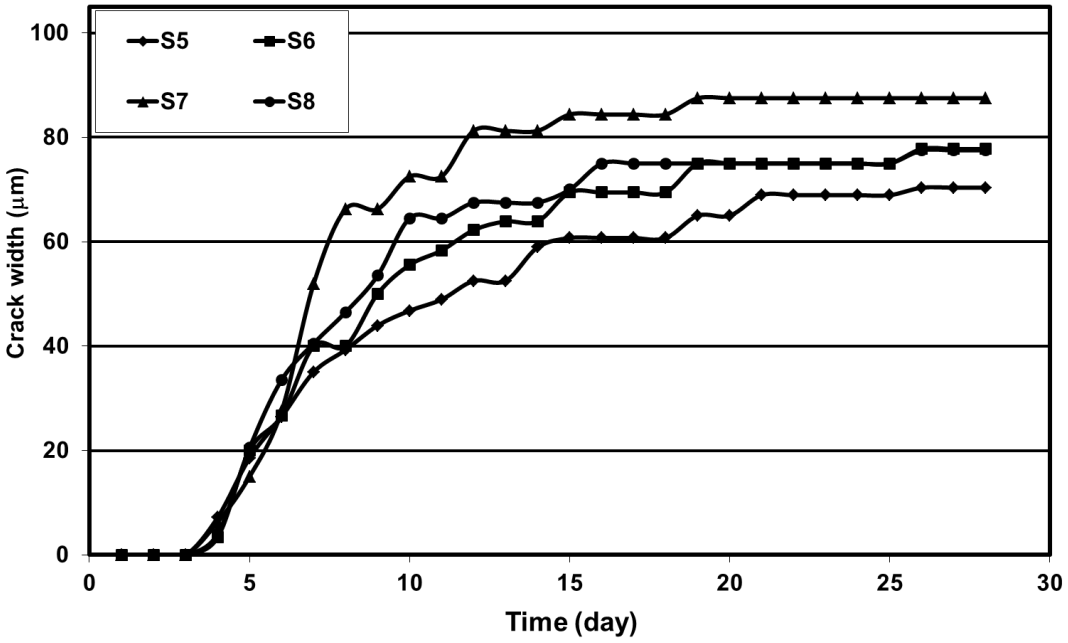

b. GGBFS/C=2.2

Figure 4.26 Crack width development in restrained shrinkage specimens with GGBFS

4.2.7 Tensile Creep

As mentioned in previous chapter, two sets of tensile creep experiments were designed. In the first set which is intended to evaluate the early age tensile creep behavior of the ECC mixtures, specimens were cured under lime saturated water for 2 days after they were demolded and kept in the laboratory conditions for the rest of the week. After the preparation of the specimens for the test, they were loaded up to 30% of their 7 day tensile strength. Tensile load gradually increased at 14 and 28 days with 30% of tensile strength determined by direct tensile test and the load was sustained 90 days on the specimens.

In the second set of experiments which is intended to evaluate standard creep behavior, specimens were cured 21 day under lime saturated water and prepared for the test during the following week and loaded at the age of 28 days with a constant tensile stress of 1.5 MPa. Together with the length change of the specimens under tensile loads, drying shrinkages were also determined in order to calculate the tensile creep of the specimens for both experimental sets. For length change measurements a digital mechanical strain gage was used with an accuracy of $\pm$ 5 x 10^{-6} strains. Two steel locating discs were glued 250 mm apart on each of four surfaces of the specimens. Average of the strains, calculated by using the length change measurements made with mechanical strain gage on total of 12 surfaces was taken. The strains calculated for each surface were sufficiently close to each other which indicate that the specimens were loaded under direct tension without eccentricity during the test. For all specimens at all ages drying shrinkage was higher than the tensile creep, hence specimens under tensile loads contracted.

Although Reinhardt and Rinder (2006) explained that the drying shrinkage of specimens under tensile creep will be higher than unloaded specimens, in order to evaluate the tensile creep behavior of the specimens, the superposition of drying shrinkage and drying tensile creep are considered as adjusted tensile creep which was calculated as algebraic sum of drying shrinkage and drying tensile creep as

depicted in Figure 4.27. Superposition of the drying tensile creep and drying shrinkage is a commonly used method for determination of the tensile creep strains.

After calculating the adjusted tensile creep, corresponding instantaneous elastic strains were also subtracted and specific creep of the specimens were determined as presented in Figure 4.28 and 4.29 for FA and GGBFS mixtures, respectively. In those plots both early age (started at 7 days) and standard creep (started at 28 days) tests were provided. Also test results are provided in Table 4.7 and 4.8.

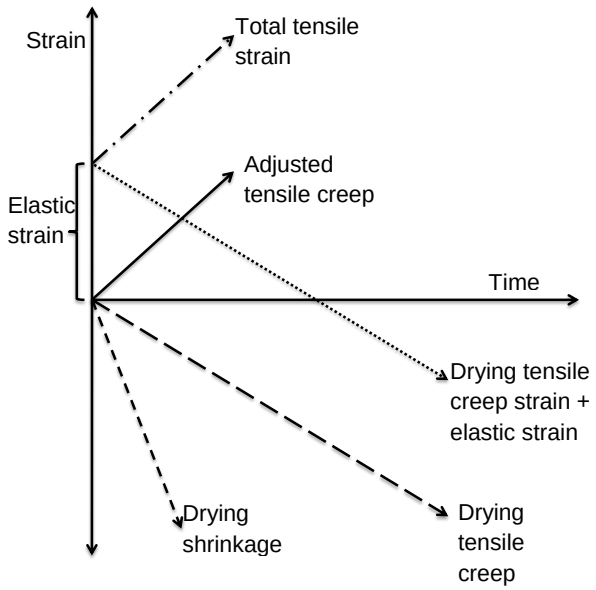

Figure 4.27 Schematic representation of elastic and time dependent strains of a tensile creep specimen

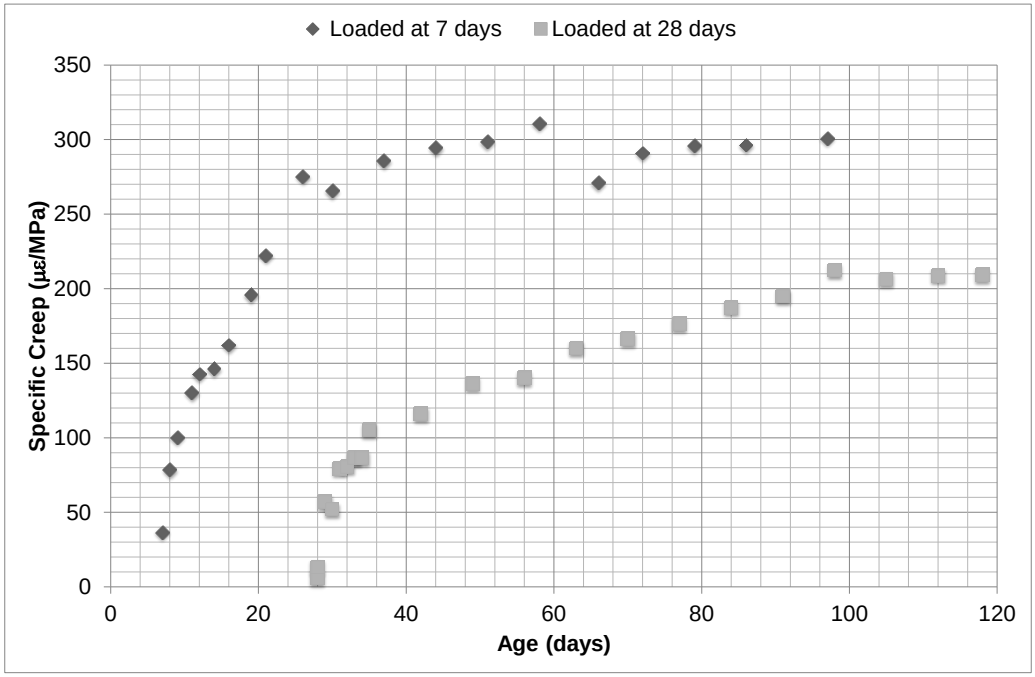

a. F1

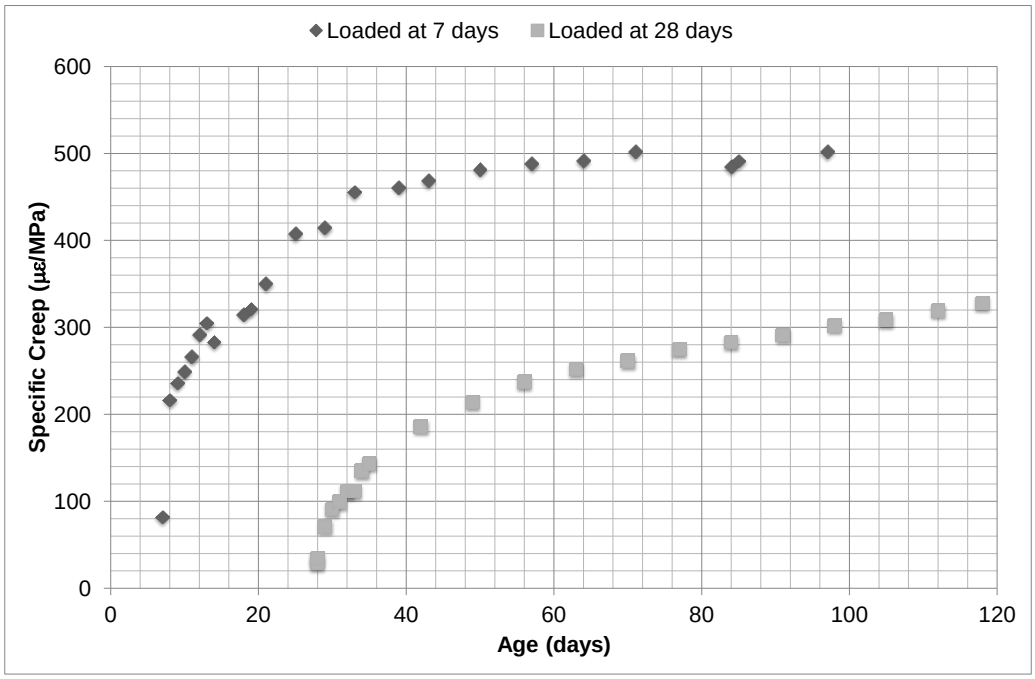

b. F5

Figure 4.28 Specific tensile creep of ECC mixtures with FA

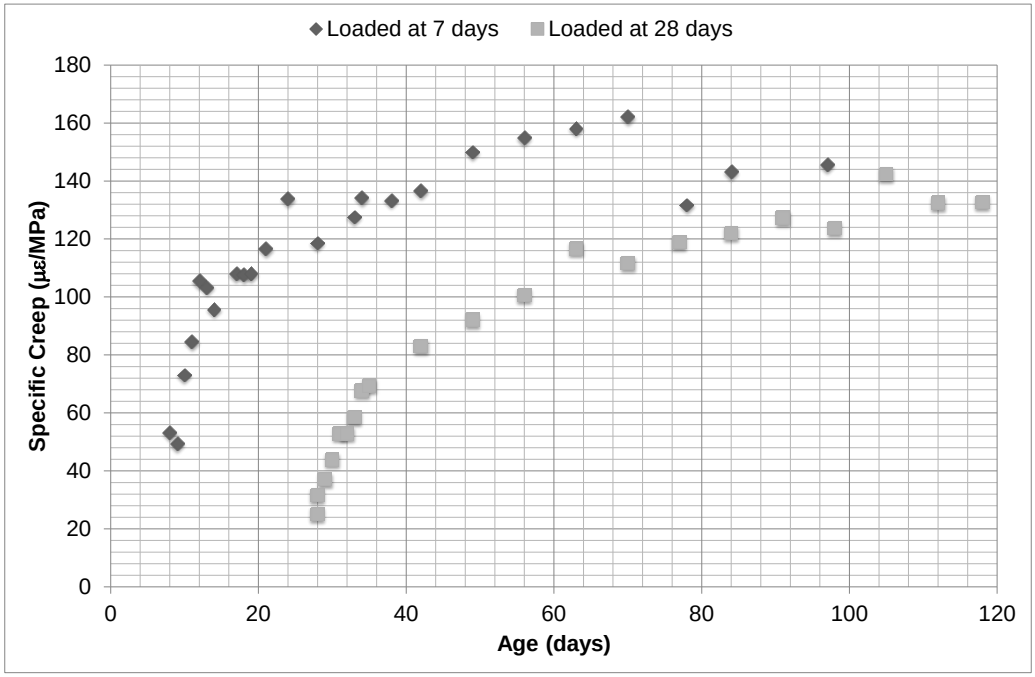

a. S1

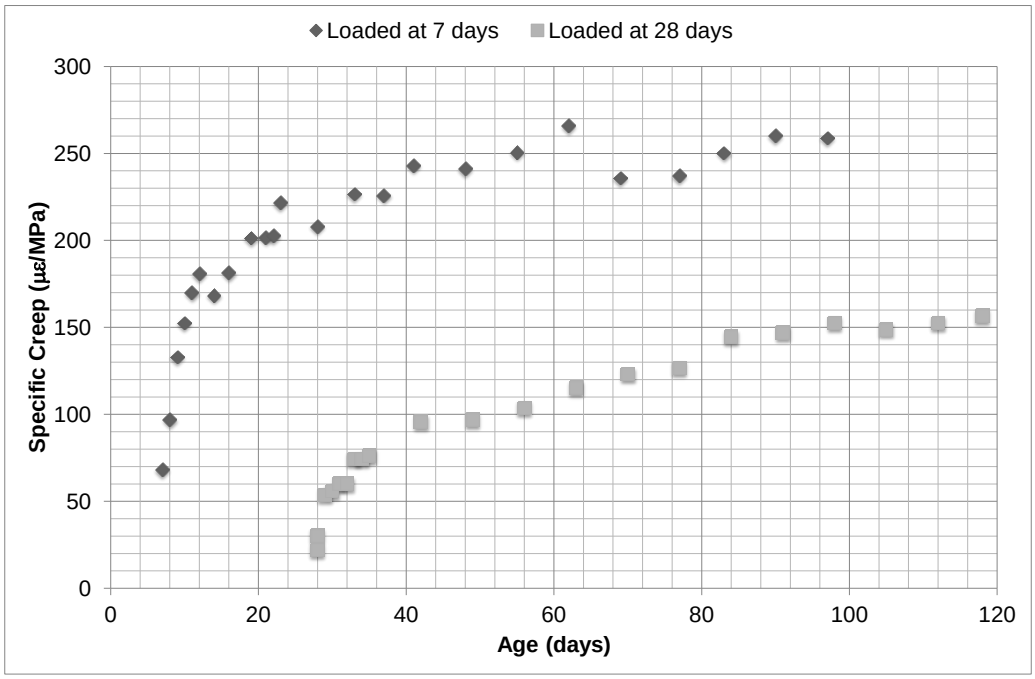

b. S5

Figure 4.29 Specific tensile creep of ECC mixtures with GGBFS

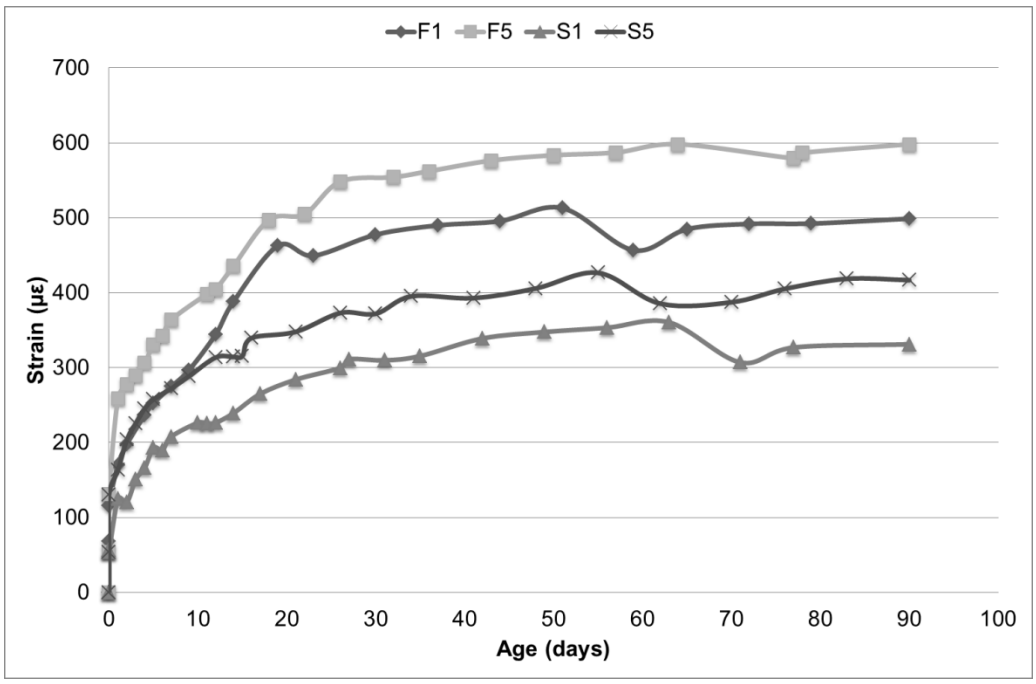

a. Specimens loaded at 7 days

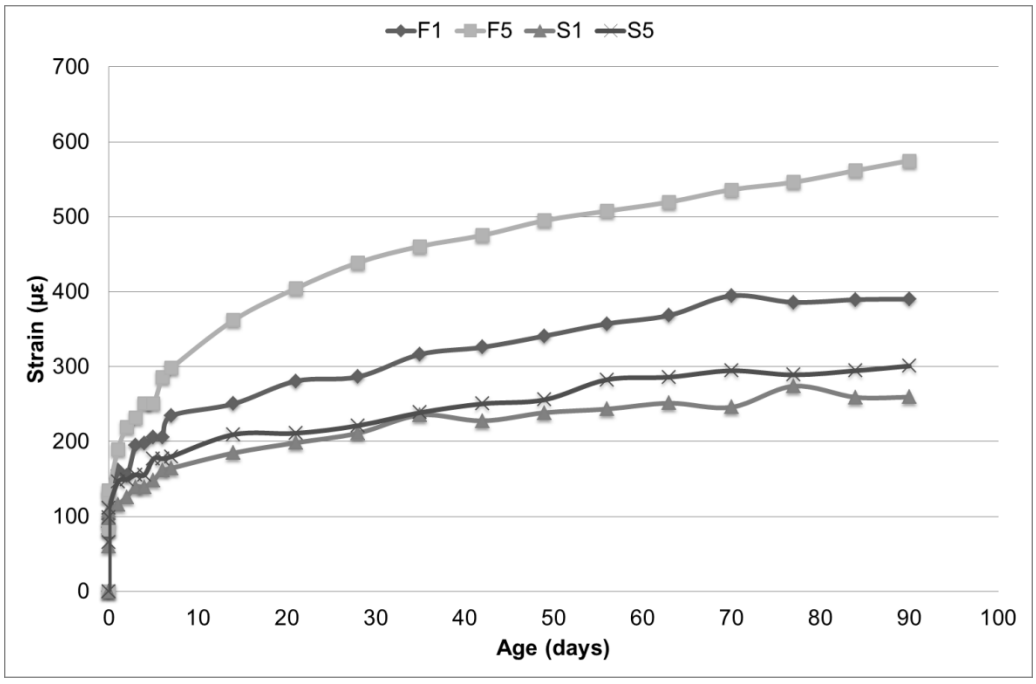

b. Specimens loaded at 28 days

Figure 4.30 Total tensile strain of ECC mixtures

As can be seen from the figures, tensile specific creep which is determined as creep strain per applied tensile stress is higher for the specimens loaded at 7 days than specimens loaded at 28 days for all tested mixtures. This may be explained by the microcracking mechanism of tensile creep together with the deformability of the ECC mixtures. As the deformability of the mixtures are higher at early ages according to the results of mid-span beam deflection tests as a result of lower matrix toughness, during the formation of microcracks under sustained tensile stresses, specimens loaded at 7 days may deform more than the specimens loaded at 28 days. This phenomenon can also be used to explain the higher tensile creep strains of FA mixtures with respect to GGBFS mixtures as seen in Figure 4.30. Moreover, higher tensile creep of mixtures with mineral admixtures to cement ratio of 2.2 with respect to that of mixtures with mineral admixture to cement ratio of 1.2, may also be explained by this theory as there is proportionality between the deformability, and tensile creep of the specimens. On the other hand, microcraks are not visible under ocular inspection; several microcracks were detected under heavy light source as seen in Figure 4.31. Boshoff and Van Zijl (2007) showed that there may be time dependent crack formation in ECC specimens under sustained tensile stresses of 50% of the materials tensile strength. However, the specimens used in that study was 16 x 30 x 80 mm in dimensions which is too small compared to the specimens used in this study and also specimens were loaded up 50% of their tensile strengths which is 30% for this study. For this reason, results are not comparable. Although, Bissonnette et al. (2007), in their study, claimed that as the calculated secant modulus of elasticity measured on companion specimens were slightly lower than that of tensile loaded specimens which validates the relation between tensile creep and microcraking for unsealed creep specimens, sealed specimens were found to be unaffected.

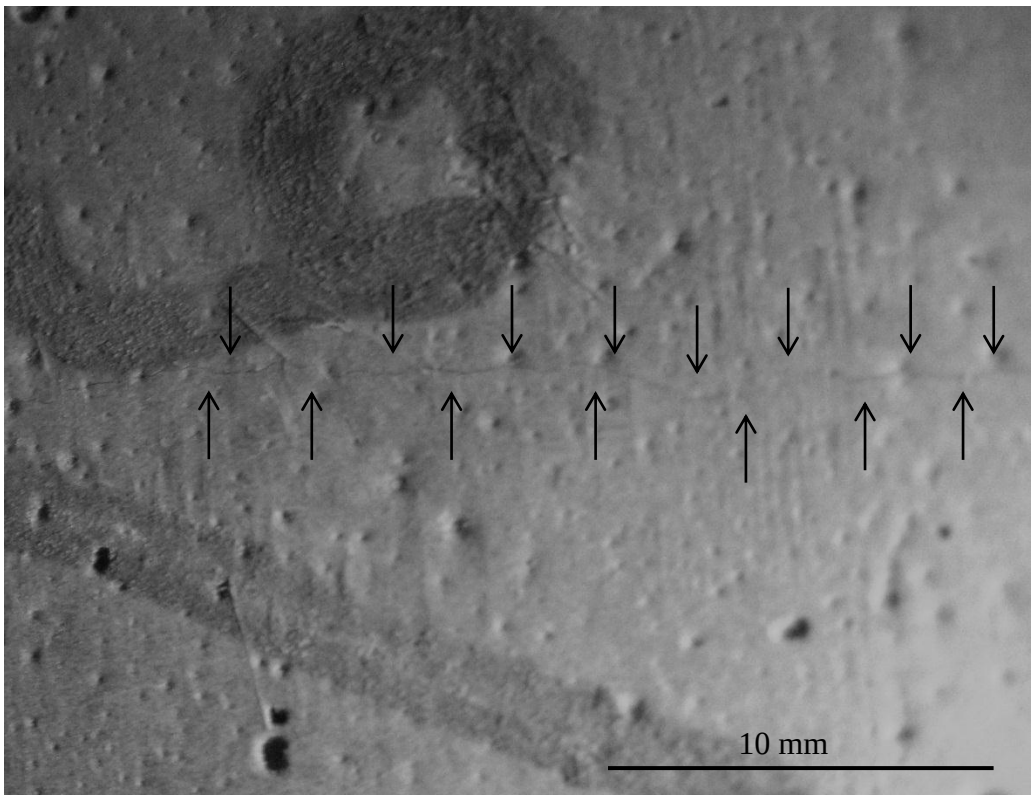

Figure 4.31 Microcrack observed on a tensile creep specimen after 90 days of loading.

Due to limited number of the observed cracks, alternative mechanism should also be considered in terms of tensile creep together with the microcracking mechanism. For this reason, seepage and viscous shear phenomenon may also be evaluated. For water seepage and viscous shear mechanisms to occur it requires deformation of the material under applied tensile load to open up the gel porosity, which in turn adsorbs the free water in large capillaries and to disturb the adsorbed water layers to facilitate gel particles to slide over each other. It was mentioned earlier that mid-span deflection of the flexural strength test specimens reflects the behavior of them under direct tensile strength test. As the mixtures exhibiting higher deformability according to mid-span deflections which is directly related with the ductility also exhibit higher tensile creep as seen in Figure 4.32, water seepage and viscous shear theories also supports the results of tensile creep tests.

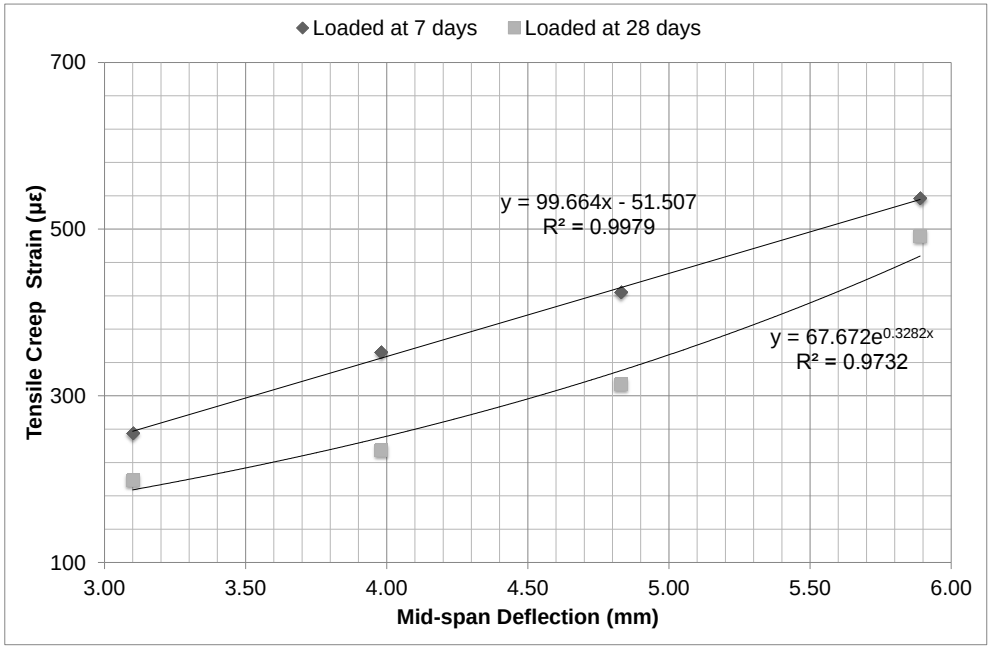

Figure 4.32 Correlation between deformability and tensile creep

4.2.8 Relation between Tensile Creep and Dimensional Compatibility

It is clearly seen that specimens exhibiting high dimensional compatibility also exhibits high ductility and high tensile creep which is consistent with the commonly accepted fact that low shrinkage, low modulus of elasticity, high elastic and tensile creep strain are in favor of dimensional compatibility. As the restrained shrinkage tests were conducted within the first 28 days after casting, the first set of tensile creep test in which the specimens were loaded at 7 days is more valuable as it also reflects the early age behavior of the mixtures including the early age after 7 days. For comparison, if the 28 day adjusted tensile creep values are considered, corresponding adjusted tensile creep values of F1, F5, S1 and S5 specimens are about 424, 537, 255 and 352 με, which are in agreement with dimensional compatibility and deformability hence ductility.

Even though the calculated adjusted tensile creep values of the mixtures are in agreement with dimensional compatibility behavior, it should be noted that the

adjusted tensile creep values are not the real basic tensile creep values of the specimens since drying shrinkage is known to increase the amount of tensile creep when tensile stress and drying acts simultaneously (Bissonnette et al., 2007). As the drying shrinkage of the mixtures with low dimensional compatibility is higher, the basic tensile creep of those mixtures may be much lower than calculated adjusted tensile creep.

Creep coefficient may also be effective on the cracking behavior since it is defined as the ability of cemetitious material to relax stresses (D'Ambrosi et al., 2004). Considering the creep coefficients of the mixtures presented in Table 4.7 and 4.8, the mixtures with high creep coefficients are the same mixtures those perform better under restrained shrinkage conditions which may show that induced tensile stresses due to drying can be relaxed by the materials with high creep coefficients which results in better dimensional compatibility.

According to the formulation (2.14) given by Li (2004), it will be more appropriate to consider the sum of elastic, shrinkage and creep strains for evaluation of cracking potential or dimensional compatibility. At the end of 90 days total percent strains or cracking potentials are calculated as 0.09, 0.06, 0.12, 0.10%, for F1, F5, S1 and S5 mixtures, respectively by using the data obtained from the first tensile creep test. The origins of the strains used in the calculations are marked in Figure 4.33. Also when the data obtained from the second tensile creep test is used; cracking potentials are calculated as 0.08, 0.04, 0.12 and 0.10% for F1, F5, S1 and S5, respectively. These values agree well with restrained shrinkage test results. On the other hand it should be noted that these values were calculated by considering the elastic and tensile creep strains corresponding to a stress of 30% of the ultimate tensile strength of the material and also inelastic strain capacity of ECC (up to 5%) was not included in the calculations which will further decrease the cracking potential to negative values.

As the tensile creep tests were started at 7 and 28 days after casting, sum of the drying shrinkage, elastic and creep strains could only be obtained after 7 and 28

days which limit to comment on dimensional compatibility by using the available data since restrained shrinkage tests were started the day after casting. For this reason, autogenous shrinkage strains, the only available data at early ages, which is also effective on dimensional compatibility, was also added to the total strains to fill the time gap between the restrained shrinkage and tensile creep tests. Autogenous shrinkage strains of the first 7 days and 28 days were prepended to the sum of the strains obtained by first and second sets of tensile creep test data, respectively. As seen in Figure 4.33, the total strains (cracking potentials in με) obtained from tensile creep and autogenous shrinkage tests agree well with the experimentally obtained dimensional compatibility of the specimens. Finally, it can be concluded that, the data obtained from the tensile creep test can also be used as a measure of dimensional compatibility along with the restrained shrinkage tests provided in the literature.

Table 4.7 Tensile creep test results for specimens loaded at 7 days

Mix ID	Tensile Strength (MPa)			Tensile Creep Coefficient	Specific Tensile Creep (με/MPa)	Drying Shrinkage (με)
	7 days	14 days	28 days	90 days		
F1	4.26	4.54	4.59	5.69	301	1372
F5	3.13	3.44	3.49	8.78	502	1155
S1	4.57	4.91	5.91	3.35	146	1550
S5	3.84	4.20	4.50	5.44	259	1436

Table 4.8 Tensile creep test results for specimens loaded at 28 days

Mix ID	Tensile Creep Coefficient	Specific Tensile Creep (με/MPa)	Drying Shrinkage (με)
F1	4.12	209	1188
F5	5.94	328	998
S1	3.31	133	1461
S5	3.57	157	1324

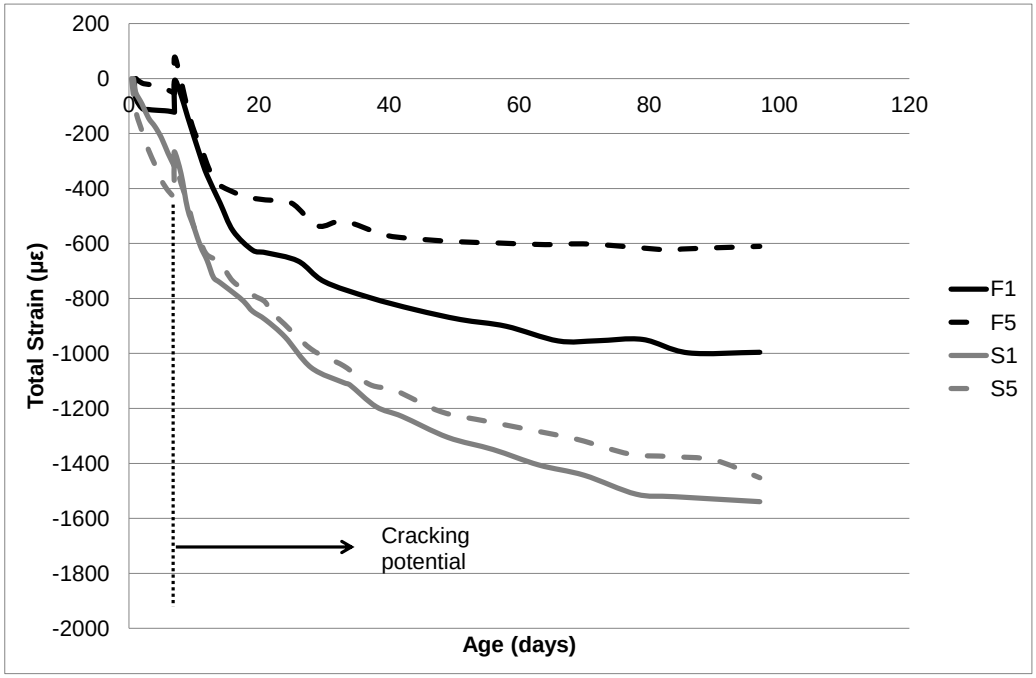

a. Specimens loaded at 7 days

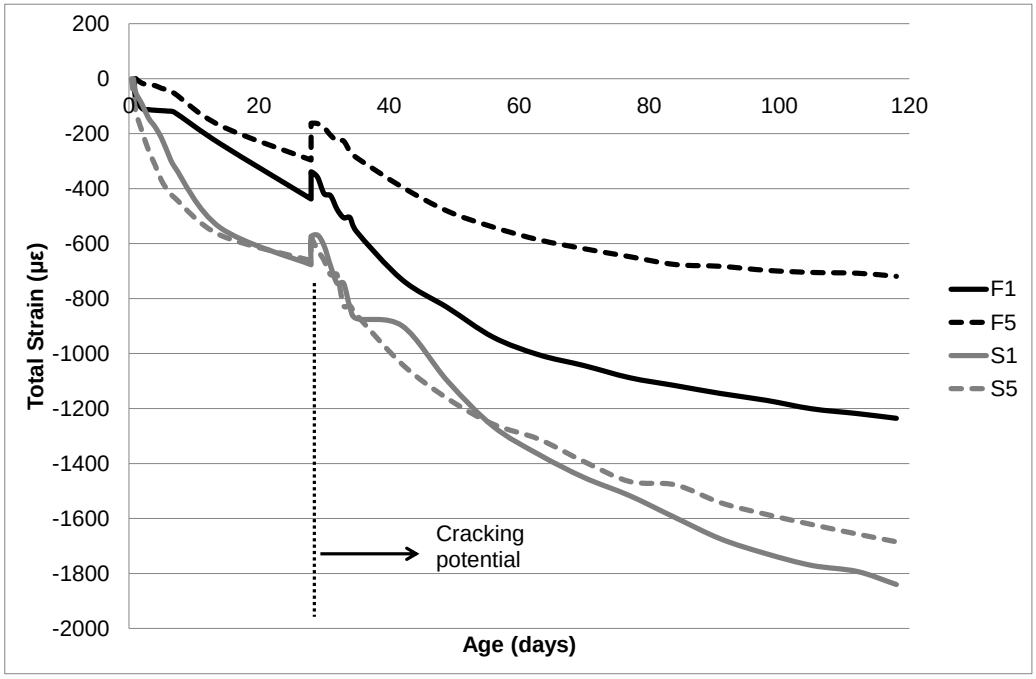

b. Specimens loaded at 28 days

Figure 4.33 Autogenous shrinkage strains prepended to total strains

4.3 Effect of Internal Curing on Mechanical and Dimensional Compatibility Properties

The aim of the second experimental set is to investigate the effect of expanded perlite aggregate replacement level as internal curing agent, especially for reducing the autogenous deformations of ECC mixtures. For this purpose three new ECC mixtures designated with P1, P2 and P3 with 10, 20 and 30% pre-soaked expanded perlite aggregate replacement levels were developed. Proportions of the new mixtures are similar to F1 mixture except that the amount of silica sand in F1 mixture was replaced with expanded perlite. Results are compared with the F1 mixture.

Before starting the tests of internal curing, it was needed to supply more amount of fly ash. Hence, even though the same mixture proportions and materials were used as control mixture designated by F1 in both experimental program, there may be slight differences in the test results since the tests were conducted at different times and the properties of fly ashes may slightly differ as the fly ash used in the internal curing experiments was dispatched at a later time.

4.3.1 Compressive Strength

Results of compressive strength tests performed at 28 and 90 days for evaluation of pre-soaked LWA replacement level are given in Table 4.9. Compressive strengths of the mixtures decrease significantly with an increase in LWA replacement level. However, the lowest compressive strength is 39.8 MPa for 30% pre-soaked LWA replacement which is still suitable for most civil engineering applications. LWA replacement is anticipated to increase the compressive strength as a result of the improved transition zone (ITZ), enhanced hydration and lack of shrinkage cracking as found in the studies conducted with pumice aggregate as internal curing agent for high performance concrete (Lura et al., 2004). However the results of this study showed that between control and P3 specimens there is nearly 35% reduction in

compressive strength. This may be a consequence of the difference between aggregate sizes and strengths of expanded perlite used as LWA and fine silica sand in the study. As expanded perlite has a larger aggregate size that aggravates the compact aggregate size distribution and also has significantly lower strength compared to silica sand and pumice which has been used in the study conducted by Lura et al. (2004), it may adversely affect the compressive strength. Also replacement levels of pre-soaked LWA are higher than that of the study conducted by Lura et al. (2004). Larger perlite aggregate particles may act as stress concentrators where initiation of cracks starts during loading. Besides, large aggregate particles hinder the uniform fiber distribution and results in fiber bundles that may act like voids. Moreover, according to Mehta and Monteiro (2006), an increase in aggregate size accompanies an increase in local water cement ratio in ITZ resulting in a weaker concrete which may be another possible reason for lower compressive strength values at higher perlite aggregate replacement levels. Considering the compressive strength development between 28 and 90 days, the increase in compressive strength values were 19.9, 15.2, 20.6 and 23.4% for F1, P1, P2 and P3, respectively. The direct proportion between compressive strength development and pre-soaked LWA replacement level may be a result of ongoing pozzolanic reaction which is supported by the internal curing water.

Table 4.9 Effect of pre-soaked LWA replacement on compressive strength

Mix ID	**Compressive Strength (MPa)**	
	28 day	**90 day**
F1	60.8	72.9
P1	53.6	61.8
P2	48.6	58.7
P3	39.8	49.1

4.3.2 Flexural Performance

The results of flexural strength tests of the mixtures containing pre-soaked LWA (Table 4.10) show that flexural strength decreases with an increase in LWA replacement level which may be due to large aggregate size and lower strength of expanded perlite aggregate behaving as stress concentrator and preventing the uniform distribution of fibers as described in discussion of compressive strength test results. Similarly, uneven fiber distribution yields bundling of fibers resulting an inadequate coating of fibers by the matrix and reduction in bond strength, hence will lower the flexural strength. As discussed earlier, flexural strength development of LWA containing mixtures are lower compared to compressive strength test results. However, flexural strength development is directly proportional with LWA replacement level, which may be attributed to expected beneficial effects of internal curing, mentioned in compressive strength test results.

Table 4.10 Effect of pre-soaked LWA replacement on flexural strength

Mix ID	**Flexural Strength (MPa)**	
	28 day	**90 day**
F1	12.5	12.7
P1	10.9	11.2
P2	9.2	9.8
P3	8.7	9.5

Mid-span beam deflections of LWA containing specimens at 28 and 90 days are presented in Table 4.11. When the effect of LWA replacement on mid-span beam deflections of the specimens is taken into account, apart from the aforementioned discussion, a positive effect of LWA replacement especially up to 20% is encountered. However, there is a reduction in ductility at the replacement level of 30% which is still higher than control mixture meaning that there is an optimum

level of LWA replacement for maximum ductility. The increase in ductility up to 20% LWA replacement may be attributed to decrease in matrix fracture toughness which will be discussed later. Although, P3 specimen possesses the lowest matrix fracture toughness, its deformability is not the highest which may be a consequence of poor fiber distribution as a result of higher amount of coarse pre-soaked perlite aggregate.

Table 4.11 Effect of pre-soaked LWA replacement on mid-span deflection

Mix ID	Mid-span Deflection (mm)	
	28 day	90 day
F1	4.52	4.04
P1	5.29	5.10
P2	5.42	5.28
P3	4.58	4.45

4.3.3 Matrix Fracture Toughness

As seen from Table 4.12, for internally cured specimens, matrix fracture toughness is inversely proportional with the level of internal curing. The LWA replacement decreased the matrix fracture toughness 20, 33 and 37% for 10, 20 and 30 pre-soaked perlite aggregate replacement, respectively. It denotes that energy required to open a crack in a specimen is 20, 33 and 37% lower compared to the control mixture. The reason for that can be imputed to the reasons discussed in compressive strength test results. In addition, as discussed earlier, during propagation, a crack prefer to propagate through the weaker zones, and as perlite aggregates are weak contrary to silica sand, instead of deflecting and travelling around the perlite aggregate along ITZ, cracks prefer to propagate through the perlite aggregate and crack path becomes smoother and energy requirement decreases which also decreases the matrix fracture toughness. It can be concluded

that LWA replacement has a positive effect on achieving strain-hardening behavior by decreasing the matrix fracture toughness.

Table 4.12 Effect of pre-soaked LWA replacement on matrix fracture toughness

Mix ID	Matrix Fracture Toughness ($MPa \times m^{1/2}$)
	28 day
F1	0.742
P1	0.597
P2	0.496
P3	0.468

4.3.4 Drying Shrinkage

Drying shrinkage development of internally cured and control specimens and corresponding mass loss due to drying up to 112 days after 28 days moist curing are presented in Figure 4.34 and 4.35. Drying shrinkage strains at the end of 112 days of drying were in the range of 1233 and 1391 με. All internally cured specimens exhibited higher drying shrinkages compared to control specimen. Contrary to restrained and autogenous shrinkage results, which will be discussed later, the LWA replacement level adversely affected the drying shrinkage. Shrinkage of normal and lightweight aggregate is expected to be similar according to Zhang et al (2005). However, concrete with LWA would have lower drying shrinkage due to lower autogenous shrinkage (Zhang et al., 2005). This contrast may be a result of higher water loss to environment from the material as LWA level increases which yield higher drying shrinkage. This can be observed in Figure 4.35 as mass loss increases with the LWA replacement level. In addition to this, even though the water to binder ratio is set constant for all mixtures, considering the absorbed water in expanded perlite aggregate, water to binder ratios become

0.29, 0.31 and 0.33 for P1, P2 and P3 mixtures which also results in higher drying shrinkage.

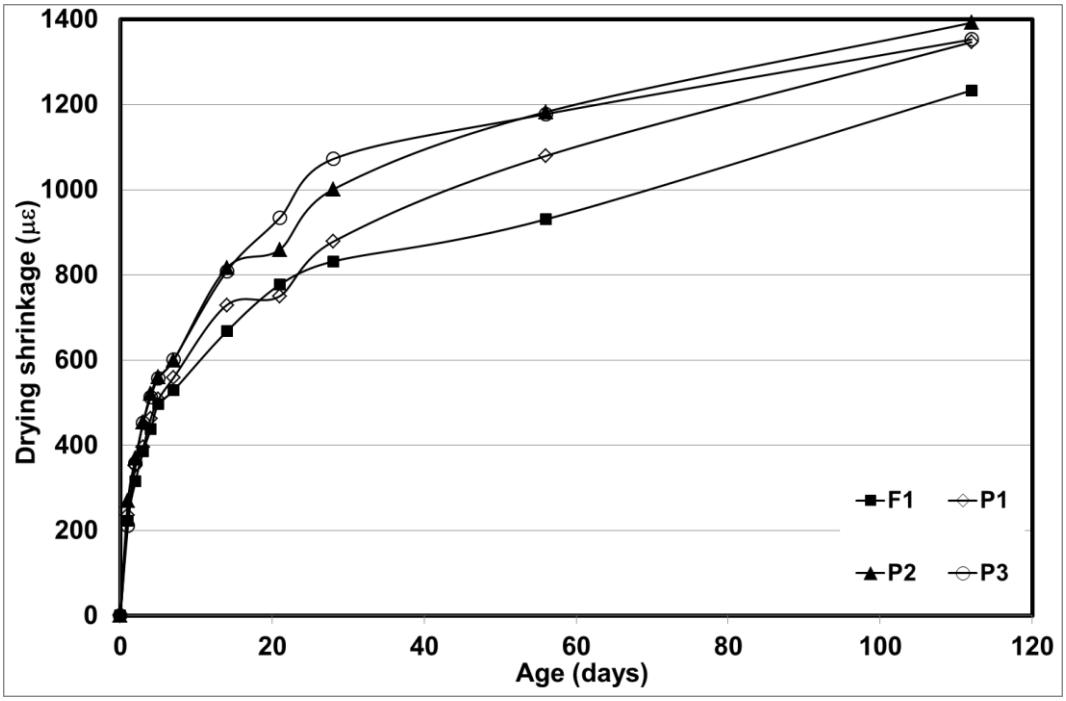

Figure 4.34 Drying shrinkages development of mixtures containing LWA

In spite of the fact that mass loss of mixtures are not close to each other, corresponding drying shrinkage values did not differ much. For instance, percent mass loss of P3 is higher than P1 and P2; however its drying shrinkage is similar to P1 and lower than P2 which means that drying shrinkage is related to other factors in addition to weight loss. Lower autogenous shrinkage may partially compensate the drying shrinkage.

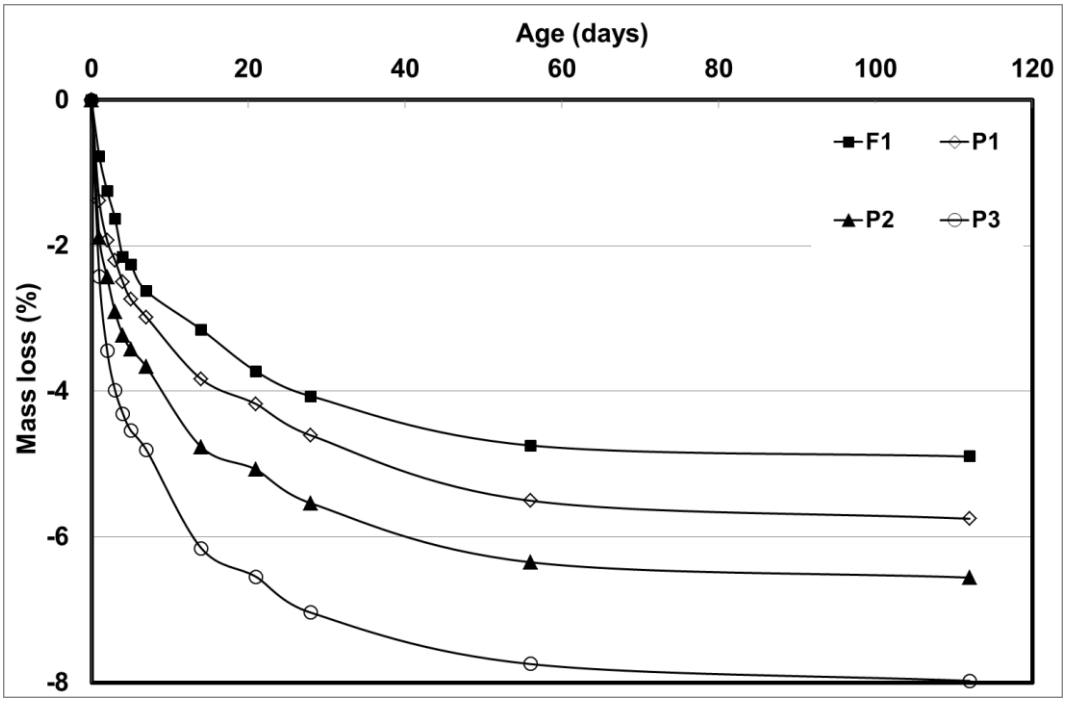

Figure 4.35 Mass loss of LWA containing mixtures due to drying

4.3.5 Autogenous Shrinkage

Incorporation of pre-soaked LWA has a significant effect on autogenous shrinkage as can be seen in Figure 4.36. As the level of LWA replacement increases, a drastic reduction in autogenous shrinkage is observed. The inclusion of LWA replacement both contributed to early and later age autogenous shrinkage, which is an evidence of its positive effect on autogenous shrinkage due to self-desiccation. According to Figure 4.36, autogenous shrinkage values of P1 and P2 are both around 25 με at the end of 3 days while it is more than 100 με for control mixture and 10 με for P3. As the level of LWA replacement increases concave portion of the plot becomes linear. Additionally, between 8^{th} and 9^{th} days instead of shrinkage, P3 exhibits swelling as a result of high internal curing.

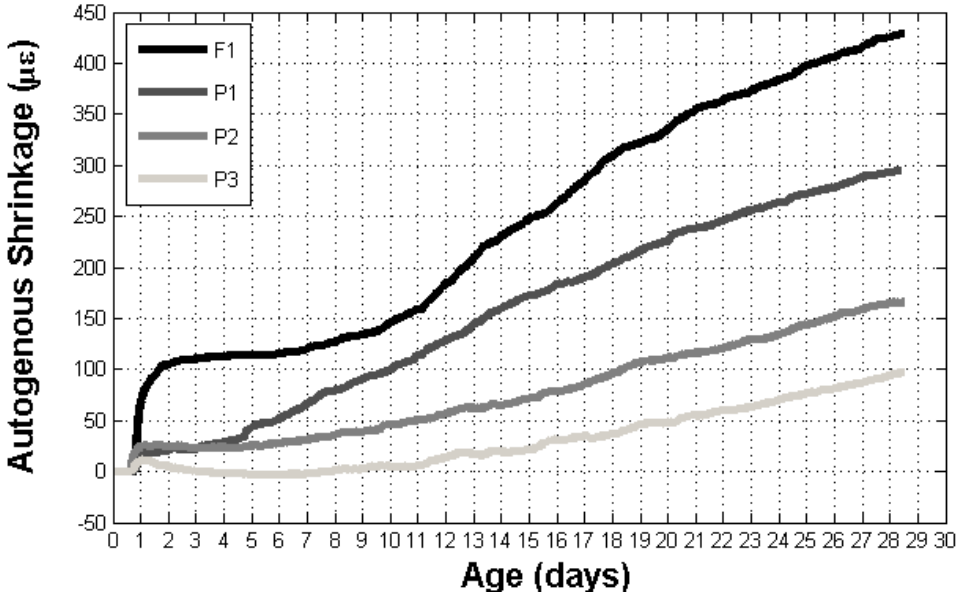

Figure 4.36 Autogenous shrinkage of mixtures with LWA

4.3.6 Restrained Shrinkage

Behavior of ECC mixtures with LWA for internal curing under restrained conditions can be seen in Figure 4.37. Mixtures incorporating LWA for internal curing began to crack after 6 and 7 days which is 5 days for control specimen. The benefit of using LWA for internal curing is clear not only in terms of onset time of first crack but also in terms of the average crack width which decreases proportionally with the pre-soaked LWA replacement level. Furthermore, the numbers of restrained shrinkage cracks are 7, 9, 11 and 13 for control, P1, P2 and P3, respectively.

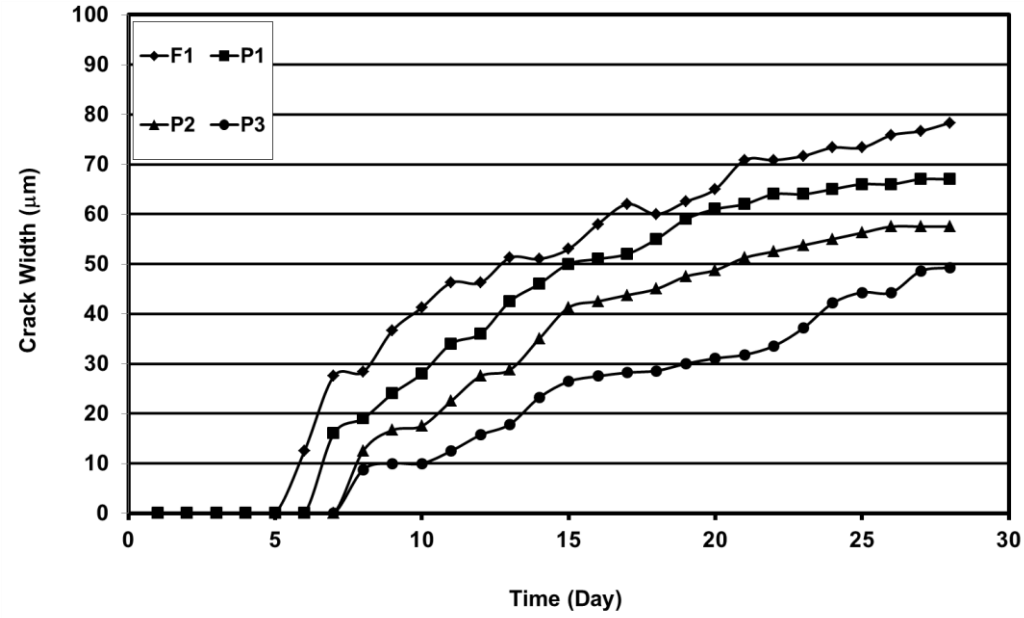

Figure 4.37 Crack width developments in restrained shrinkage specimens with LWA replacement

It can be concluded that pre-soaked LWA replacement has beneficial effect on restrained shrinkage performance hence dimensional compatibility. This can be attributed to low matrix fracture toughness and high mid-span beam deflection capacity hence ductility attained by LWA usage. However, the total crack width is slightly increased which may be a result of increased drying shrinkage of mixtures with LWA replacement. On the other hand it is the maximum width of a crack that influences the durability of a cementitious composite rather than the total crack width (Şahmaran and Li, 2009-a).

CHAPTER 5

SUMMARY AND CONCLUSIONS

This study had two main objectives. The first one of these objectives is the evaluation of the effect of mixture proportioning on mechanical properties and on autogenous, drying and restrained shrinkage behaviors of micromechanically designed, strain-hardening, high performance, fiber-reinforced cementitious composites, also known as Engineered Cementitious Composites (ECC), produced with locally available materials. Together with the abovementioned properties, behavior of the selected mixtures under sustained tensile loads were also investigated in order to relate shrinkage, elastic and time dependent tensile properties with the dimensional compatibility of the mixtures.

In the first experimental program, sixteen different mixtures were used. In half of the mixtures, fly ash (FA) was used as mineral admixture as it is generally used in ECC production and ground granulated blast furnace slag (GGBFS) was used for the rest of the mixtures. This was intended to evaluate the use of different available pozzolanic materials and their effect on properties of the produced ECC. Hence each set of eight mixtures were similar to the other set in terms of mixture proportions except the type of mineral admixtures used. Half of the eight mixtures possessed a mineral admixture to cement ratio of 1.2 while this ratio was 2.2 for the rest of the mixtures which was aimed to evaluate the effect of the mineral admixture amount. Sand to cementitious material ratios of the mixtures were selected as 0.36, 0.45 and 0.55 so that the effect of the sand amount could also be

investigated. For the mixtures with sand to cementitious material ratio of 0.36 a companion mixture with a maximum aggregate size of 1000 μm was designed while for the rest of the mixtures the maximum aggregate size remained 400 μm.

The following specific conclusions were drawn from the test results of the first experimental program:

1. Compressive strength of the mixtures containing GGBFS is higher than that of containing FA due to the early reaction, hydraulic binding property and high specific surface area of the GGBFS compared to FA. As mineral admixture to cement ratio is increased from 1.2 to 2.2, compressive strength decreases. The effect of aggregate amount on compressive strength is not consistent in the range tested. As the amount of sand decreased, the amount of binder increases, however due to the high amount of binders used; some of the binding materials remain unhydrated and act as aggregates which hinder their effect on compressive strength. Moreover, maximum aggregate size does not have a significant effect on compressive. Even though the GGBFS mixtures have higher compressive strength, rate of strength gain is higher for FA mixtures especially at later ages due to slow pozzolanic reactions with respect to GGBFS. Moreover, rate of compressive strength gain is higher for mixtures with higher amount mineral admixture.

2. Type and amount of mineral admixture are very effective on flexural performance of ECC mixtures. GGBFS mixtures have higher flexural strengths compared to FA mixtures. Aggregate content does not have a significant effect on flexural strength as in compressive strength. However, increase in maximum aggregate size slightly reduced the flexural strength for all ages of testing.

3. Mid-span beam deflections, as a measure of tensile ductility of the materials, obtained from flexural strength tests showed that GGBFS

mixtures have lower mid-span deflections compared to FA mixtures. This is attributed to high matrix fracture toughness and higher bond between the matrix and PVA fibers in specimens with GGBFS, compared to FA mixtures. Mid-span beam deflections, hence ductility increases when the amount of mineral admixture increase especially for FA mixtures due to the low matrix fracture toughness and enhanced fiber slippage. Mid-span beam deflections also decrease with the age of the specimen as a result of increase in the matrix fracture toughness and bond between the matrix and fibers.

4. All mixtures exhibit a degree of multiple cracking with tight and fine cracks. Average crack widths are higher for mixtures with GGBFS, compared to FA mixtures and reduces as the amount of FA is increased. This may be attributed to better workability of FA mixtures providing a more uniform fiber distribution and better fiber pull out performance due to spherical shape of FA particles. Average crack widths are not influenced from the amount and maximum size of aggregates used in this study.

5. GGBFS mixtures have higher matrix fracture toughness compared to FA mixtures which is a consequence of lower porosity and smaller pore sizes. Aggregate amount and maximum size also increase the matrix fracture toughness because as cracks meet aggregate particles they prefer to travel around the weaker ITZ which requires higher energy. Aggregate size and amount should be limited in order to attain strain-hardening behavior. Besides, an inverse proportionality between matrix fracture toughness and mid-span deflection is found.

6. Increase in the mineral admixture amount significantly decreases the drying shrinkage of the mixtures. This may be attributed to denser matrix affected by shape, micro filler effect and pozzolanic property of FA, which prevents moisture loss from the material. Alternatively, unhydrated FA particles may act like aggregates and result in coarser pore structure which decreases the

capillary tension hence shrinkage. GGBFS mixtures have higher drying shrinkage with respect to FA mixtures due to enhanced pore size refinement. Aggregate amount has a clear effect on drying shrinkage; maximum aggregate size on the other hand has a slight effect as a result of restraining effect and coarser pore structure.

7. GGBFS mixtures exhibit higher autogenous shrinkage compared to FA mixtures. Also increase in the aggregate amount decrease the autogenous shrinkage. Moreover maximum aggregate size has slight effect on autogenous shrinkage as in drying shrinkage tests. Those results are in compliance with drying shrinkage measurements as the mechanism of drying and autogenous shrinkages are similar. On the other hand, development of autogenous shrinkage strains differs for FA and GGBFS mixtures on account of their rate of reactivity.

8. Under restrained shrinkage conditions, all specimens exhibit multiple cracking. The first crack occurs between 2 to 3 days and 4 to 8 days, for GGBFS and FA containing mixtures, respectively depending on the amount of mineral admixtures and aggregate. As the aggregate amount increases, first crack formation is delayed which is a consequence of restraining effect of aggregates. Average crack widths are lower for FA mixtures compared to GGBFS mixtures. Low compatibility of GGBFS is due to higher shrinkage hence higher induced tensile stresses together with the lower ductility and lower tensile creep of GGBFS.

9. FA mixtures exhibit higher tensile creep strain compared to GGBFS mixtures. Also, increase in the amount of mineral admixture yields tensile creep strains to increase. Specific creep values are higher for the specimens loaded at 7 days with respect to the specimens loaded at 28 days. Both the effect of mineral admixture amount and startup time of loading are

attributed to the deformability of the specimens and explained by microcraking, water seepage and viscous shear theories.

10. Tensile creep properties of the mixtures are found to be related with the dimensional compatibility properties of the mixtures. Calculated cracking potentials by the use of tensile creep test results reflect the real cracking behavior of ECC specimens under restrained shrinkage conditions. Thus, tensile creep test results may also be used as a measure of dimensional compatibility of the mixtures.

The second objective of this study is to evaluate the effect of internal curing provided by expanded perlite aggregate as pre-soaked lightweight aggregate, for mitigating autogenous shrinkage as ECC is expected to experience significantly high autogenous shrinkage as a result of its low water to cementitious material ratio. Using saturated lightweight aggregate is an existing practice in the literature, however in this study its effect on the mechanical properties and the drying and restrained shrinkages were also investigated. 10, 20 and 30% of the silica sand which is used as aggregate in ECC production was replaced with pre-soaked expanded perlite aggregate and results were compared with a standard ECC mixture without any LWA replacement. The following specific conclusions were drawn:

1. Compressive strength is adversely affected by the pre-soaked LWA replacement. Low strength together with large aggregate size of expanded perlite compared to silica sand may result in a reduction in compressive strength. As a result of enhanced hydration due to internal curing provided by pre-soaked perlite aggregate, compressive strength development over time is better for mixtures containing LWA.

2. As the pre-soaked expanded perlite replacement level increases, fracture toughness of ECC matrices reduce. This is attributed to low strength of

perlite aggregate as cracks prefer to propagate through them instead of deflecting and travelling around as in silica sand. However, lower fracture toughness is beneficial for multiple cracking in accordance with micromechanics based design theory of ECC.

3. Under flexural loading, all ECC mixtures exhibit deflection-hardening behavior and multiple cracking. As a result of weak perlite particles, flexural strengths are inversely proportional with the LWA replacement rate. Up to 20% of LWA replacement level, mid-span beam deflections proportionally increase. However, mid-span beam deflection of 30% LWA replacement is not found to be the highest even though it has the lowest 28 day matrix fracture toughness. This discrepancy can be attributed to poor fiber distribution resulted by the high amount of LWA replacement. It can be concluded that for the 30% LWA replacement level the positive effect of low matrix fracture toughness is outweighed by the negative effect of the LWA replacement on uniform fiber distribution. Hence, there is an optimum level of LWA replacement to attain strain-hardening together with dimensional stability properties.

4. Autogenous shrinkage of ECC mixtures, both at early and late ages are significantly affected positively by the pre-soaked expanded perlite replacement. About 78% decrease in the autogenous shrinkage strain at the age of 28 days was observed for 30% pre-soaked perlite replacement, revealing that pre-soaked expanded perlite aggregate replacement can be used to almost eliminate autogenous shrinkage in ECC.

5. As a result of restrained shrinkage tests conducted, it can be concluded that pre-soaked expanded perlite type LWA replacement improves the dimensional compatibility of ECC mixtures. As the level of pre-soaked expanded perlite replacement increase, the first crack onset time and number of the cracks increase while the average crack widths decreases.

This may be attributed to the higher ductility and dimensional stability as a result of reduced autogenous shrinkage with pre-soaked LWA replacement.

6. Pre-soaked expanded perlite replacement slightly increased the drying shrinkage of the ECC specimens compared to control specimen. This may attributed to the increase in the effective water to cementitious material ratio with the increase in pre-soaked expanded perlite aggregate replacement level calculated by summing the total amount of mixing water and the water absorbed inside the LWA particles.

Finally, as a result of the experimental study, it could be concluded that ECC produced with locally available materials have similar mechanical performance when compared to the standard ECC mixture. ECC mixtures may suffer from early age cracking due to restrained shrinkage, because of their lower water to cementitious material ratio. However, besides shrinkage, deformability and ductility are also important on restrained shrinkage cracking performance of a material. Thus, tensile creep data, together with shrinkage data needs to be used to evaluate the dimensional compatibility of a material to be used adjacent to another construction material. Although some mixtures have better dimensional stability properties, such as low drying and autogenous shrinkage, their performance under restrained shrinkage conditions, and therefore their dimensional compatibility becomes worse when they have low deformability. Among the pozzolanic materials used in this study, flexural and compressive strength of GGBFS mixtures are higher compared to FA mixtures, however FA mixtures have better dimensional compatibility. Therefore, ECC mixtures with high volumes of FA seems to be more appropriate for repair and strengthening works owing to their low autogenous and drying shrinkage, high tensile creep and better performance under restraining shrinkage conditions. Furthermore, those ECC mixtures with perlite addition as an internal curing agent have enhanced dimensional compatibility properties which make them also ideal candidates for repair works.

CHAPTER 6

RECOMMENDATIONS

In this experimental study, it was shown that mechanical properties including the compressive strength, flexural strength, mid-span beam deflection, matrix fracture toughness, and properties related to dimensional compatibility including the autogenous, drying, restrained shrinkage and tensile creep are dependent on the type and amount of ingredients. It was also revealed that by the use of expended perlite as pre-soaked LWA, ECC with sufficient mechanical properties with low autogenous shrinkage can be produced. For further studies on the subject, following can be recommended:

1. Tensile creep tests were started at 7 days after casting; however, restrained shrinkage tests were started the day after casting. Due to the time gap between tensile creep and restrained shrinkage test, effect of early age tensile creep on dimensional compatibility could not be evaluated accurately. On the other hand, it is not possible to start the tensile creep test before 7 days as it requires time for the epoxy, used to mount to specimens to the steel plates, to set and reach sufficient bond strength. However, by the use of special mold that does not require epoxy; early age tensile creep can be measured.

2. Tensile creep tests were conducted on a limited number of mixtures due to the long duration of the test and limited number of test setups. In order to

establish the correlation between tensile creep and other related properties the number of the mixtures can be increased.

3. The restrained shrinkage test provides data about the cracking potential and dimensional compatibility. In ASTM C 1581 (ASTM, 2009), restrained shrinkage rings are standardized and the mold used in the standard provides a test material thickness of 37.5 mm. This thickness may be appropriate for normal concrete; however ECC, especially produced with FA, may not experience any cracking. For this reason, it may not be useful for evaluating the cracking potential of ECC according to this standard by determining the age at cracking and crack widths. For this purpose modified molds which provide a thinner test specimen may be used to observe cracks due to drying-induced tensile stresses. Otherwise, the setup proposed in the same standard to monitor the hoop strains inside the inner ring should be used.

4. For materials to be used for repair and strengthening purposes like ECC, it is important to determine bonding ability of the material to substrate. It is recommended to conduct additional bond tests for further studies.

REFERENCES

ACI Committee 232. (2003). *Use of fly ash in concrete* (ACI 232.2R-03).

ACI Committee 233, (2003). *Slag cement in concrete and mortar* (ACI 233R-03).

Aïtcin, P.-C. (1998). *High-performance concrete*. London, New York: E. & F.N. Spon.

American Society for Testing and Materials. (1987). *Standard test method for creep of concrete in compression* (ASTM C 512) West Conshohocken, PA: ASTM International.

American Society for Testing and Materials. (1995). *Standard test method for change in height at early ages of cylindrical specimens from cementitious mixtures* (ASTM C 827) West Conshohocken, PA: ASTM International.

American Society for Testing and Materials. (2003). *Test method for plane-strain fracture toughness of metallic materials* (ASTM E 399) West Conshohocken, PA: ASTM International.

American Society for Testing and Materials. (2006-a). *Standard test method for evaluating plastic shrinkage cracking of restrained fiber reinforced concrete (using a steel form insert)* (ASTM C 1579) West Conshohocken, PA: ASTM International.

American Society for Testing and Materials. (2006-b). *Standard test method for length change of hardened hydraulic-cement mortar and concrete* (ASTM C 157) West Conshohocken, PA: ASTM International.

American Society for Testing and Materials. (2007). *Standard test method for chemical shrinkage of hydraulic cement paste* (ASTM C 1608) West Conshohocken, PA: ASTM International.

American Society for Testing and Materials. (2009). *Standard test method for determining age at cracking and induced tensile stress characteristics of mortar and concrete under restrained shrinkage* (ASTM C 1581) West Conshohocken, PA: ASTM International.

Bentur, A., and Mindess, S. (2007). *Fibre reinforced cementitious composites* (2nd ed.). London, New York: Taylor & Francis.

Bisaillon, A., Rivest, M. and Malhotra, V. M. (1994). Performance of high-volume fly ash concrete in large experimental monoliths. *ACI Materials Journal, 91*(2), 178-187.

Bissonnette, B., Pigeon, M. and Vaysburd, A. M. (2007). Tensile creep of concrete: Study of its sensitivity to basic parameters. *ACI Materials Journal, 104*(4), 360-368.

Boshoff, W. P. and van Zijl, G. P. A. G. (2007). Time-dependent response of ECC: Characterisation of creep and rate dependence. *Cement and Concrete Research, 37*(5), 725-734.

Boshoff, W. P., Mechtcherine, V. and van Zijl, G. P. A. G. (2009-a). Characterising the time-dependant behaviour on the single fibre level of SHCC: Part 1: Mechanism of fibre pull-out creep. *Cement and Concrete Research, 39*(9), 779-786.

Boshoff, W. P., Mechtcherine, V. and van Zijl, G. P. A. G. (2009-b). Characterising the time-dependant behaviour on the single fibre level of SHCC: Part 2: The rate effects on fibre pull-out tests. *Cement and Concrete Research, 39*(9), 787-797.

Brooks, J. (2003). Elasticity, shrinkage, creep and thermal movement. In J. B. Newman & B. S. Choo (Eds.), *Advanced concrete technology: Concrete properties* Burlington MA: Butterworth-Heinemann.

Bucher, E. B. (2009). *Shrinkage and shrinkage cracking behavior of cement systems containing ground limestone, fly ash, and lightweight synthetic particles.* MSc Thesis. Purdue University.

Cetin, A. and Carrasquillo, R. L. (1998). High-performance concrete: Influence of coarse aggregates on mechanical properties. *ACI Material Journal, 95*(3), 252-261.

Chen, B. and Liu, J. (2004). Effect of aggregate on the fracture behavior of high strength concrete. *Construction and Building Materials, 18*(8), 585-590.

Davis, D. E. and Alexander, M. G. (1989). *Properties of aggregate in concrete (Part 1).* Hippo Quarries, Sandton, South Africa: Hippo Quarries Technical Publication.

Davis, D. E. and Alexander, M. G. (1992). *Properties of aggregate in concrete (Part 2).* Hippo Quarries, Sandton, South Africa: Hippo Quarries Technical Publication.

Decter, M. H. and Keeley, C. (1997). Durable concrete repair - importance of compatibility and low shrinkage. *Construction and Building Materials, 11*(5-6), 267-213.

De Larrard, F. and Belloc, A. (1997). The influence of aggregate on the compressive strength of normal and high-strength concrete. *ACI Material Journal, 94*(5), 417-426.

D'Ambrosia, M. D., Lange, D. A. and Grasley, Z. C. (2004). Measurement and modeling of concrete tensile creep and shrinkage at early age. *ACI Special Publication, 220*, 99-112.

Emberson, N. K. and May, G. C. (1990). Significance of property mismatch in the patch repair of structural concrete Part 1: Properties of repair systems. *Magazine of Concrete Research, 42*(152), 147-160.

Emmons, P. H., Vaysburd, A. M. and McDonald, J. E. (1993). A rational approach to durable concrete repairs. *Concrete International, 15*(9), 40-45.

Emmons, P. H. and Vaysburd, A. M. (1995). *Performance criteria for concrete repair materials, Phase 1*: US Army Corp of Engineers.

Emmons, P. H., Vaysburd, A. M., McDonald, J. E., Poston, R. W. and Kesner, K. E. (2000). Selecting durable repair materials: Performance criteria. *Concrete International, March* 38-45.

Evardsen, C. (1999). Water permeability and autogenous healing of cracks in concrete. *ACI Materials Journal, 96*(4), 448-454.

Garas, V. Y., Kahn L. F. and Kurtis K. E. (2009). Short-term tensile creep and shrinkage of ultra-high performance concrete. *Cement and Concrete Composites 31*, 147–152.

Garas, V. Y., Kurtis, K. E. and Kahn, L. F. (2012). Creep of UHPC in tension and compression: Effect of thermal treatment. *Cement and Concrete Composites 34*, 493-502.

Goodwin, F. (2006). Volume change. In J. F. Lamond & J. H. Pielert (Eds.), *Significance of tests and properties of concrete and concrete-making materials*. Bridgeport, NJ: ASTM International.

Holt, E. E. (2001). *Early age autogenous shrinkage of concrete*. Espoo: Technical Research Centre of Finland.

Japan Society of Civil Engineers. (2008). *Recommendations for design and construction of high performance fiber reinforced cement composites with multiple fine cracks (HPFRCC).* Retrieved from: http://www.jsce.or.jp/committee/concrete /e/hpfrcc_JSCE.pdf

Jawed, I., Skalny, I. J., Bach, T., Schubert, P., Bijen, J., Grube, H., Nakagataki, S., Ohga, H. and Ward, M. A. (2005). Hardened mortar and concrete eith fly ash. In K. Wesche (Ed.), *Fly ash in concrete properties and performance* London, New York, Tokyo, Melbourne, Madras: E & FN Spon.

Kabele, P., Li, V. C., Horii, H., Kanda, T. and Takeuchi, S. (1997). *Use of BMC for ductile structural members.* Paper presented at the Proc. of 5th Int'l Symposium on Brittle Matrix Composites (BMC-5) Warsaw, Poland.

Kanda, T. and V.C. Li. (1998). Interface property and apparent strength of high strength hydrophilic fiber in cement matrix. *Journal of Materials in Civil Engineering, 10*(1), 5-13.

Kanda, T., Watanabe, S. and Li, V. C. (1998). *Application of pseudo strain-hardening cementitious composites to shear resistant structural elements.* Paper presented at the Fracture Mechanics of Concrete Structures Proceedings FRAMCOS-3, Freiburg, Germany.

Kanda, T., Saito T. and Sakata N. (2003). Tensile and anti-spalling properties of direct sprayed ECC. *Advanced Concrete Technology, 1*(3), 269-282.

Keoleian, G. A., Kendall, A., Dettling, J. E., Smith, V. M., Chandler, R. F., Lepech, M. D. and Li V. C. (2005). Life Cycle Modeling of Concrete Bridge Design: Comparison of ECC Link Slabs and Conventional Steel Expansion Joints. *Journal of Infrastructure Systems, 11*(1), 51-60.

Kim, Y. Y., Fischer, G. and Li V. C. (2004-a). Performance of bridge deck link slabs designed with ductile engineered cementitious composites. *ACI Structural J.,101*(6), 792-801.

Kim, Y. Y., Fischer, G., Lim Y. M. and Li V. C. (2004-b). Mechanical performance of sprayed engineered cementitious composite (ECC) using wet-mix shotcreting process for repair. *ACI Materials J., 101*(1), 42-49.

Kong, H. J., Bike S. and Li V. C. (2003). Constitutive rheological control to develop a self-consolidating engineered cementitious composite reinforced with hydrophilic poly(vinyl alcohol) fibers. *Cement and Concrete Composites, 25*(3), 333-341.

Kosmatka, S. H., Kerkhoff, B. and Panarese, W. C. (2003). *Design and control of concrete mixtures* (Fourteenth Edition ed.). Skokie, Illinois: Portland Cement Association.

Lawrence, C. D. (2004). Physicochemical and mechanical properties of portland cements. In P. C. Hewlett (Ed.), *Lea's chemistry of cement and concrete* (4th ed.). Oxford: Butterworth Heinemann.

Lepech, M. and Li, V. C. (2005). *Water permeability of cracked cementitious composites.* Paper presented at the 11th International Conference on Fracture, Turin, Italy.

Lepech, M. D. and Victor C. Li. (2009). Application of ECC for bridge deck link slabs. *Materials and Structures, 42*(9), 1185-1195.

Li, M. and Li, V. C. (2006). Behavior of ECC/concrete layered repair system under drying shrinkage conditions. *Journal of Restoration of Buildings and Monuments, 12*(2), 143-160.

Li, M. and Li V. C. (2007). *Durability of HES-ECC repair under mechanical and environmental loading conditions.* Paper presented at the High Performance Fiber Reinforced Cement Composites (HPFRCC5), Mainz, Germany.

Li., M., Şahmaran M. and Li V.C. (2007). *Effect of cracking and healing on durability of engineered cementitious composites under marine environment.* Paper presented at the High Performance Fiber Reinforced Cement Composites (HPFRCC5), Mainz, Germany.

Li, M., and Li, V. C. (2009). Influence of material ductility on the performance of concrete repair. *ACI Materials Journal, 106*(5), 419-428.

Li, M. and V.C. Li. (2011). High-early-strength ECC for rapid durable repair - material properties. *ACI Materials Journal, 108*(1), 3-12.

Li, V. C., Wang, Y. and Backer, S. (1991). A micromechanical model of tension-softening and bridging toughening of short random fiber reinforced brittle matrix composites. *Journal of Mechanics and Physics of Solids, 39*(5), 607-625.

Li, V. C. and Leung, C. K. Y. (1992). Steady state and multiple cracking of short random fiber composites. *ASCE Journal of Engineering Mechanics, 188*(11), 2246-2264.

Li, V. C. and Wu, H. C. (1992). Conditions for pseudo strain-hardening in fiber reinforced brittle matrix composites. *Applied Mechanics Review, 45*(8), 390-398.

Li, V. C. (1993). From micromechanics to structural engineering - the design of cementitious composites for civil engineering applications. *JSCE Journal of Structural Mechanics and Earthquake Engineering, 10*(2), 37-48.

Li, V. C., Mishra, D. K., Naaman, A. E., Wight, J. K., LaFave, J. M., Wu, H. C., Inada, Y. (1994). On the shear behavior of engineered cementitious composites. *Journal of Advanced Cement Based Materials, 1*(3), 142-149.

Li, V. C., Mishra, D. K. and Wu, H. C. (1995). Matrix design for pseudo strain-hardening fiber reinforced cementitious composites. *Materials and Structures, 28*(10), 586-595.

Li, V. C. (1998). Engineered cementitious composites - tailored composites through micromechanical modeling. In N. Banthia, A. Bentur and A. Mufti (Eds.), *Fiber Reinforced Concrete: Present and the Future* (pp. 64-97). Montreal, Canada: Canadian Society for Civil Engineering.

Li, V. C. and Kanda, T. (1998). Engineered cementitious composites for structural applications. *Journal of Materials in Civil Engineering, 10*(2), 66-69.

Li, V. C., Horii, H., Kabele, P., Kanda, T. and Lim, Y. M. (2000). Repair and retrofit with engineered cementitious composites. *Int'l J. of Engineering Fracture Mechanics, 65*(2-3), 317-334.

Li, V. C. (2001). J-integral applications to characterization and tailoring of cementitious materials. In T.J. Chuang and J.W. Rudnicki (Eds.), *Multiscale deformation and fracture in materials and structures* (Vol. The J.R. Rice 60th Anniversary Volume, pp. 385-406). Dordrecht: Kluwer Academic Publishers.

Li, V. C., Wang, S. and Wu, C. (2001). Tensile strain-hardening behaviour of PVA-ECC. *ACI Materials Journal, 98*(6), 483-492.

Li, V. C. (2002). Advances in ECC research. *SP 206-23 ACI Special Publication on Concrete: Material Science to Applications*, 373-400.

Li, V. C., Wu C., Wang S., Ogawa A. and Saito T. C. (2002). Interface tailoring for strain-hardening PVA-ECC. *ACI Materials Journal, 99*(5), 463-472.

Li, V. C. (2003). On engineered cementitious composites (ECC) – a review of the material and ıts applications. *Journal of Advanced Concrete Technology, 1*(3), 215-230.

Li, V. C., Fischer, G., Kim, Y. Y., Lepech, M., Qian, S., Weimann, M. and Wang, S. (2003). *Durable link slabs for jointless bridge decks based on strain-hardening cementitious composites* (Research Report RC-1438): Michigan Department of Transportation.

Li, V. C. (2004). High performance fiber reinforced cementitious composites as durable material for concrete structure repair. *Journal for Restoration of Buildings and Monuments, 10*(2), 163-180.

Li, V. C. and Lepech, M. (2004). *Crack resistant concrete material for transportation construction Paper No. 04-4680.* Paper presented at the Transportation Research Board 83rd Annual Meeting, Washington D.C.

Li, V. C. and Stang, H. (2004). *Elevating FRC material ductility to infrastructure durability.* Paper presented at the 6th International RILEM Symposium on Fibre-Reinforced Concretes (BEFIB'2004), Varenna, Lake Como, Italy.

Li, V. C., Lepech, M. and Li, M. (2005). *Field demonstration of durable link slabs for jointless bridge decks based on strain-hardening cementitious composites* (Research Report RC- 1471): Michigan Department of Transportation.

Lim, Y. M. and Li, V. C. (1997). Durable repair of aged infrastructures using trapping mechanism of engineered cementitious composites. *Cement and Concrete Composites, 19*(4), 373-385.

Lin, Z., Kanda, T., and Li, V. C. (1999). On interface property characterization and performance of fiber reinforced cementitious composites. *Concrete Science and Engineering, 1*, 173-184.

Loukili, A., Chopina, D., Khelidjb, A. and Touzo, J. Y. L. (2000). A new approach to determine autogenous shrinkage of mortar at an early age considering temperature history. *Cement and Concrete Research 30*(6), 915-922.

Lura, P., Bentz, D. P., Lange, D. A., Kovler, K. and Bentur, A. (2004). *Pumice aggregates for internal water curing.* Paper presented at the International RILEM Symposium on Concrete Science and Engineering: A Tribute to Arnon Bentur, Evanston, IL.

Mai, Y.-W. and Cotterell, B. (1985). Porosity and mechanical properties of cement mortar. *Cement and Concrete Research, 15*(6), 995–1002.

Mangat, P. S. and Limbachiya, M. K. (1995). Repair material properties which influence long-term performance of concrete structures. *Construction and Building Materials, 9*(2), 81-90.

Maslehuddin, M., Saricimen, H. and Al-Mani, A. (1987). Effect of fly ash addition on the corrosion resisting characteristics of concrete. *ACI Materials Journal, 84*(1), 42-50.

Mehta, P. K. and Monteiro, P. J. M. (2006). *Concrete; microstructure, properties, and materials* (3rd ed.). New York: McGraw-Hill.

Mindess, S., Young, J. F., and Darwin, D. (2003). *Concrete* (2nd ed.). Upper Saddle River, NJ: Prentice Hall.

Miyazato, S. and Hiraishi Y. (2005). *Transport properties and steel corrosion in ductile fiber reinforced cement composites.* Paper presented at the 11th International Conference on Fracture Turin, Italy.

Mokarem, D. W., Weyers R. E. and Lane, D. S. (2005). Development of a shrinkage performance specifications and prediction model analysis for supplemental cementitious material concrete mixtures. *Cement and Concrete Research, 35*(5), 918-925.

Morgan, D. R. (1996). Compatibility of concrete repair materials systems. *Construction and Building Materials, 10*(1), 51-61.

Neville, A. M. and Brooks, J. J. (1987). *Concrete technology* (2nd ed.). Essex: Pearson Education Limited.

Neville, A. M. (2003). *Properties of concrete* (4th ed.). Essex: Pearson Educational Limited.

Poston, R. W., Kesner, K., McDonald, J. E., Vaysburd, A. M., & Emmons, P. H. (2001). Concrete repair material performance—laboratory study. *ACI Materials Journal, 98*(2), 137-147.

Qian, S. and Li, V. C. (2006). Influence of concrete material ductility on shear response of stud connections. *ACI Materials Journal, 103*(1), 60-66.

Qian, S. and Li, V. C. (2007). Simplified inverse method for determining the tensile strain capacity of strain hardening cementitious composites. *Journal of Advanced Concrete Technology 5*(2), 235-246.

Qian, S., Zhou, J., Rooij, M. R., Schlangen, E., Ye, G. and van Breugel, K. (2009). Self-healing behavior of strain hardening cementitious composites incorporating local waste materials. *Cement and Concrete Composites, 31*(9), 613-621.

Rao, G. A. (2001). Long-term drying shrinkage of mortar-influence of silica fume and size of fine aggregate. *Cement and Concrete Research, 31*(2), 171-175.

Reinhardt, H. W. and Jooss, M. (2003). Permeability and self-healing of cracked concrete as a function of temperature and crack width. *Cement and Concrete Research, 33*(7), 981-985.

Reinhardt, H. W. and Rinder, T. (2006). Tensile creep of high-strength concrete. *Journal of Advanced Concrete Technology, 4*(2), 277-283.

Rizzo, E. M. and B.Sobelman, M. (1989). Selection criteria for concrete repair materials. *Concrete International, September,* 46-49.

Roy, D. M. and Idorn, G. M. (1983). Hydration, structure, and properties of blast furnace slag cements, mortars, and concrete. *ACI Journal, 79*(6), 445-457.

Russell, H. G. (1999). ACI defines high-performance concrete. *Concrete International, February*, 56-57.

Şahmaran M. and Li V. C. (2007). De-icing salt scaling resistance of mechanically loaded engineered cementitious composites. *Cement and Concrete Research, 37*(7), 1035-1046.

Şahmaran M., Li M. and Li V. C. (2007). Transport properties of engineered cementitious composites under chloride exposure. *ACI Materials Journal, 104*(6), 604-611.

Şahmaran, M., Yaman, İ. Ö., and Tokyay, M. (2007). Development of high volume low-lime and high-lime fly-ash-incorporated self consolidating concrete. *Magazine of Concrete Research, 59*(2), 97-106.

Şahmaran M. and Li V. C. (2008). Durability of mechanically loaded engineered cementitious composites under highly alkaline environments. *Cement and Concrete Composites, 30*(2), 72-81.

Şahmaran, M., Keskin, S. B., Ozerkan, G. and Yaman, I. O. (2008-a). Self-healing of mechanically-loaded self consolidating concretes with high volumes of fly ash. *Cement and Concrete Composites, 30*(10), 872-879.

Şahmaran M., Li V. C. and Andrade C. (2008-b). Corrosion resistance performance of steel-reinforced engineered cementitious composite beams. *ACI Materials Journal, 105*(3), 243-250.

Sahmaran, M., Lachemi, M., Hossain, K. M. A. and Li, V. (2009). Internal curing of engineered cementitious composites for prevention of early age autogenous shrinkage cracking. *Cement and Concrete Research, 39*(10), 893-901.

Sahmaran, M., and Li, V. C. (2009-a). Durability properties of micro-cracked ECC containing high volumes fly ash. *Cement and Concrete Research, 39*(11), 1033-1043.

Sahmaran, M. and Li, V. C. (2009-b). Influence of microcracking on water absorption and sorptivity of ECC. *Materials and Structures 42*(5), 593-603.

Schneider, B. (1991). *Development of SIFCON through applications.* paper presented at the high performance fiber reinforced cement composites, Mainz, Germany.

See, H. T., Attiogbe, E. K. and Miltenberger, M. A. (2003). Shrinkage cracking characteristics of concrete using ring specimens. *ACI Materials Journal, 100*(3), 239-245.

Soroushian, P., Nagi, M. and Hsu, J. (1992). Optimization of the use of lightweight aggregates in carbon fiber reinforced cement. *ACI Materials Journal, 89*(3), 267-276.

Tasdemir, M. A., Tasdemir, C., Akyüz, S., Jefferson, A. D., Lydon, F. D. and Barr, B. I. G. (1998). Evaluation of strains at peak stresses in concrete: a three-phase composite model approach. *Cement and Concrete Composites, 20*(4), 301-318.

Wang, S. and Li V. C. (2003). *Tailoring of PVA fiber/matrix interface for engineered cementitious composites (ECC).* Paper presented at the Fiber Society 2003 Symposium in Advanced Flexible Materials and Structures: Engineering With Fiber, Loughborough, UK.

Wang S. and Li V. C. (2007). Engineered cementitious composites with high-volume fly ash. *ACI Materials Journal, 104*(3), 233-241.

Ward, M. A. and Cook, D. J. (1969). The mechanism of tensile creep in concrete. *Magazine of Concrete Research, 21*(68), 151-158.

Wei, Y. (2008). *Modeling of autogenous deformations in cementitious materials, restraining effect from aggregate, and moisture warping in slabs on grade.* PhD Thesis. University of Michigan.

Wei, Y., Hansen, W., Biernacki, J. J. and Schlangen, E. (2011). Unified shrinkage model for concrete from autogenous shrinkage test on paste with and without ground-granulated blast-furnace slag. *ACI Materials Journal, 108*(1), 13-20.

Wongtanakitcharoen, T. and Naaman, A. E. (2007). Unrestrained early age shrinkage of concrete with polyproplene, PVA, and carbon fibers. *Materials and Structures, 40*(3), 289-300.

Yang, Y., Lepech, M. and Li, V. C. (2005). *Self -healing of ECC under cyclic wetting and drying.* Paper presented at the International Workshop on Durability of Reinforced Concrete under Combined Cechanical and Climatic Loads, Qingdao, China.

Yang, E. H. and Li, V. C. (2007). Numerical study on steady- state cracking of composites. *Composites Science and Technology, 67*(2), 151-156.

Yang, E. H. and Li, V. C. (2010). Strain-hardening fiber cement optimization and component tailoring by means of a micromechanical model. *Construction and Building Materials, 24*(2), 130-139.

Zhang, M. N. (1995). Microstructure, crack propagation, and mechanical properties of cement pastes containing high volumes of fly ashes. *Cement and Concrete Research, 25*(6), 1165-1178.

Zhang, J. and Li, V. C. (2002). Monotonic and fatigue performance in bending of fiber reinforced engineered cementitious composite in overlay system. *Cement and Concrete Research, 32*(3), 415-423.

Zhang, J., Li, V. C., Nowak, A. and Wang, S. (2002). Introducing ductile strip for durability enhancement of concrete slabs. *Journal of Materials in Civil Engineering, 14*(3), 253-261.

Zhang, M. H., Li, L. and Paramasivum, P. (2005). Shrinkage of high-strength lightweight aggregate concrete exposed to dry environment. *ACI Materials Journal, 102*(2), 86-92.

CURRICULUM VITAE

PERSONAL INFORMATION

Surname, Name: Keskin, Süleyman Bahadır
Nationality: Turkish (TC)
Date and Place of Birth: 20 October 1979, Uşak
Phone: +90 505 396 08 37
email: bkeskin@metu.edu.tr

EDUCATION

Degree	Institution	Year of Graduation
MS	Pamukkale University Civil Engineering	2005
BS	Pamukkale University Civil Engineering	2002
High School	Sekine Evren Anatolian High School	1997

WORK EXPERIENCE

Year	Place	Enrollment
2006-.....	METU Department of Civil Engineering	Research Assistant
2005-2006	Muğla Uni. Department of Civil Engineering	Research Assistant
2004-2005	Sismik Yapı Denetimi Limited Co.	Engineer

FOREIGN LANGUAGES

Fluent English, Intermediate German

PUBLICATIONS

Journals

- **S. B. Keskin**, K. Sulaiman, M. Şahmaran, İ. Ö. Yaman, "Effect of Pre-Soaked Expanded Perlite Aggregate on the Dimensional Stability and Mechanical Properties of ECC" Journal of Materials in Civil Engineering, doi:10.1061/(ASCE)MT.1943-5533.0000553 (In Press)

- M. Şahmaran, N. Özkan, **S. B. Keskin**, B. Uzal, İ.Ö. Yaman, T.K. Erdem "Evaluation of Natural Zeolite as a Viscosity-Modifying Agent for Cement-Based Grouts", Cement and Concrete Research, 38 (2008) 930–937.

- M. Şahmaran, **S. B. Keskin** , Gözde Özerkan, İsmail Ö. Yaman "Self-Healing of Mechanically-Loaded Self Consolidating Concretes with High Volumes of Fly Ash" , Cement and Concrete Composites, 30 (2008) 872–879.

Proceedings

- **S. B. Keskin**, İ. O.Yaman "Ground Granulated Blast Furnace Slag, Fly Ash and Zeolite as Cement Replacement Materials" The 1st International Conference on Civil Engineering - Towards A Better Environment, Coimbra, Portugal, 2009

- Ö. Kasap Keskin, **S. B. Keskin**, İ. Ö. Yaman, "The Effect of Various Water-Reducing Admixtures on Alkali-Silica Reaction ", 3rd Chemical Admixtures for Structures Symposium and Exhibition, Ankara, Turkey, 2009, 155-166 (In Turkish)

- **S. B. Keskin**, M. Güngör, M. Fırat "The Investigation of Seepage Event Inside the Body of an Earthfill Dam" 3rd National Water Engineering Symposium, İzmir, Turkey, 2007, 281-292 (In Turkish)

- **S. B. Keskin**, M. Güngör, M. Fırat "The Influence of Soil Type, Vertical Wall and Upstream Blanket on Velocity and Potential Occured by Seepage under Regulator Foundation" Symposium on Recent Applications in Engineering Geology, Denizli, Turkey, 2006, 191-200 (In Turkish)